NUMERICAL ANALYSIS FOR MAGNETIC EFFECTS ON NEWTONIAN AND NON-NEWTONIAN FERROFUID FLOW AROUND A CIRCULAR CYLINDER

by

Ömer Barış Adıgüzel

M.S., Mechanical Engineering, Boğaziçi University, 2017

Submitted to the Institute for Graduate Studies in
Science and Engineering in partial fulfillment of
the requirements for the degree of
Master of Science

Graduate Program in Mechanical Engineering
Boğaziçi University
2017

ACKNOWLEDGEMENTS

Special thanks to my thesis advisor Prof. Kunt Atalık for his constant support throughout this study.

Thanks anyone supported me and my study this whole time.

ABSTRACT

NUMERICAL ANALYSIS FOR MAGNETIC EFFECTS ON NEWTONIAN AND NON-NEWTONIAN FERROFUID FLOW AROUND A CIRCULAR CYLINDER

In this study, the effects of magnetic field applications are investigated on ferromagnetic flow around cylinder. The analyses are made for Newtonian and non-Newtonian flow types. In order to investigate the non-Newtonian fluids, shear thinning and shear thickening models are used in numerical studies. The magnets on the cylinder are located on $90^o - 150^o$ and $210^o - 270^o$ clockwise. All of these three types of fluids, whose Reynolds values ranging from 50 to 1500, are experimented to show deviation on the drag coefficient, separation point, wake region and vortex formation length with magnetostatic effects by means of various tables and graphics. Consequently, the magnetostatic force shows a decreasing effect on drag coefficient for any type of fluid. Drag coefficient becomes higher for shear thickening fluid on each Reynolds number; on the other hand, this value for shear thinning fluids becomes smaller than that, belongs to Newtonian fluid, for smaller Re number cases, and higher for higher Re number cases. Besides, the largest change on drag coefficient is observed on shear thickening fluids. Vortex formation length decreases with magnetostatic effects, although the change is not as high as drag coefficient observations. This value for shear thickening fluid becomes higher than values for Newtonian fluids for low Re number cases, and lower for high Re number cases. Vortex formation of shear thinning fluid is observed as higher than any type of fluid. Separation point and wake formation can be observed clearer for higher magnetic force values. Vortex formation length gets also bigger values with magnetic force. When the magnets are placed on the front side, separation point gets on the front side in a clear way and increased the drag coefficient largely.

ÖZET

NEWTONYEN VE NEWTONYEN OLMAYAN FERROMANYETİK AKIŞKAN MODELLERİ İÇİN MANYETİK ALANIN SİLİNDİR ETRAFI AKIŞ ÜZERİNDEKİ ETKİLERİNİN SAYISAL ANALİZİ

Silindir etrafı ferro parçacıklı akış üzerinde manyetik alan uygulanması sonucu ortaya çıkan etkiler incelenmiştir. Newtonyen ve Newtonyen olmayan akışlar için analizler yapılmıştır. Newtonyen olmayan akışkanları incelemek için, kayma kalınlaşması ve incelmesi modelleri kullanılmıştır. Silindir üzerine mıknatıslar saat yönünde $90^o - 150^o$ ve $210^o - 270^o$ açılara yerleştirilmiştir. Re=50 ve Re=1500 arasında Reynolds sayısına sahip bu üç tip akışkanın, manyetik etki altında sürüklenme katsayısı, ayrılma noktası, iz bölgesi ve girdap oluşumunda nasıl değişimler meydana geldiği tablolar ve grafiklerle gösterilmiştir. Sonuçta manyetostatik kuvvet, sürüklenme katsayısını azaltmıştır. Kayma kalınlaşması olan akışkanlar, Reynols sayısına bağlı olmaksızın diğer sıvılardan yüksek sürüklenme katsayısına sahipken, kayma incelmesi olan akışkanlar için sürüklenme katsayısı, Newtonyen akışkanlara göre düşük Reynolds değerlerinde düşük, yüksek Reynolds değerlerinde ise yüksek olmuştur. Ayrıca, sürüklenme katsayısında en yüksek değişim kayma kalınlaşması olan akışkanlarda görülmüştür. Girdap oluşum frekansı, sürüklenme katsayısına göre az da olsa manyetik etkiyle düşüş göstermiştir. Girdap oluşumu frekansı için kayma kalınlaşması olan akışkanlar, Newtonyen akışkanlara göre düşük Reynolds değerlerinde daha yüksek değerlere sahipken, Reynolds arttıkça daha düşük seviyede olmuştur. Kayma incelmesi olan akışkanların girdap oluşum frekansı da manyetik alan kuvveti ve Reynolds sayısına bağlı olmaksızın daha yüksek olarak gözlemlenmiştir. Ayrılma noktası ve iz bölgelerinde değişim, manyetik kuvvet değeri arttıkça daha net olarak gözlemlenmiştir. Girdap oluşum uzaklığı manyetik etki altında yükselmiştir. Cismin önündeki mıknatısların, üç akışkan tipi için ayrışma noktasını net bir şekilde daha öne aldığı ve sürüklenme katsayısını arttırdığı görülmüştür.

TABLE OF CONTENTS

LIST OF FIGURES

LIST OF TABLES

LIST OF SYMBOLS

$\overrightarrow{A}$	Magnetic Field Potential Vector
$\overrightarrow{B}$	Magnetic Field Induction Vector
B_0	Amplitude of the Magnetic Field
D	Rate of Deformation Tensor
D	Diameter of Cylinder
$\overrightarrow{F}$	Body Force fo Unit Volume
$\overrightarrow{H}$	Magnetic Field Vector
H	Intensty of Magnetic Field Vector $\overrightarrow{H}$
I_2	Second Invariant of the Stress Deformation Tensor
$\overrightarrow{M}$	Magnetization Vector
M	Intensty of Magnetization Vector $\overrightarrow{M}$
N	Interaction Parameter
n	Power Law Index
p	Pressure
Re	Reynolds Number
St	Strouhal Number
t	Time
T	Stress Tensor
w	Mass Fraction of the Ferroparticles in the Base Fluid
U	Free Stream Velocity
$\overrightarrow{v}$	Velocity Vector
μ	Fluid Viscosity
μ_0	Vacuum Magnetic Permeability
κ	Consistency Index
ω	Frequency of Vortex Shedding
ψ	Volume Fraction of the Ferroparticles in the Base Fluid

LIST OF ACRONYMS/ABBREVIATIONS

2D	Two Dimensional
3D	Three Dimensional
EM	Electromagnetic
MHD	Magnetohydrodynamic
NACA	National Advisory Committee for Aeronautics

1. INTRODUCTION

1.1. Literature Survey

1.1.1. Electromagnetic Flow Control

In order to control the flow field, electromagnetic force has been an important element in fluid mechanics especially for flow around an object and flow inside a tube cases. After realization of feasibility of electromagnetic force creation to control the flow, fluids are used with many different geometries as airfoil, circular cylinder and rectangular objects.

There are many studies as this has been popular subject due to its importance and applicability. Berger *et al*. [1] used Lorenz force to reduce skin friction of a tube channel flow by using direct numerical simulation for low Reynolds number as 100, 200 and 400. This simulation showed that the required power is decreased for propel objects through viscous conducting fluids. Posdziech and Grundmann [2] investigated numerically the electromagnetic control of sea water flow over an infinitely long circular cylinder between Re= 10 and Re=300. According to this study; the pressure, frictional and total drag have a clear dependency on the position of Lorenz application, Lorenz force magnitude and Reynolds number. Weier *et al*. [3] used Lorentz force to modify the boundary layer around a circular cylinder. By using electromagnetic force, it is possible to have smaller wake region. They used periodic Lorenz force to control the flow. They used hydrofoil NACA 0015 on the Reynolds Number range 10^4 < Re < 10^5. They showed that the maximum lift gain can be increased by using oscillatory momentum instead of stationary.

Kim and Lee [4] investigated the influence of electromagnetic forces, that applied on the cylinder surface in the range of $70^o - 130^o$ as shown in Figure 1.1. They applied the force on both clockwise and counterclockwise. Their experimental study expressed that, both separation point and drag coefficient have dependency on Reynolds number, electromagnetic force direction and magnitude. As a result, for lower Reynolds number the effect of Lorenz force is higher on drag reduction. Positive Lorenz force accelerates the separation and increases the drag, and magnitude of electromagnetic force has a positive effect on drag reduction.

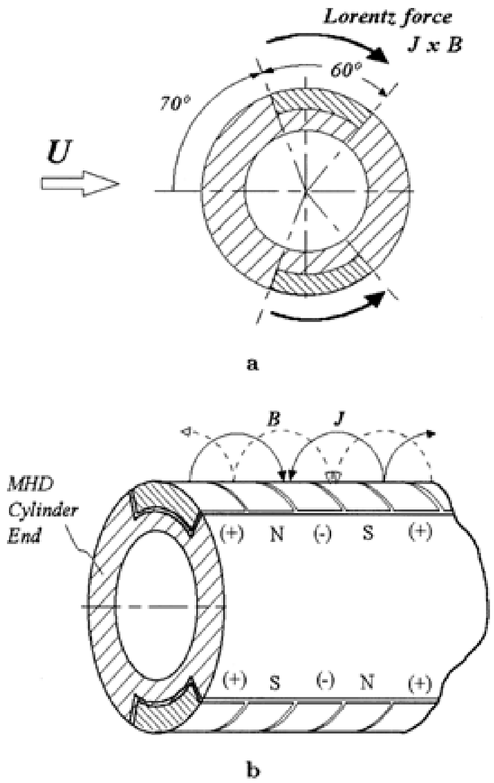

Figure 1.1. Problem domain for the flow past on a cylinder of experiment by Kim and Lee [4]

There are some other applications for electromagnetic and magnetostatic flow control as recent studies expressed. Papadapoulos *et al*. [17] used cylindrical coil around a section of a pipe to create magnetostatic force. The 3D numerical simulations are made on ferrofluid inside the pipe. They showed that axial velocity is mostly dependent on volumetric concentration. On another research of Rosa *et al*. [18] on laminar pipe flow, the drag reduction is aimed for ferrofluid by the help of a magnet, located in the end of the pipe. That created a magnetic field gradient favorable to the flow direction. They observed that a controllable magnetic field can be used for drag reduction. Kalter *et al.* [19] used electromagnetic forces to control a flow with very high Reynolds number (Re= 3,1x103) in a rectangular cavity, and with this study, they showed that oscillatory frequency can be altered significantly by the help of Lorentz forces. Sedaghat and Badri [20] used NACA0015 aerofoil to investigate flow control with electromagnetic force numerically. They used different angle of attack values and realized that hydrodynamic performance is increase in a significant manner. Also, flow separation area is decreased and overall lift is increased. Zhao *et al.* [21] also worked on airfoil. They tried to control the flow separation behind the airfoil in plasma by changing the angle of attack. By optimal angle of attack and frequency, the experiment showed that it is possible to reduce the drag up to 22,4%. Also, there are some researches, related to flow around sphere. Shatrov and Gerberth [22] used electromagnetic forces to create strong drag reductions. They used higher Reynolds numbers to express that very high drag reductions are available by electromagnetic field use. Sekhar *et al.* [23] investigated MHD flow around a sphere object. In this study, they used finite difference method for Re=100 and Re=200 and the magnetic interaction parameter N= [0,10]. In the end, they found a linear correlation between total and pressure drag with square root of interaction parameter. Zhang *et al.* [24] worked on cylinder flow and tried to suppress the wake region by using electromagnetic forces that alter by time $N(t)$. The results of their work show that drag oscillation can be made to the optimal force.

1.1.2. Ferrofluids

A ferromagnetic colloidal solution is a colloid suspension that consisting of nano magnetic particles in a liquid dispersion. The stated particle size is usually considered to be in the range of 5nm to 20nm [5]. The solutions are mostly very dilute magnetic suspensions. Montgomery [6,7] used the solutions of Nickel Magnetite (Fe_3O_4) and gamma iron (γFe_2O_3) with concentration of 0,1% by weight. Berkovsky and Bashtoyov [8] showed the ferromagnetic fluids can be used for loudspeakers with the use of DC magnetic fields from permanent magnets to create dampers in stepper motors and shock observers. Additionally, Gazeau *et al.* [9] showed thet ferrofluid particles can be used nanoduct flows, nanomotors, nanogenerators, nanpumps, nanoactuators and some similar nanoscale devices. In Bioengineering, there are fields that ferrofluids can be used. Voltairas *et al.* [10] used ferrofluid behavior to target the medication in the artery. As stated at Figure 1.2, by the help of magnet a magnetostatic current is created and the flow regime is changed where the drug needs to be addressed. Also, as stated, the ferrofluid is blood in this experiment.

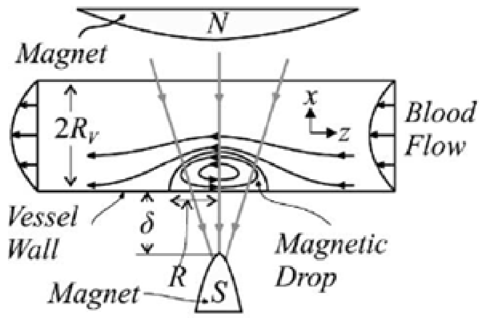

Figure 1.2. Problem domain for the magnetic drug targeting experiment by Votairas *et al.*[10]

The flow regime is affected by the magnets and the created magnetic force in this study. The main reason of that is the blood has iron containing proteins. This enables the blood to be affected by strong magnetic fields. Blood is considered as Newtonian in many studies. But, there are some non-Newtonian examples especially in narrow arteries or variable sectioned arteries. Reynolds range can vary from 1 to 4000 for different cases of blood flow [11].

1.1.3. Rheology

The definition of Newtonian fluids is simply made by existence of a linear relationship between the applied stress and shear rate. Mostly, low molecular weight substances such as organic and inorganic liquids, inorganic salts, molten metals and gases have Newtonian flow characteristics [12]. In other words, Newtonian fluids have constant dynamic viscosity.

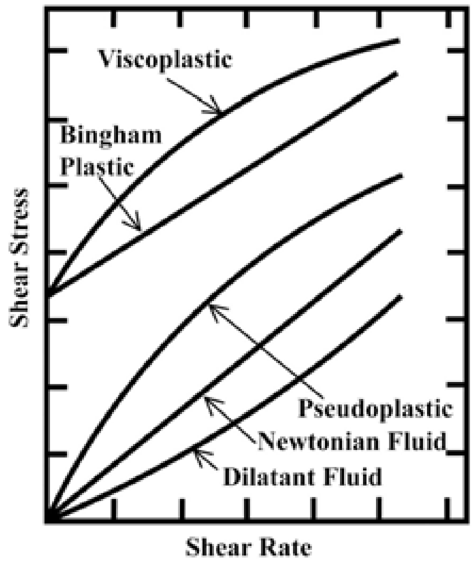

Figure 1.3. Shear stress and shear rate curves of Newtonian and non-Newtonian fluids [13]

Adhesives, biological fluids (as saliva, blood, synovial fluid etc.), cement paste, foams, molten lava and polymer melt and solutions have different behavior compared to Newtonian fluids mentioned above. These fluids are called as non-Newtonian fluids [13]. There is no linear relationship between shear rate and shear stress and also these data may not pass from the origin as seen at Figure 1.3.

Shear thinning flow behavior is one of the most common Non-Newtonian behavior types. This model is time independent. The apparent viscosity decreases gradually with increasing shear rate in these fluids. There are many studies that aim to observe pseudoplstic flow behavior of polymer melts such as studies made by Ibarz and Barbosa [14] and Goiver and Aziz [15]. They showed the viscosity decreases with shear rate and at the same time the shear stress increases with negative gradient with shear rate.

Shear thickening or dilatant behavior has similarities with shear thinning fluids, since they show no yield stress. But in contrary, their viscosity increases with increasing shear rate. Metzner and Withlock [16] worked on TiO_2 suspensions to investigate this behavior at many different concentrations.

There are many time independent models generated to express the non-Newtonian behavior of the fluids. Power law model is one of them. In this model, there are 2 different parameters to characterize the fluid. First one is n (power law index). This determines the behavior whether shear thinning or shear thickening, by its value. If the power law index is smaller than 1, this fluid is named as shear-thinning fluid. For n greater than 1, the flow shows shear thickening behavior, and the power law index for Newtonian fluids is 1. For example, experiments show that many polymer melts have power law index in the range on n=0,3 and n=0,7. The other parameter is κ (consistency index). This is used for a better approximation for manifesting the flow characteristics.

1.2. Objective

The study investigates the flow characteristic changes and effects on wake region under magnetostatic force application for flow around circular cylinder. In order to understand the results of those changes, magnetic and flow parameters are determined, and these parameters are used for Newtonian and power law flow models, after the verification of the numerical model with the literature review. The used fluids are considered to be ferrofluids as Newtonian, shear thinning and shear thickening. The geometry of the problem is considered to be infinitely long and wide for the used finite element method.

The main purpose of the study is to investigate the magnetostatic effects with different amounts on flow with different Reynolds numbers and models (different power law index, n). In order to do that, more than Reynolds number values ranges from Re=50 to Re=1500, different magnetic magnitude values ranges from N=0 to N=100, different power law indexes from n=0,2 to n=1,5 and 3 different magnet locations are used with different combinations. The desired outputs are to obtain the exact values and changes on drag coefficient, Strouhal number, vortex formation length and the effects of the magnet positions.

1.3. Outline of the Thesis

In the following chapters of the study, mathematical formulation and solution method as Chapter 2, results and discussion as Chapter 3 and conclusion and future works as Chapter 4 are presented.

In Chapter 2, the details of formulation are given. Non-dimensionalization of combined formulas is presented and non-dimensional parameters are introduced. Afterwards, the results of mesh independency test are shown and selected meshes are presented for both Newtonian and non-Newtonian cases. Lastly, the details of numerical method are explained.

In Chapter 3, the numerical simulation results are shown. The validation with literature data is given for Newtonian flow past a circular cylinder. Then, a parametric study is conducted to elucidate the effects of parameters as interaction parameter and Reynolds number on flow. The results are discussed in terms of the changes in drag coefficient, Strouhal number and vortex formation length.

In Chapter 4, the study is concluded briefly and possible future works are presented.

2. MATHEMATICAL FORMULATION AND SOLUTION METHOD

2.1. Mathematical Formulation

The mass and linear momentum conservation laws for the incompressible flow of a fluid under the action of a magnetic field can be written respectively as:

$$\nabla.\overrightarrow{v} = 0 \tag{2.1}$$

$$\rho(\frac{\partial\overrightarrow{v}}{\partial t} + \overrightarrow{v}.\nabla\overrightarrow{v})) = -\nabla p + \nabla.T + \rho\overrightarrow{F} \tag{2.2}$$

where $\overrightarrow{v}$ is the velocity vector, t is the time, ρ is the fluid density, p is the pressure, T is the stress tensor. The body force vector represents the action of the magnetic field.

For a Newtonian fluid the stress tensor can be written as:

$$T = \mu(\nabla\overrightarrow{v} + (\nabla\overrightarrow{v})^T) \tag{2.3}$$

where μ is the fluid viscosity.

For non-Newtonian fluids, different constitutive laws must be used. In this work, an inelastic non-Newtonian model, the Power-Law model is chosen. This model is able to describe the dependence of the viscosity on the shear rate and to represent shear thinning or shear thickening effects. The fluid's viscosity is then written as a function of the rate of deformation tensor D as:

$$\mu(D) = \kappa I_2^{\frac{(n-1)}{2}} \tag{2.4}$$

where κ is the consistency index, I_2 is the second invariant of the rate of deformation tensor, and n is the Power-Law index.

In the flow of a ferrofluid under the application of a magnetic field, the electromagnetic body force can be written as:

$$\overrightarrow{F} = \mu_0 M \nabla H \tag{2.5}$$

where μ_0 represents the vacuum magnetic permeability, M represents the intensity of magnetization vector $\overrightarrow{M}$ and H is the intensity of the magnetic field vector $\overrightarrow{H}$.

Magnetic field induction vector can be written as:

$$\overrightarrow{B} = \mu_0(\overrightarrow{H} + \overrightarrow{M}) \tag{2.6}$$

Magnetic field and induction vectors are assumed to satisfy the following equations:

$$\nabla \times \overrightarrow{H} = 0 \tag{2.7}$$

$$\nabla . \overrightarrow{B} = 0 \tag{2.8}$$

According to these conditions, it is possible to define a magnetic field potential vector through:

$$\overrightarrow{B} = \nabla \times \overrightarrow{A} \tag{2.9}$$

Under magnetostatic assumption, the magnetic field is uncoupled from the flow field. For the magnet only, magnetic field induction vector reduces to,

$$\overrightarrow{B} = \mu_0 \overrightarrow{H} + \overrightarrow{B_0} \tag{2.10}$$

where $\overrightarrow{B_0}$ is the remanent magnetic flux vector.

With the combination of the equations stated above, the equation to be solved for the permanent magnet becomes:

$$\nabla \times (\mu_0^{-1}(\nabla \times \overrightarrow{A} - \overrightarrow{B_0})) = 0 \tag{2.11}$$

Using this relation in Equation (2.7) with Equation (2.6) , the equation to be solved for fluid magnetization becomes:

$$\nabla \times (\mu_0^{-1}(\nabla \times \overrightarrow{A}) - \overrightarrow{M}) = 0 \tag{2.12}$$

By solving the Equation (2.12), the magnetization vector can be determined. This value is critical, because the force vector, that connects the magnet with the fluid in our domain, can be determined by the help of this magnetization vector. In the end, the force vectors are created only the surfaces, touching the fluid, by the help of insulation boundary conditions of other surfaces.

2.2. Non-dimensional Parameters

The simulation results are evaluated in terms of four non-dimensional parameters: the Reynolds number, the interaction parameter, the Power-Law index and the Strouhal number. The velocity and length scales are chosen as the free stream velocity U and the diameter of the cylinder D. The time scale is therefore D/U. The pressure variable is scaled with ρU^2. The magnetic field induction vector $\overrightarrow{B}$ is scaled with the magnitude of the remanent magnetic flux B_0. Then, the scale for both magnetic field and magnetization vectors becomes B_0/μ_0.

With the guidance of reference scales, the non-dimensional momentum equation becomes,

$$(\frac{\partial \overrightarrow{v}}{\partial t} + \overrightarrow{v}.\nabla\overrightarrow{v})) = -\nabla p + \frac{1}{Re}\nabla.T + N\overrightarrow{F} \tag{2.13}$$

The Power-Law Reynolds number, Re, represents the ratio of inertia effects to viscous effects and is defined as:

$$Re = \frac{\rho U^{2-n} D^n}{\kappa} \tag{2.14}$$

where U represents the free stream velocity, and D represents the cylinder diameter. The other non-dimensional parameter is the interaction parameter N, characterizing magnetic effects to inertia effects ratio.

The other non-dimensional parameter is the interaction parameter N, characterizing magnetic effects to inertia effects ratio. This parameter is defined as:

$$N = \frac{B_0^2}{\mu_0 \rho U^2} \tag{2.15}$$

where B_0 is the magnitude of the remanent magnetic flux.

The Strouhal number, St, represents the non-dimensional vortex formation frequency, and is defined as,

$$St = \frac{\omega D}{U} \tag{2.16}$$

where ω represents the frequency of vortex shedding. This frequency is calculated from the Fast Fourier transform analysis of the drag coefficient time evolution signal.

2.3. Geometry and Mesh Selection

The geometry of the study is basically consisting of a 2D cylinder and infinitely long and high domain as seen Figure 2.1. There are additionally two magnets as stated clearly in Figure 2.2. The magnets are placed from 90^o to 150^o and 210^o to 270^o.

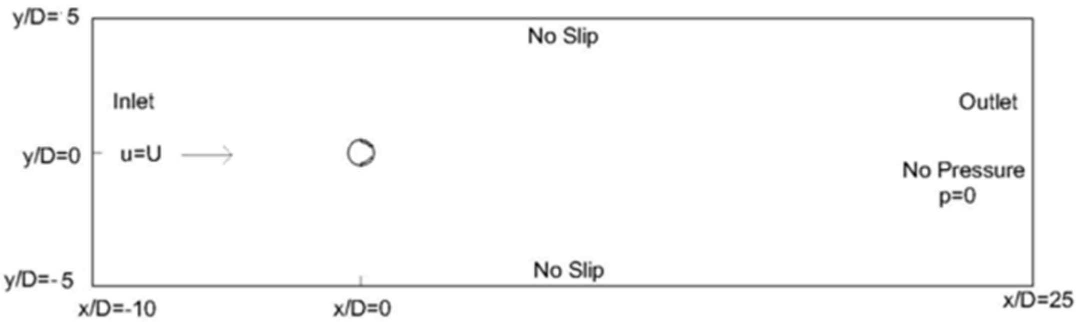

Figure 2.1. Computational domain (D=2mm)

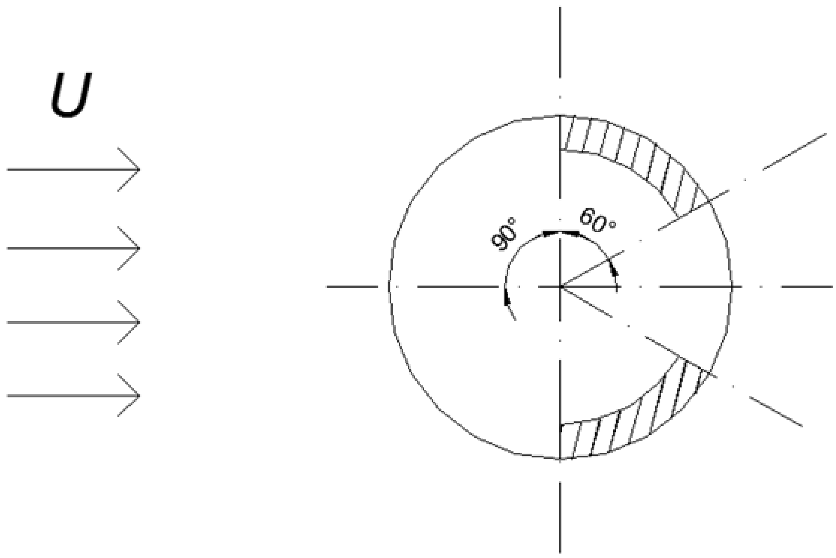

Figure 2.2. Flow geometry with magnets placed at $90^o - 150^o$ section

On the top and bottom boundaries, there is no slip condition. At the end, there is no pressure. The ferrofluid enters the domain with a uniform velocity.

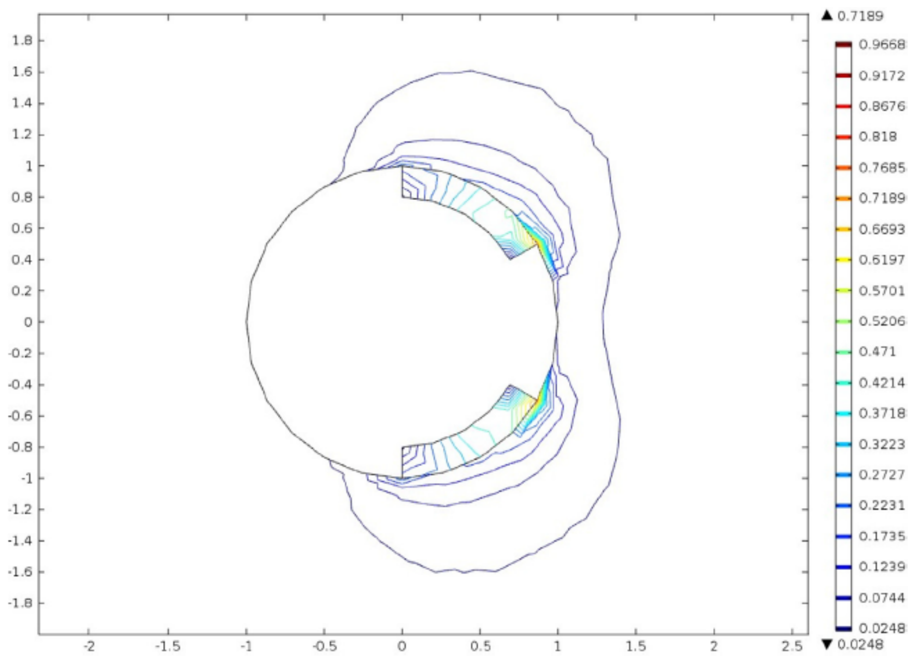

Figure 2.3. Magnetic field induction lines B = constant lines for $N = 100$.

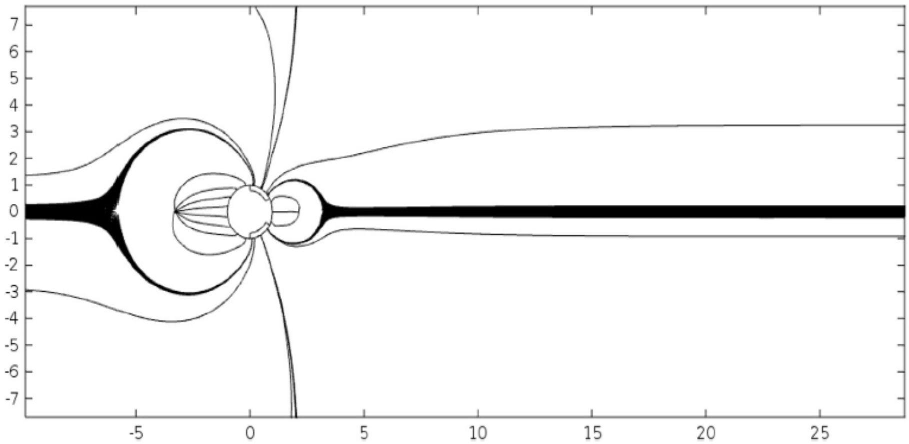

Figure 2.4. Magnetic body force lines F = constant lines for $N = 100$.

For illustrative purposes, the magnetic field induction (or magnetic flux density) lines (B = constant lines) and the magnetic body force lines (F = constant lines) are shown in Figure 2.3 and Figure 2.4 , for the $N = 100$ case. The magnetic field induction vector is tangent to the lines shown in Figure 2.3 . The direction of the vectors are from top to bottom around both magnets, since the north poles are located at the upper part of the magnets. In Figure 2.4 , the magnetic body force vectors which are tangent to F = constant lines are directed towards the cylinder where the magnets are placed.

Many mesh alternatives are tried for validation from 3000 total elements to 17500 elements as seen at Figure 2.5.

By the independency test, the selected mesh is the one with 8082 elements. As tabulated at Table 2.1, there is no distinctive change between Grid II and Grid III. After validation with Grid IV consisting of 17500 elements, the Grid III is decided as the suitable mesh selection with consideration of computational power either.

Grid III, seen at Figure 2.5, contains 7530 triangular elements, 552 quadrilateral elements, 344 edge elements and 15 vertex elements. Therefore, it is used in all of the simulations mentioned in this study.

Table 2.1. Mesh Selection Trials for Newtonian Case

Mesh Selection	**I**	**II**	**III**
Drag Coefficient	1.0164	1.0533	1.0564
Element Number	3214	4710	8082

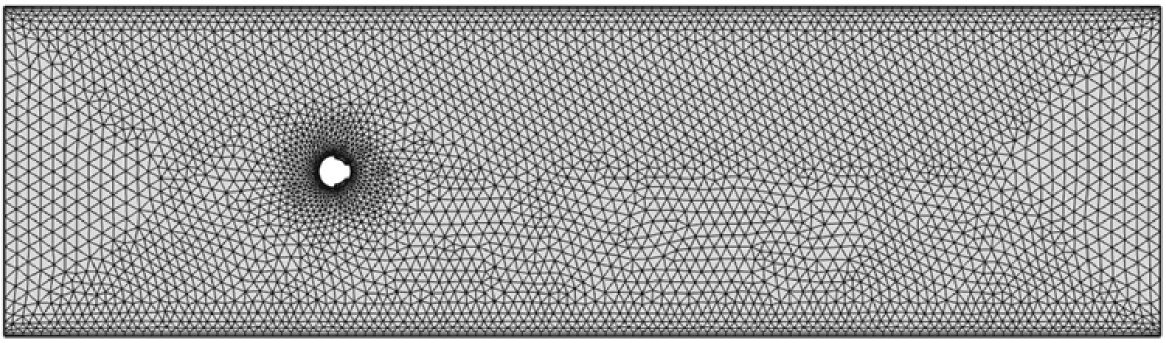

Figure 2.5. Grid III

For non-Newtonian case, the mesh grid is selected by higher element numbers as seen at Figure 2.6. There are 17534 elements consisting of 16392 triangular elements, 1132 quadrilateral elements, 662 edge elements and 15 vertex elements. This is basically because of the complexity of the fluid types and the need for better convergence.

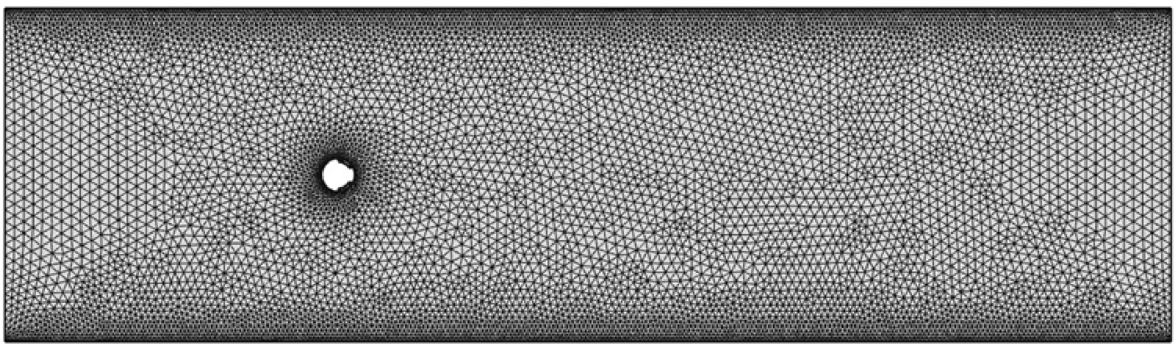

Figure 2.6. Mesh grid example for non-Newtonian simulations

2.4. Method of Solution

In numerical simulations, COMSOL commercial software is used. This software is suitable for our study, because it can model the electromagnetic effects successfully compared to its equivalents. There are two steps for solution as time dependent and time independent part. Velocity, pressure and magnetic vector potential equations are solved for both of the parts. They are coupled by volumetric force parameter as explained.

In the numerical method, equal order Lagrange linear shape functions are used for both velocity and pressure, and quadratic shape functions are used for magnetic vector potential. Backward Euler method is used for time discretization. Typical time step for simulations is of the order of 10^{-5}. A direct solver for sparse matrices is used in the solution of discretized equations. The convergence criterion is chosen to be of the order of 10^{-4}. The run time for simulations vary from 60 minutes to 300 minutes according to fluid type, Reynolds number and interaction parameter.

3. RESULTS AND DISCUSSION

The study is performed to express the changes on drag coefficient and Strouhal number with magnetic effects by Reynolds number and fluid type. The magnetic effects are parameterized with N (interaction parameter). It is chosen as N=0 to show no magnetic effect case, N=10 to express the low magnetic values and N=100 to show the effect of higher magnetic values. Also, the fluid types are determined upon the value of power-law index (n). This index is chosen as n=1 for Newtonian fluid, n=0.2 for shear thinning fluid and n= 1.5 for shear thickening fluid case.

In this study, two dimensional simulations are applied in order to show the effects, those stated above. There is a widely believed opinion, two dimensional simulations are not sufficient for expressing the aspects on higher Reynolds values than Re=200. Although this opinion is correct, it is impractical to simulate all of the cases on three dimensional base with our current computational power. Also; in the literature, it can be inferred that, two dimensional analyses can be used to show the general trends of drag coefficient and Strouhal number for much higher Reynolds numbers. In the following sections, the general drag coefficient and Strouhal number closeness with literature data is stated.

Drag coefficient is the main parameter for the comparison of effects in this study. The equation of drag coefficient is expressed as;

$$C_D = \frac{2.F_D}{\rho.U^2.D} \tag{3.1}$$

where F_D is the total drag force per unit length. This force is obtained by integration of magnetic, viscous and pressure forces, created around the cylinder. For higher Re values, the evolution of drag coefficients with time is periodic. In order to obtain the value of drag coefficient, after stabilization of the flow, mean value is calculated for a period of flow.

$$\overrightarrow{F_s} = \oint \overrightarrow{t}_{(\overrightarrow{n})}\, dS \tag{3.2}$$

where $\overrightarrow{t}_{(\overrightarrow{n})}$ denotes the total stress vector on the surface with outward unit normal vector $\overrightarrow{n}$.

3.1. Newtonian Cases

At first, the fluid is modeled as Newtonian in order to validate the solution method and express the changes in drag coefficient, Strouhal number and vortex formation length parameters with interaction parameter. In Figure 3.1 and Figure 3.2, literature data of the drag coefficient versus Reynolds number are presented [25,26].

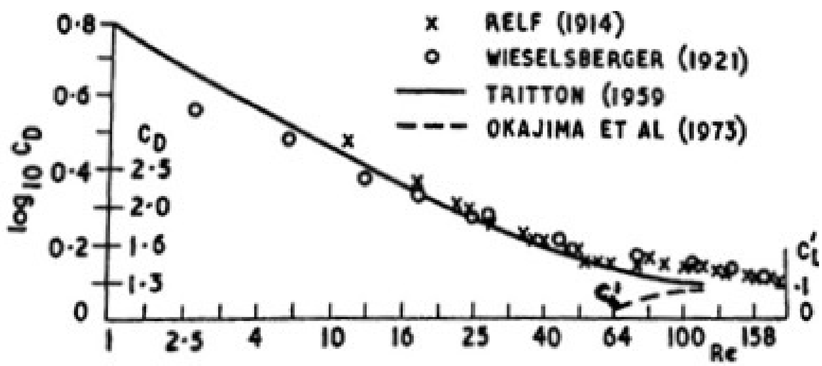

Figure 3.1. Mean drag coefficient for different Reynolds number for Newtonian Fluid [25]

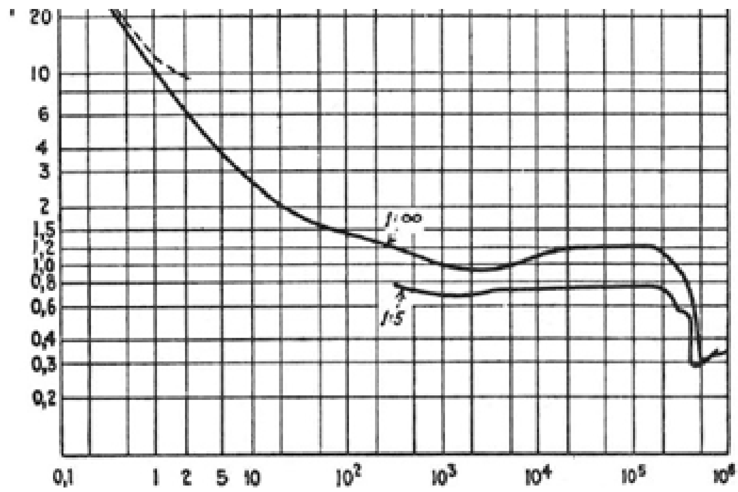

Figure 3.2. Mean drag coefficient for different Reynolds number for Newtonian Fluid [26]

In Table 3.1, the results of numerical simulations for Re=50, Re=100, Re=200, Re=500, Re=1000 and Re=1500 with N=0, N=10 and N=100 are tabulated. As denoted, there is a consistency between literature data and simulation results. For instance, at Re=50 and N=0, the drag coefficient is around 1.5, which is obviously close to the literature data seem slightly over 1.5. Also, after Re=500, the calculated drag coefficient values are constant as expected. This implies, the general trends can be obtained by applied simulation method. Afterwards, the trend suggests that interaction parameter has a decreasing effect on drag coefficient. That effect can also be seen at Figure 3.3 clearly. Both of the table and figure enable us to see the drag reduction is significant enough, which is almost 20%.

Strouhal number is another non-dimensional parameter of our study. The literature data is given at Figure 3.4 [26].

The applied inverse Fourier transform method on drag coefficient is used to determine the tabulated data, seen at Table 3.2. These values and literature data are consistent. It can be implied that interaction parameter has clearly low effect on Strouhal number for the considered range of Reynolds numbers as seen in Figure 3.5.

Table 3.1. Mean drag coefficients (C_D) with different Reynolds number(Re) values for different interaction parameter(N)

	N=0	**N=10**	**N=100**
Re=50	1.4847	1.43757	1.3969
Re=100	1.3095	1.2654	1.1531
Re=200	1.2404	1.20409	1.0649
Re=500	1.0637	1.02218	0.8924
Re=1000	1.0564	1.02381	0.8704
Re=1500	1.0727	1.0615	0.8873

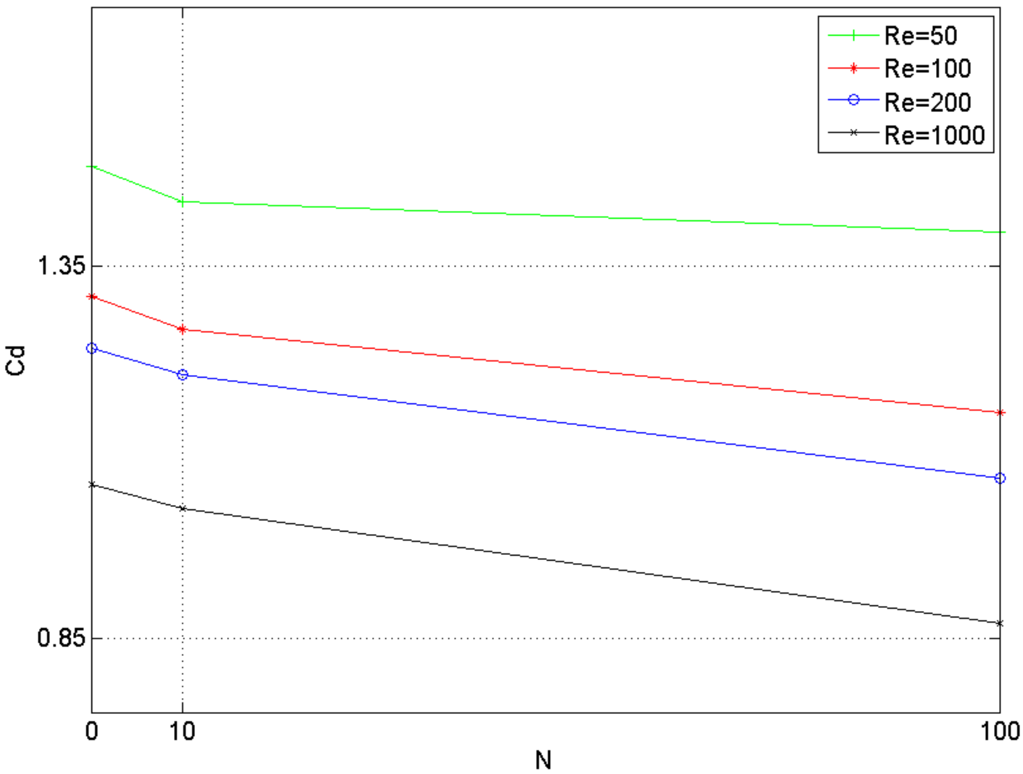

Figure 3.3. Mean drag coefficients (C_D) with different Reynolds number(Re) values for different interaction parameter(N)

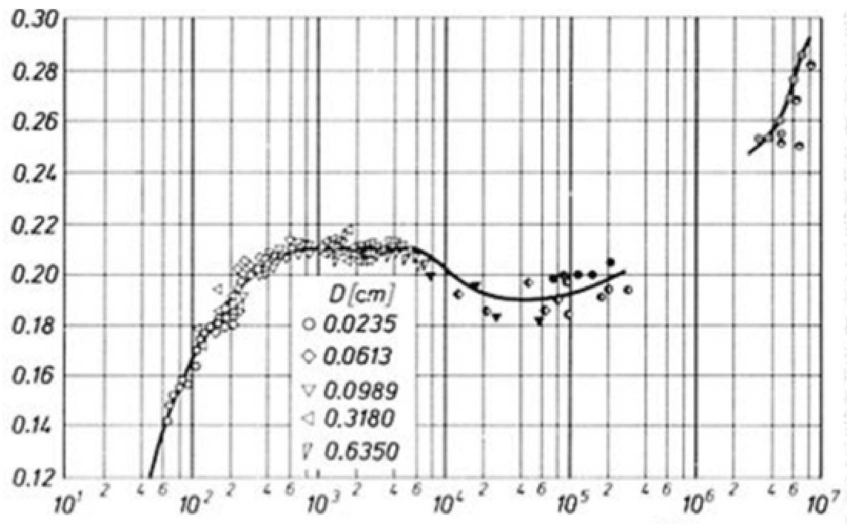

Figure 3.4. Strouhal number change with different Reynolds numbers for Newtonian Fluid [25]

Table 3.2. Strouhal number(St) with different Reynolds number(Re) values for different interaction parameter(N)

	N=0	**N=10**	**N=100**
Re=100	0.1678	0.1670	0.1672
Re=200	0.18182	0.17176	0.17122
Re=500	0.21176	0.20903	0.20129
Re=1000	0.21770	0.21593	0.21039
Re=1500	0.21898	0.21802	0.21532

Third important parameter is separation point location in our study. Previous mentioned studies show that the separation point shifts on the front side of the cylinder because of electromagnetic field application. Two different streamline plots are presented at Re=1000 with N=0 and N=100 at Figure 3.6. The red marks indicate that the separation point shifts on the front side as expected. Although it is not a drastic shift, it is a significant result for expressing the drag reduction, since this movement creates a relatively smaller wake region.

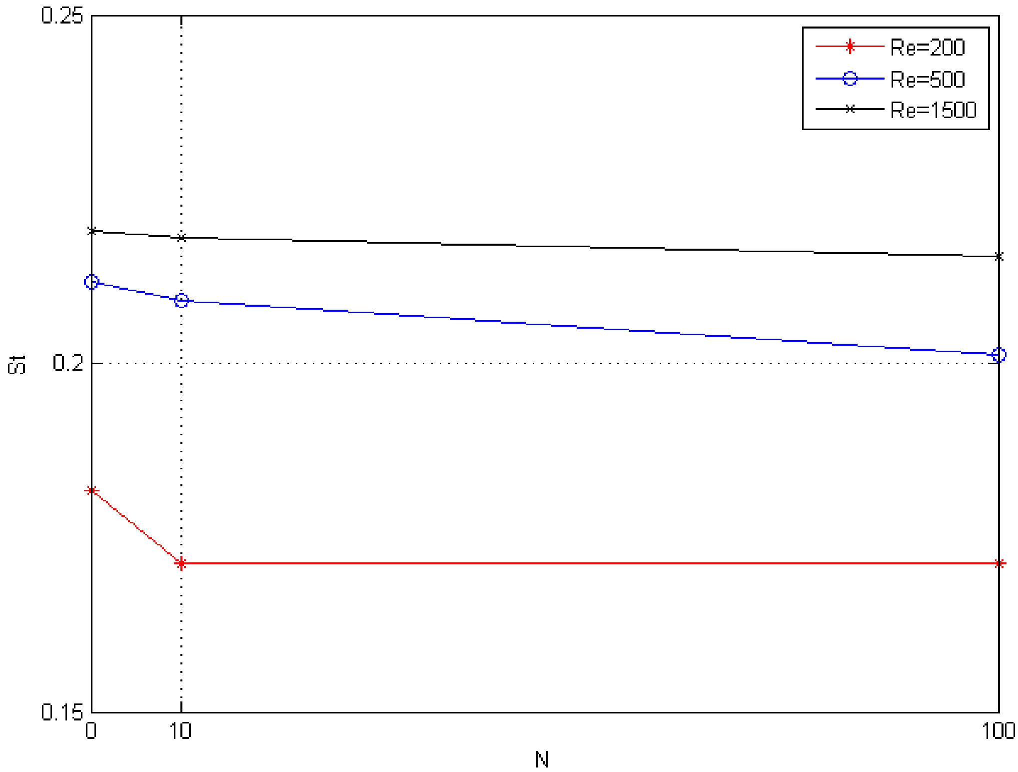

Figure 3.5. Strouhal Number (St) with different Reynolds number(Re) values for different interaction parameter(N)

At Re=50, we have a pair of vortices as seen at Figure 3.7, however the formation of a vortex street s observed in Figure 3.11 to 3.19 for higher Reynolds numbers(Re=200, Re=1000 and Re=1500). After some simulations starting from Re=50, it is observed that the transition to vortex shedding begins between Re=50 and Re=60.

In order to see if the vortex shedding can be delayed by magnetostatic field application, flows at Re=100 are simulated with various interaction parameters. Some of the streamline plots are presented at Figure 3.8, Figure 3.9 and Figure 3.10. These results show that the vortex shedding can be delayed with magnetic field application. As the vortex shedding can be delayed and wake region can become smaller, eliminating the wake region also seems possible for higher values of interaction parameter. For very large N values, for example Re=50 and N=2500, negative drag coefficient values are observed with backflow near the cylinder. This situation may be unphysical due to unrealistic magnetic intensity.

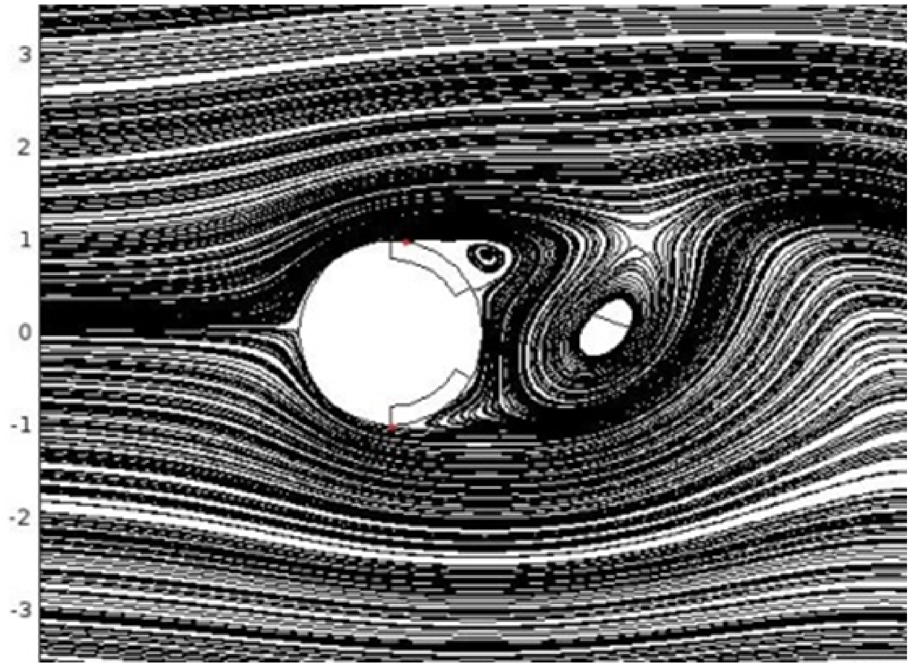

(a)

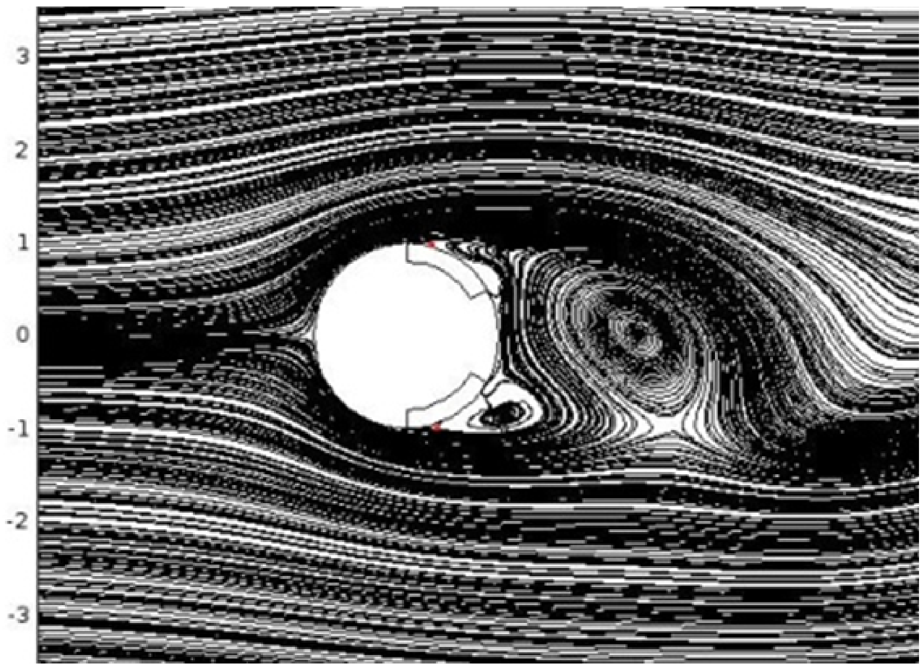

(b)

Figure 3.6. Streamlines for Newtonian case Re=1000 for (a) N=0 and (b) N=100

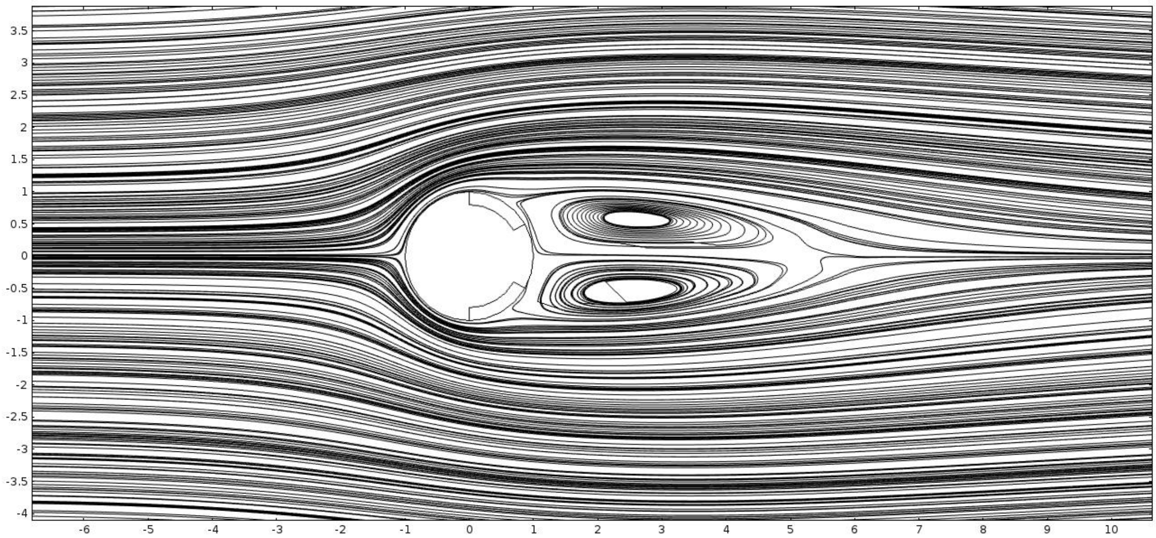

Figure 3.7. Streamlines for Newtonian case Re=50 for N=10

Figures from Figure 3.11 to Figure 3.19 include streamline plots, velocity distribution plots and time evolution of drag coefficients graphs for a Newtonian fluid at Re=200, Re=1000 and Re=1500 with N=0, N=10 and N=100. These results are mentioned to underline the tabulated calculations visually. First, the frequency changes can be seen when Figure 3.14 and Figure 3.16 and Figure 3.17 and Figure 3.19 are compared. It can be inferred that time evolution of drag coefficients graphs have relatively different frequency patterns. For higher Reynolds numbers, the frequency seems to decrease with interaction parameter as stated at Table 3.1. Secondly, the streamline plots show that the length of the vortex formation and vortex structure change with interaction parameter and Reynolds number. Vortex formation length increases with magnetic field application as seen.

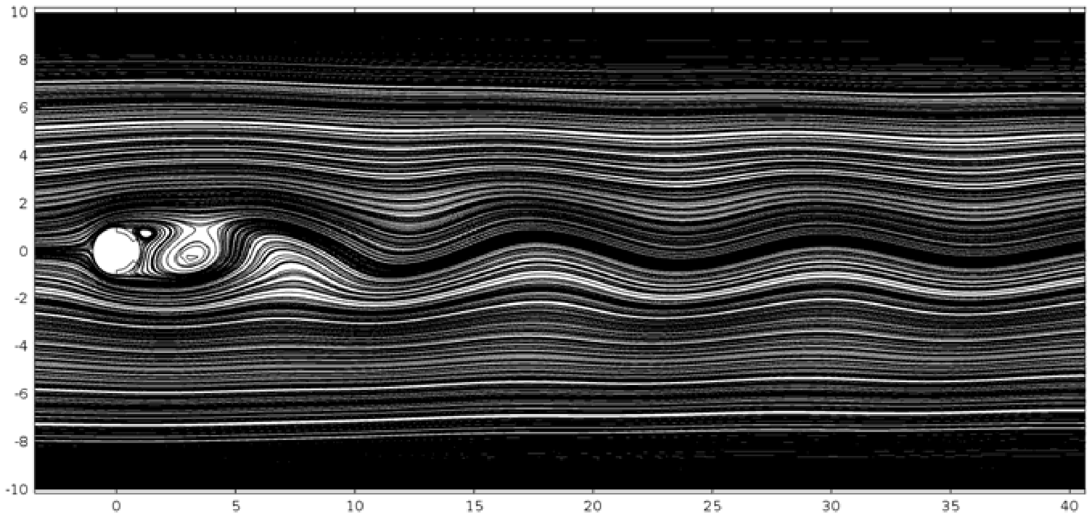

Figure 3.8. Streamlines for Newtonian case Re=100 for N=0

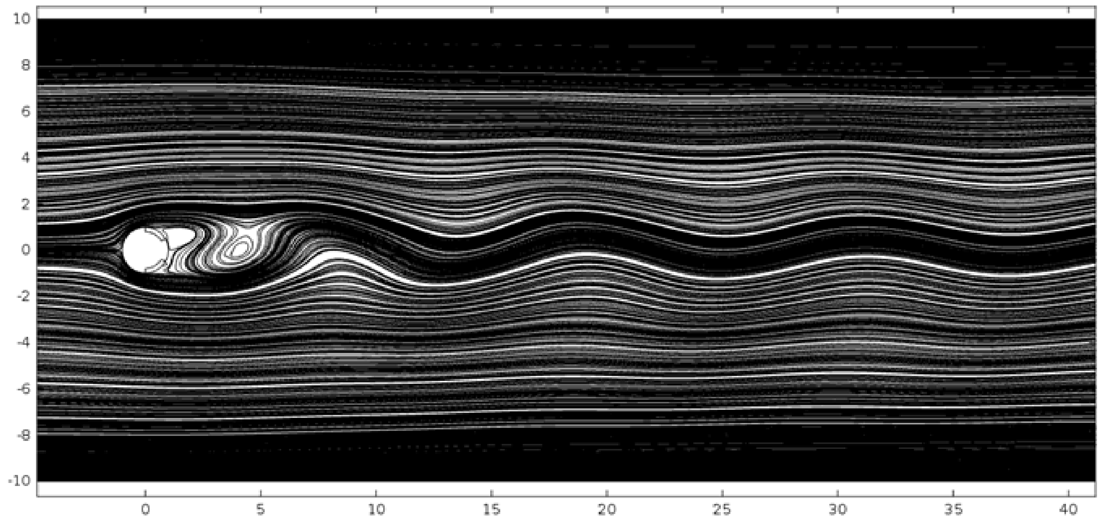

Figure 3.9. Streamlines for Newtonian case Re=100 for N=100

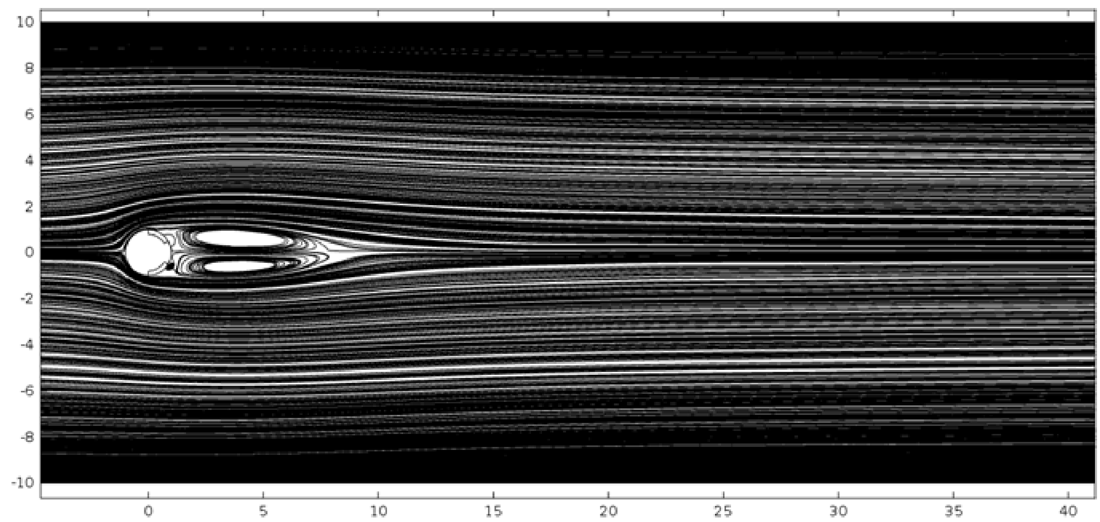

Figure 3.10. Streamlines for Newtonian case Re=100 for N=250

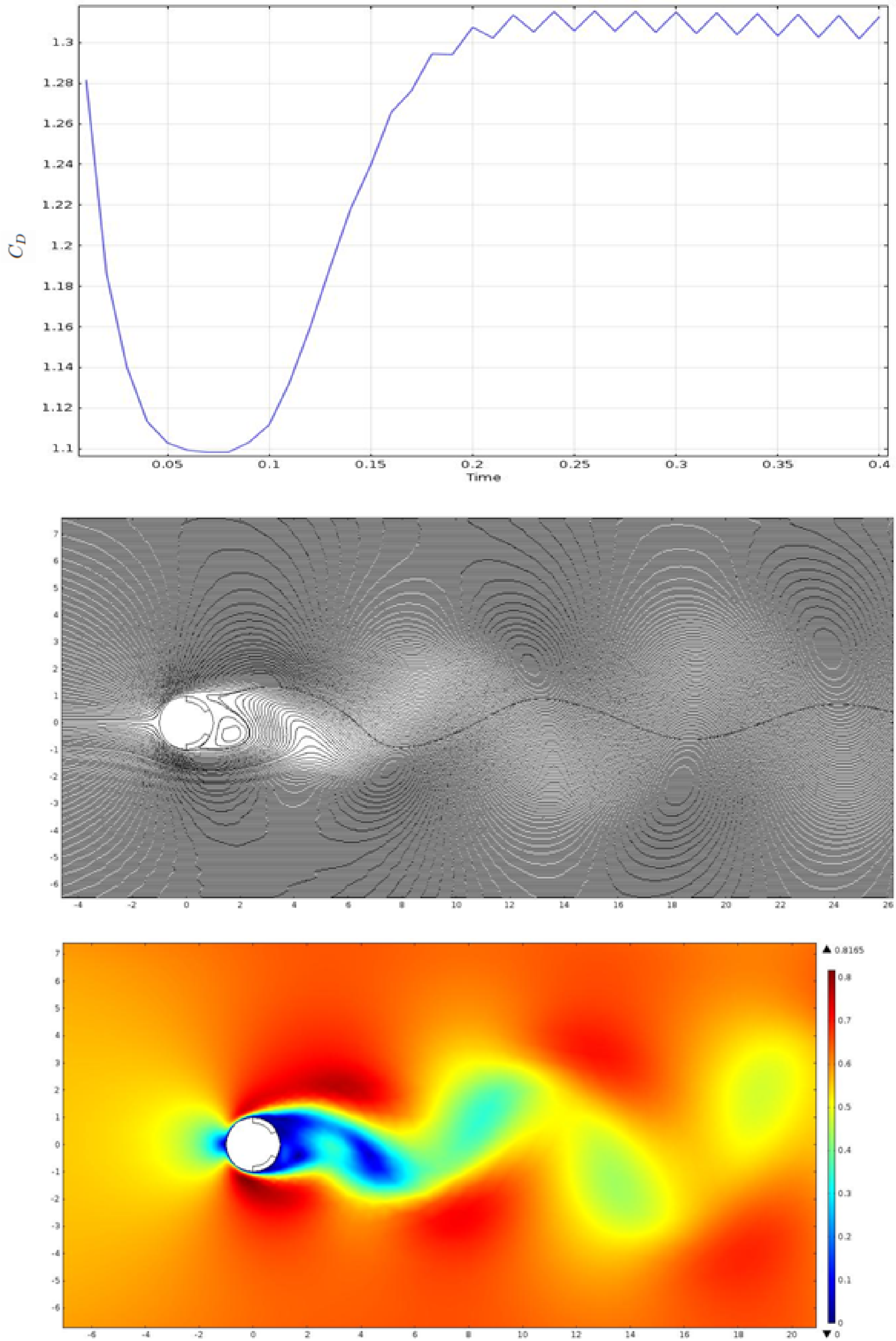

Figure 3.11. Drag Coefficient Graph, Streamline and Velocity Plots for Re=200, N=0

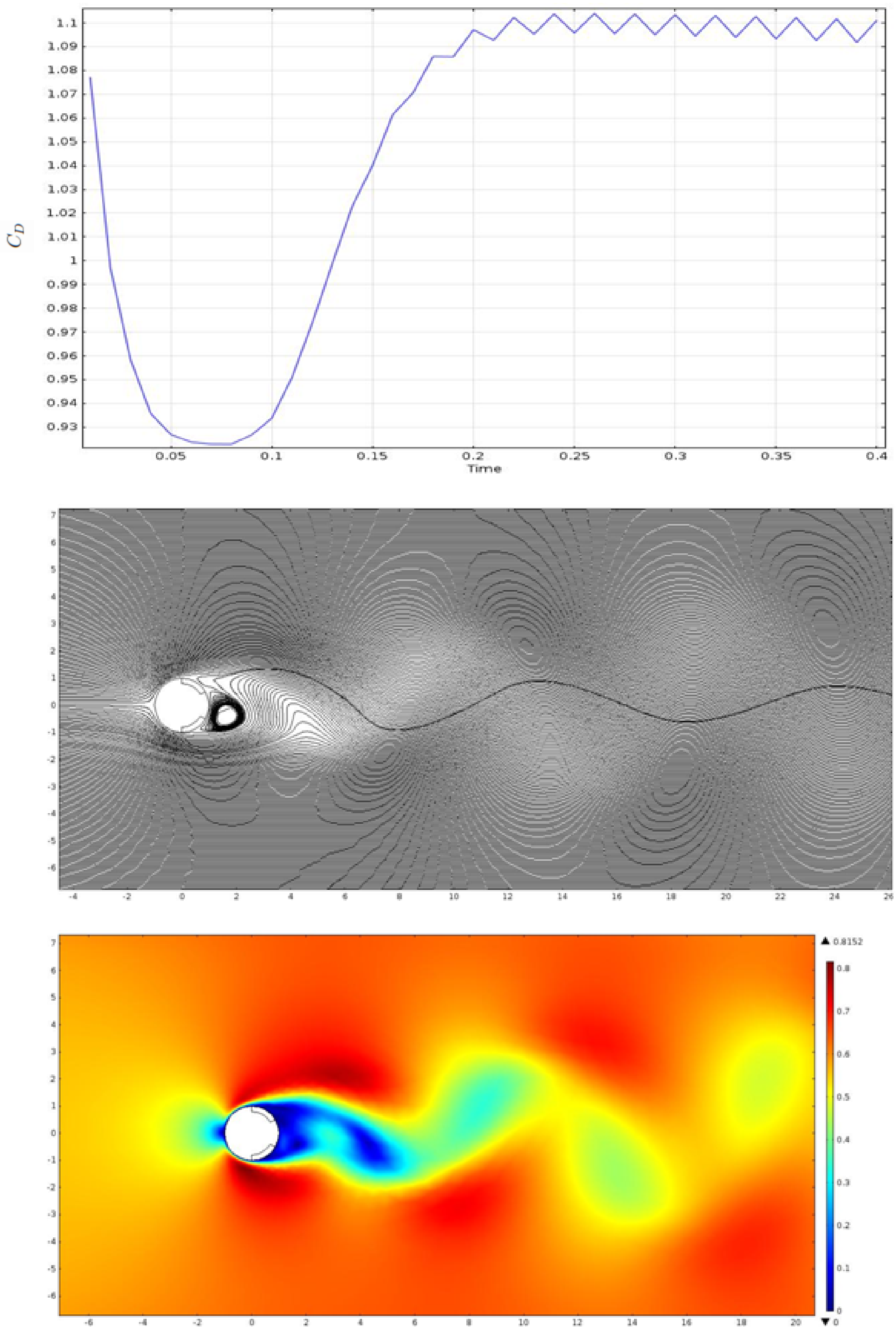

Figure 3.12. Drag Coefficient Graph, Streamline and Velocity Plots for Re=200, N=10

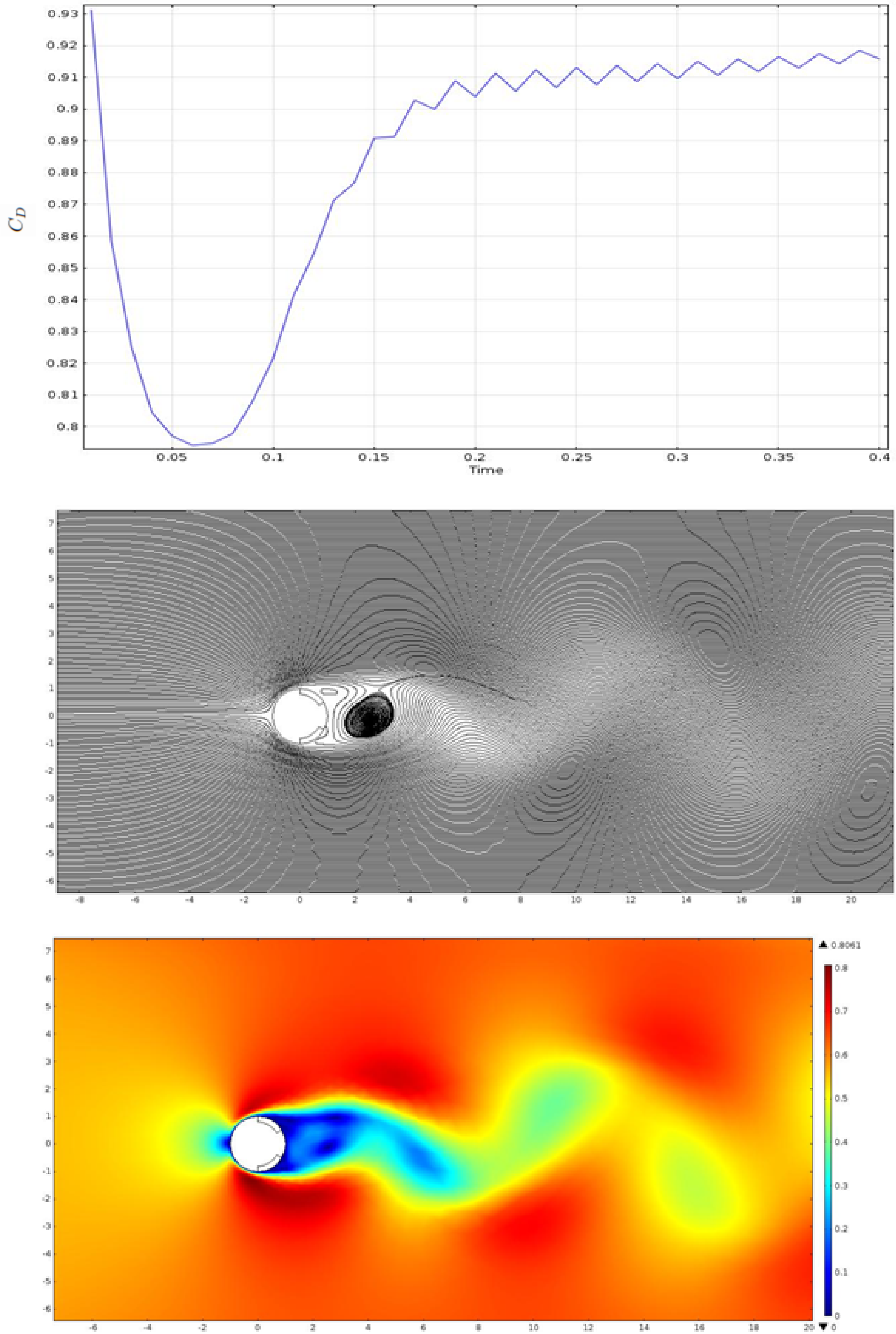

Figure 3.13. Drag Coefficient Graph, Streamline and Velocity Plots for Re=200, N=100

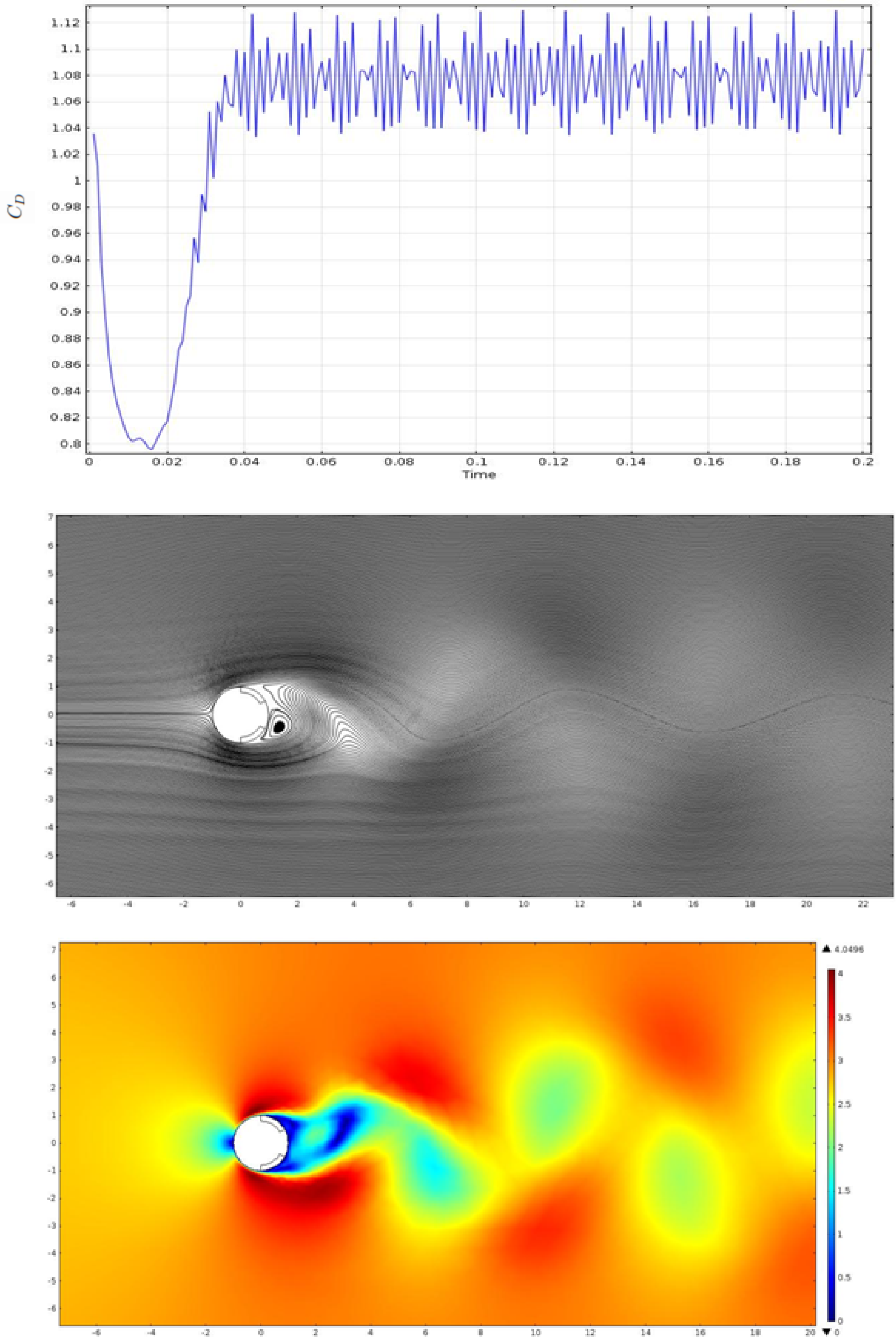

Figure 3.14. Drag Coefficient Graph, Streamline and Velocity Plots for Re=1000, N=0

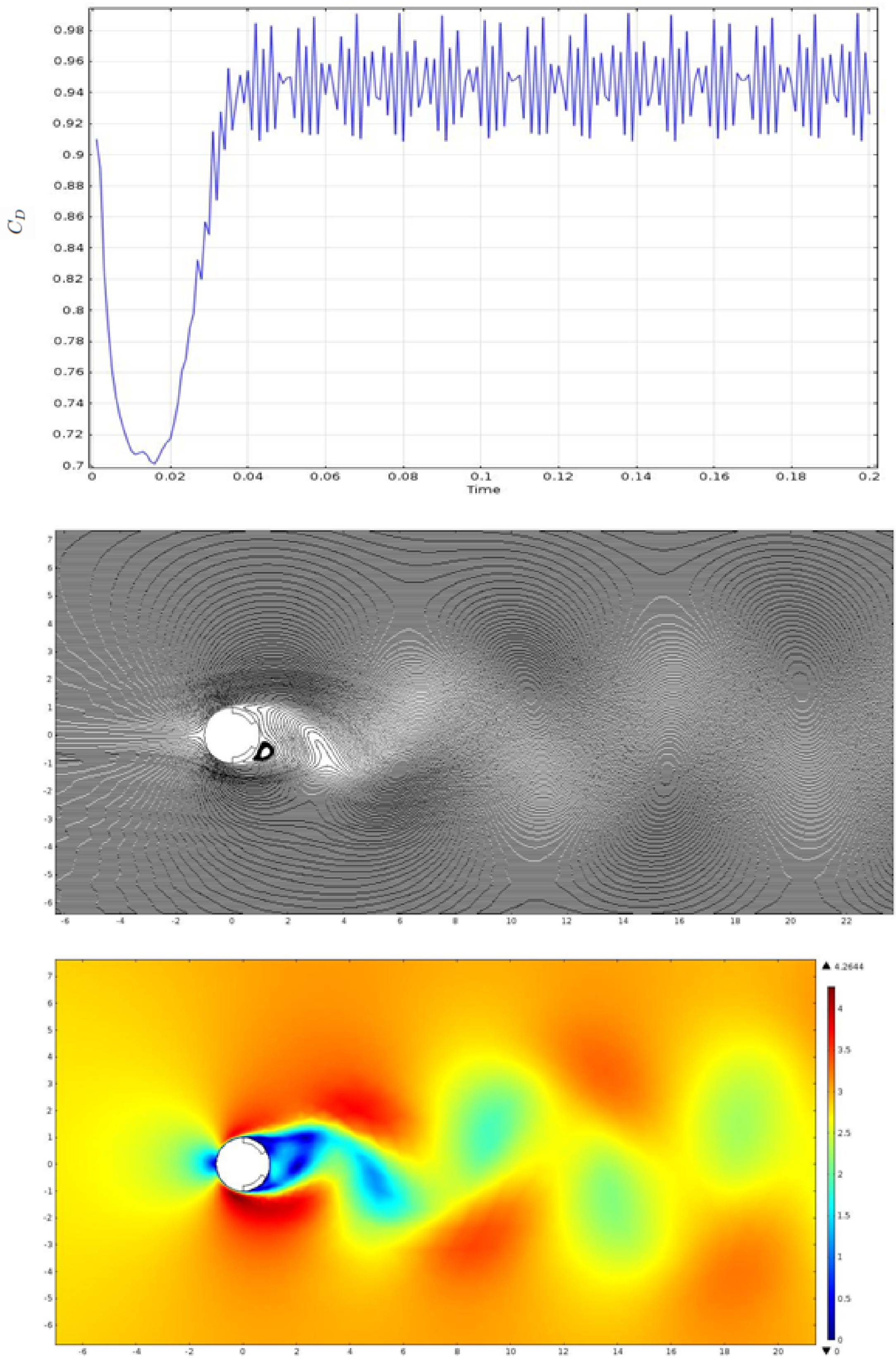

Figure 3.15. Drag Coefficient Graph, Streamline and Velocity Plots for Re=1000, N=10

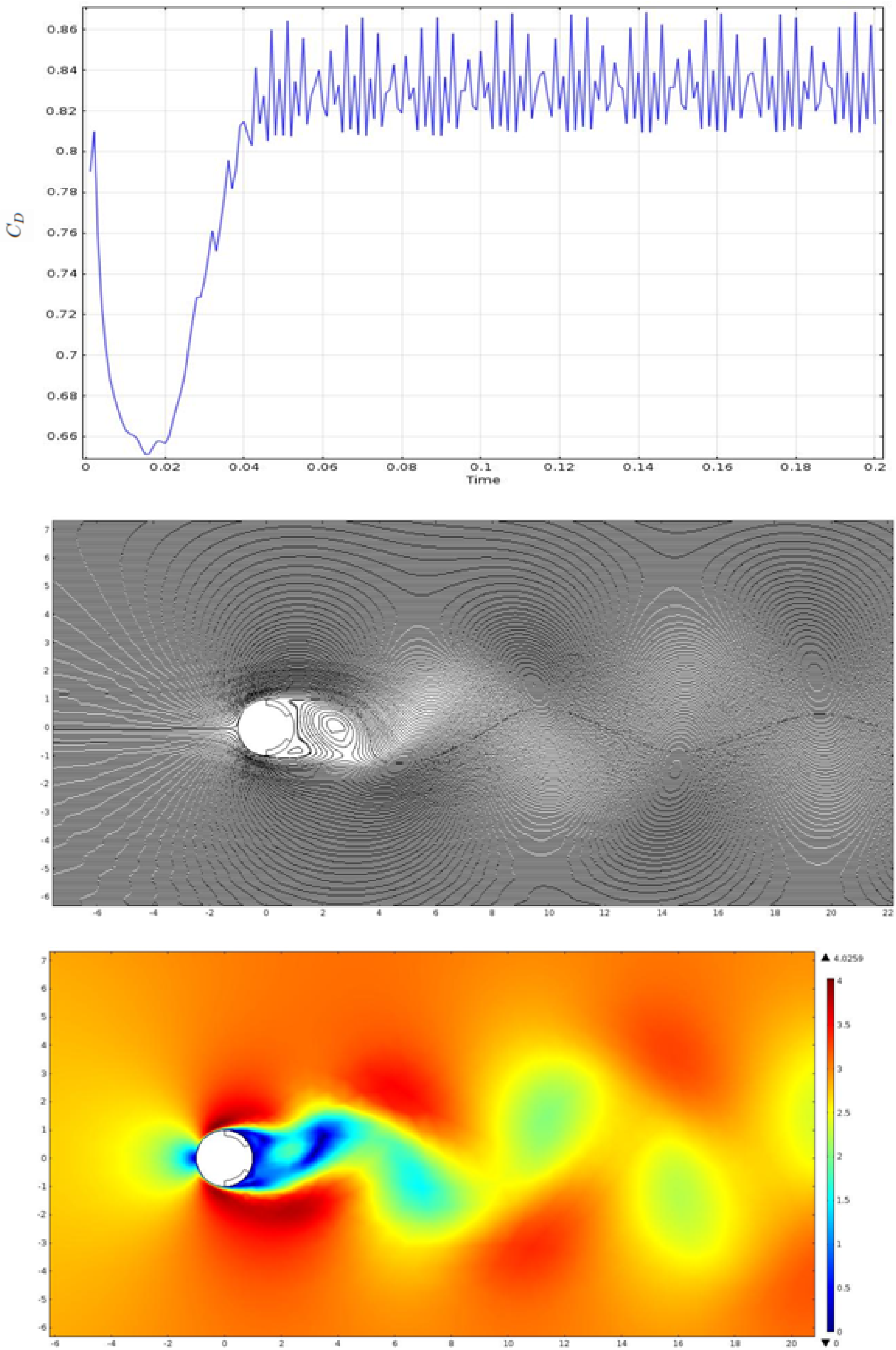

Figure 3.16. Drag Coefficient Graph, Streamline and Velocity Plots for Re=1000, N=100

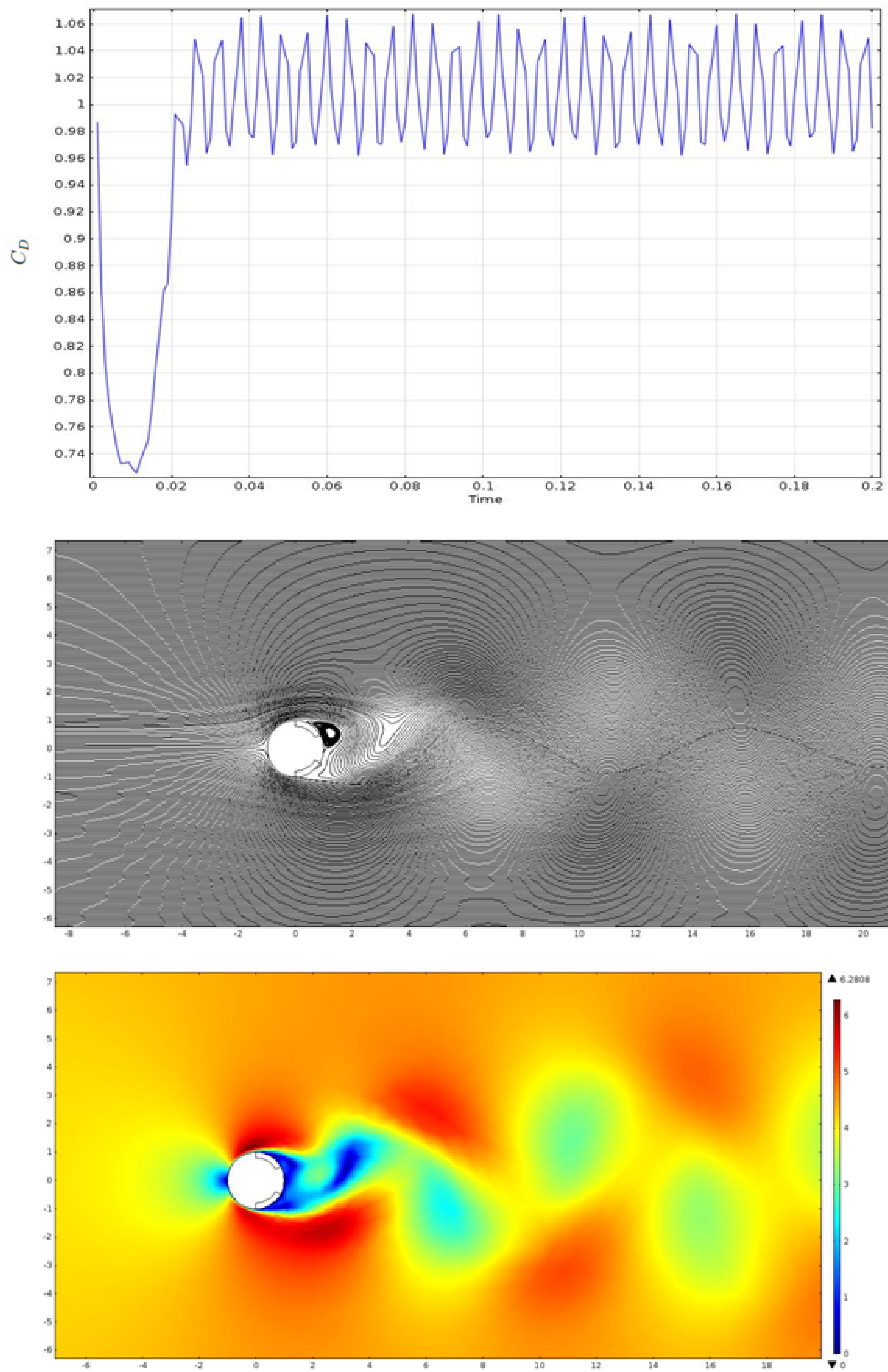

Figure 3.17. Drag Coefficient Graph, Streamline and Velocity Plots for Re=1500, N=0

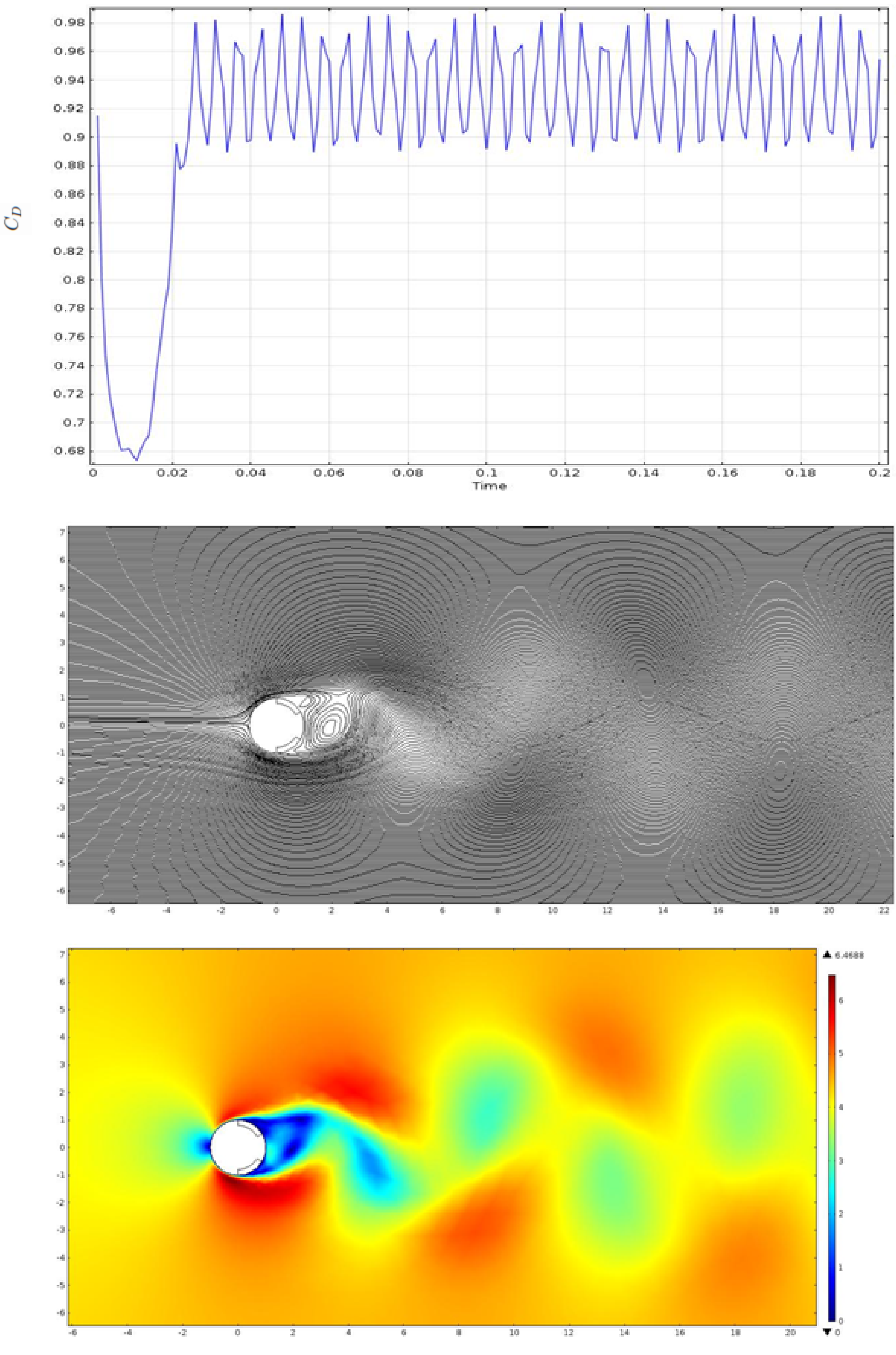

Figure 3.18. Drag Coefficient Graph, Streamline and Velocity Plots for Re=1500, N=10

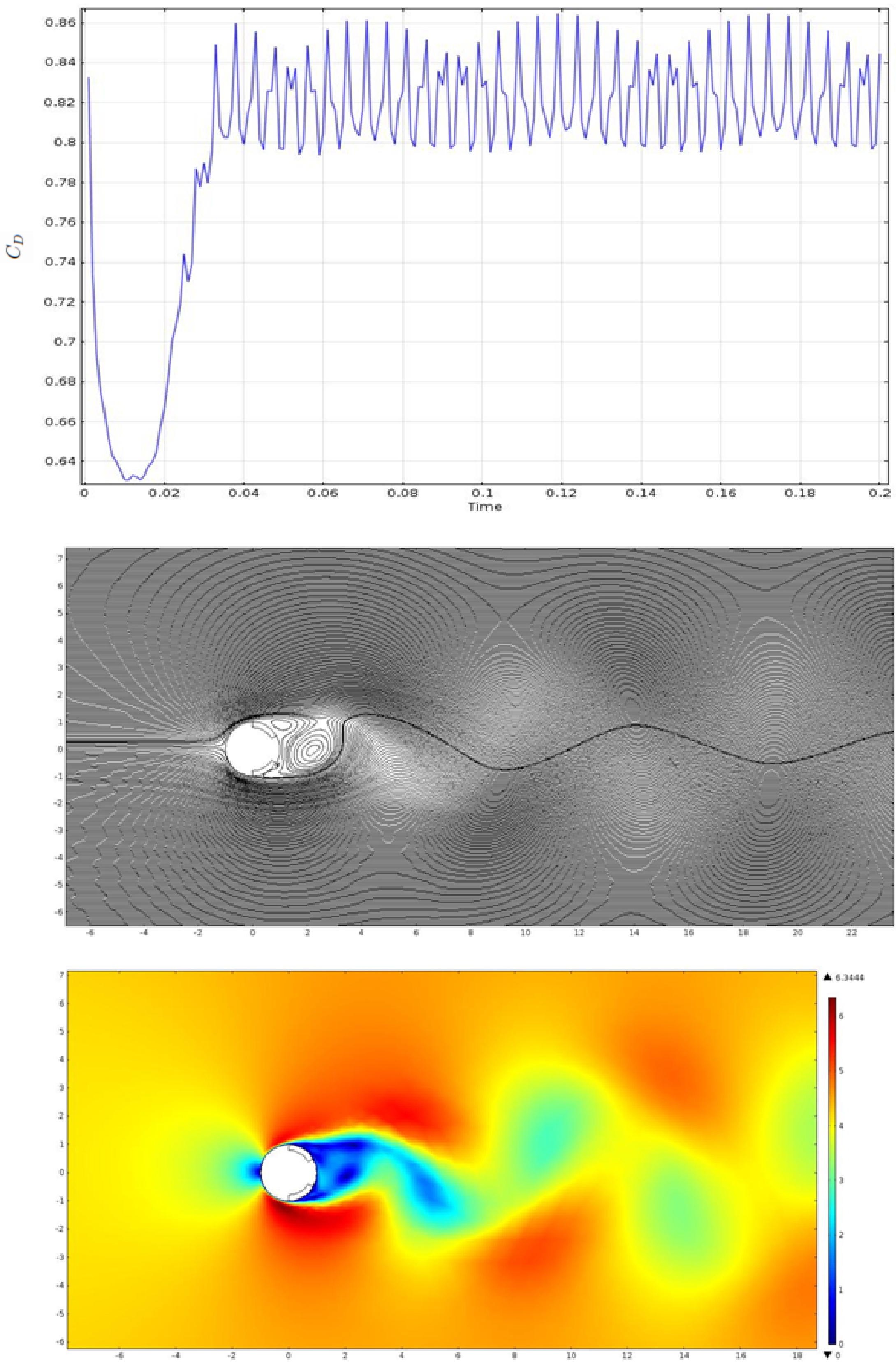

Figure 3.19. Drag Coefficient Graph, Streamline and Velocity Plots for Re=1500, N=100

3.2. Shear Thinning Cases

The ferrofluids can be expressed as non-Newtonian as stated in some of the studies reviewed in literature. There are two non-Newtonian models mentioned in this study, which are shear thinning and shear thickening models.

In order to express the shear thinning behavior of fluid explicitly, power law index (n) is chosen as n=0.2. In Table 3.3, it is shown that drag coefficients for Reynolds numbers Re=50, Re=100, Re=200, Re=500, Re=1000 and Re=1500 with interaction parameter N=0, N=10 and N=100. As seen in Table 3.3 and Figure 3.20, the drag coefficient decreases when interaction parameter increases for each Reynolds number. The amount of decrease is between 15% and 20%, which is not far from the decrease rate of Newtonian fluid simulations. That implies magnetic forces have a decreasing effect on shear thinning fluids for any Reynolds number.

In Table 3.4, Strouhal numbers are tabulated for Re=200, Re=500, Re=1000 and Re=1500 with N=0, N=10 and N=100. There is no data for Re=50 and Re=100, because vortex shedding has not started for these Reynolds numbers yet. As stated in Table 3.2, there are vortex shedding frequency values for Re=100 for Newtonian fluids.

Table 3.3. Mean drag coefficients (C_D) with different Reynolds number(Re) values for different interaction parameter(N) of shear thinning fluid (n=0.2)

	N=0	**N=10**	**N=100**
Re=50	1.2458	1.1991	1.0614
Re=100	1.1476	1.1095	0.9654
Re=200	1.1338	1.1071	0.9308
Re=500	1.0593	1.03914	0.869
Re=1000	1.0923	1.0549	0.8648
Re=1500	1.0938	1.0697	0.8687

This result shows that vortex shedding starts later for shear thinning fluids as expected from our literature pre-knowledge. In both Table 3.4 and Figure 3.21, it is shown that interaction parameter has a decreasing effect on shear thinning fluids. For low Reynolds numbers (Re=200 and Re=500), the decrease rate is smaller compared to the cases with higher Reynolds numbers (Re=1000 and Re=1500).

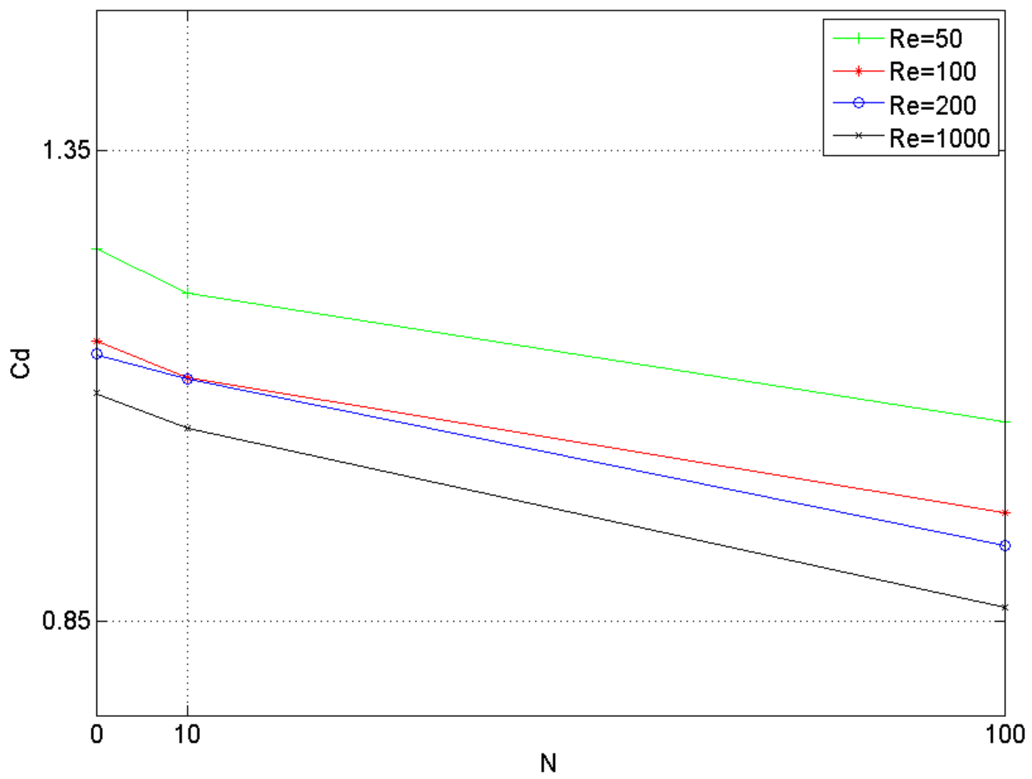

Figure 3.20. Mean drag coefficients (C_D) with different Reynolds number (Re) values for different interaction parameter(N) of shear thinning fluid (n=0.2)

In between Figure 3.22 and Figure 3.30, streamline plots, velocity distribution plots and time evolution of drag coefficients graphs for flow of a shear thinning fluid at Re=200, Re=1000 and Re=1500 with N=0, N=10 and N=100 are stated. Similar to implications of Newtonain simulations, the vortex formation lengths increase with interaction parameters, which is shown in streamline and velocity distribuion plots.

Also, the structure of vortex shedding frequency is changed with interaction parameter variation as seen at time evolution of drag coefficients plots.

Table 3.4. Strouhal number(St) with different Reynolds number(Re) values for different interaction parameter(N) of shear thinning fluid(n=0.2)

	N=0	**N=10**	**N=100**
Re=200	0.22540	0.20814	0.20472
Re=500	0.22800	0.22400	0.22020
Re=1000	0.23803	0.22935	0.21769
Re=1500	0.23077	0.22637	0.21858

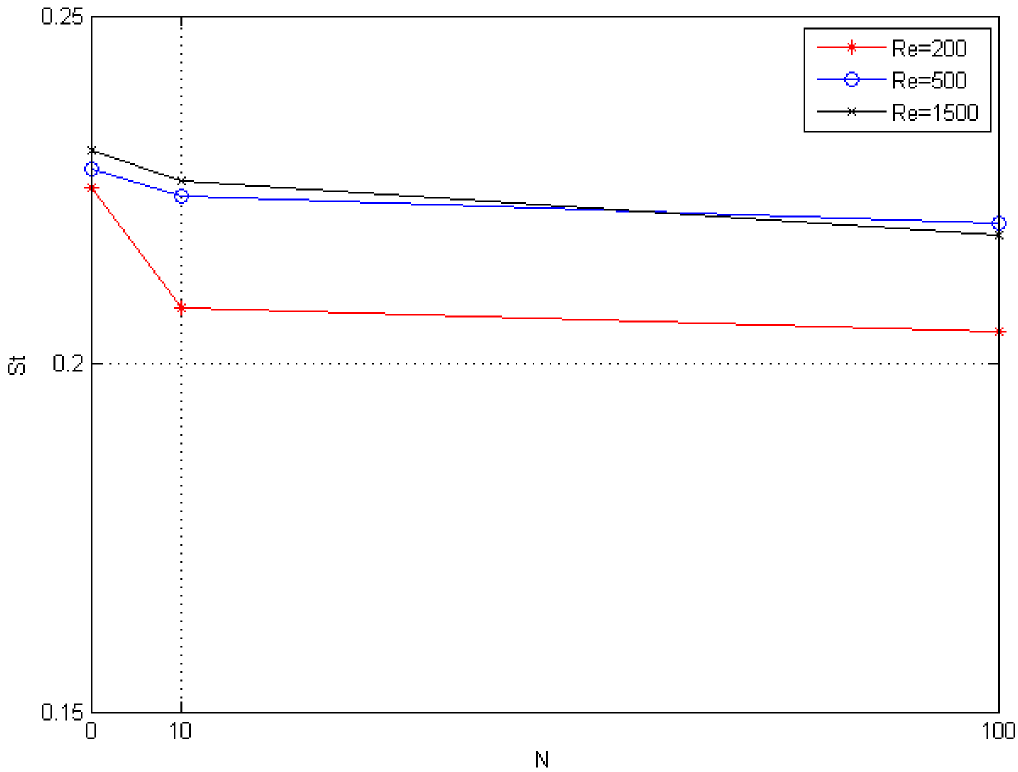

Figure 3.21. Strouhal Number (St) with different Reynolds number(Re) values for different interaction parameter(N) of shear thinning fluid(n=0.2)

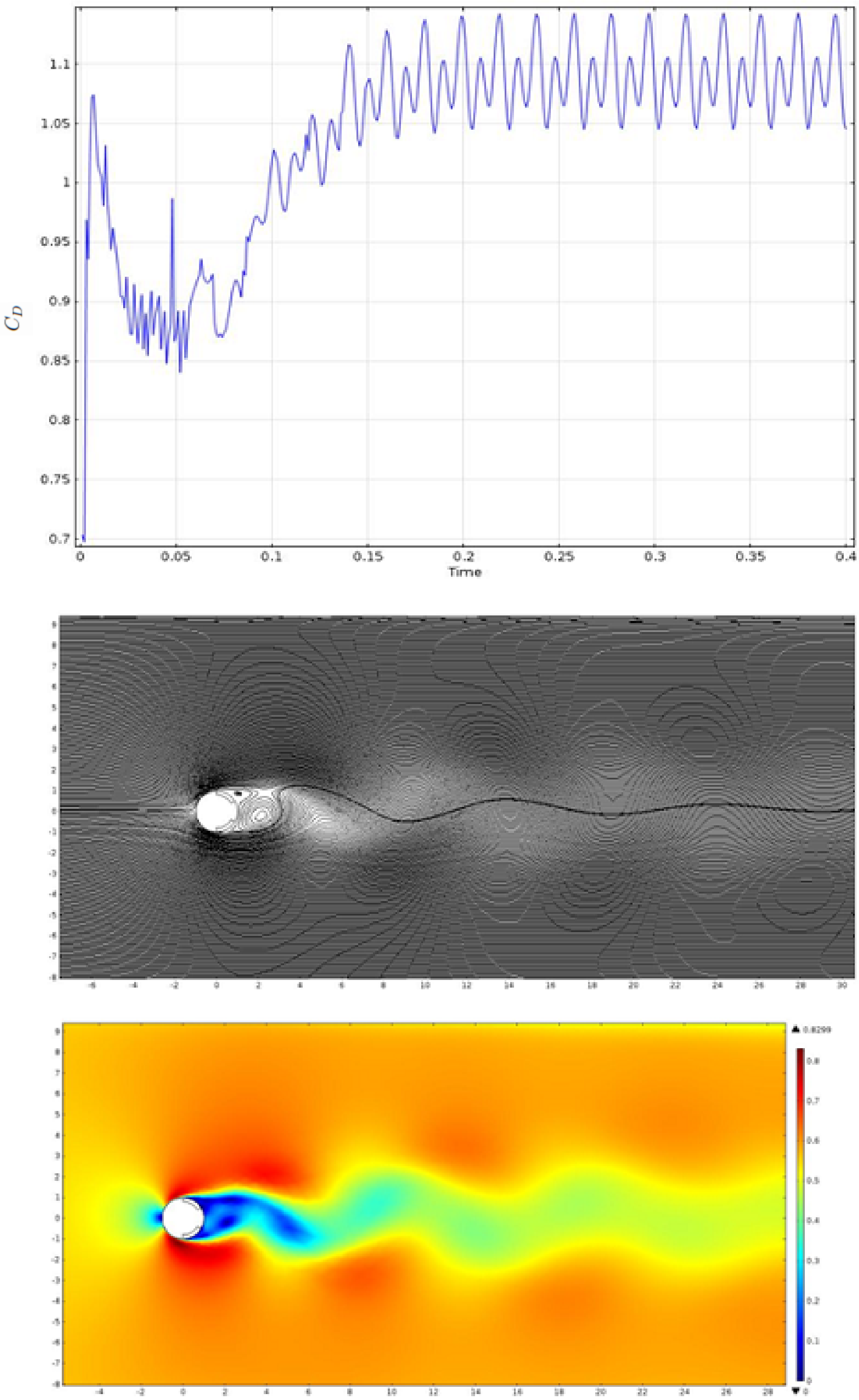

Figure 3.22. Drag Coefficient Graph, Streamline and Velocity Plots for Re=200, N=0 of shear thinning fluid(n=0.2)

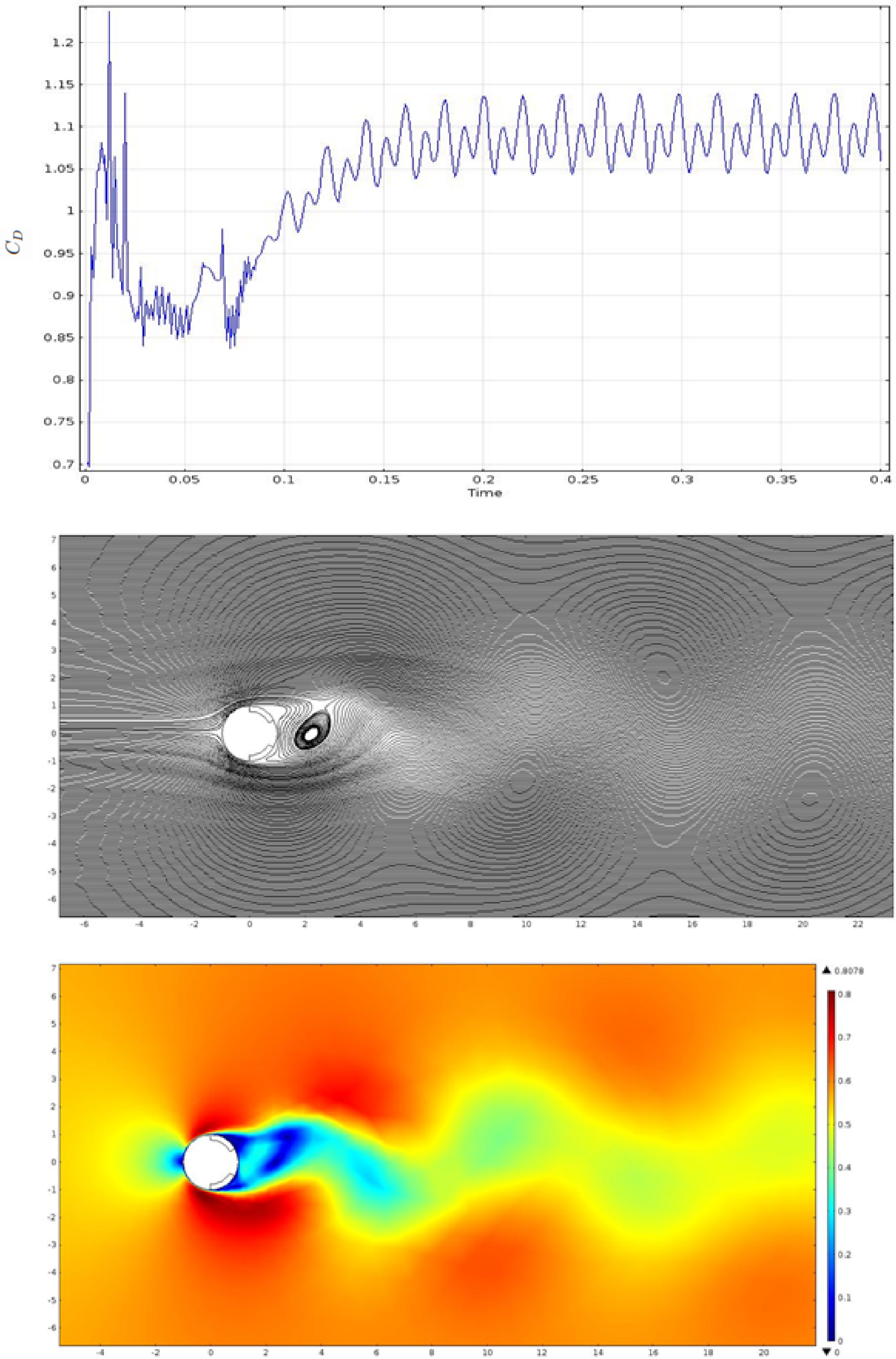

Figure 3.23. Drag Coefficient Graph, Streamline and Velocity Plots for Re=200, N=10 of shear thinning fluid(n=0.2)

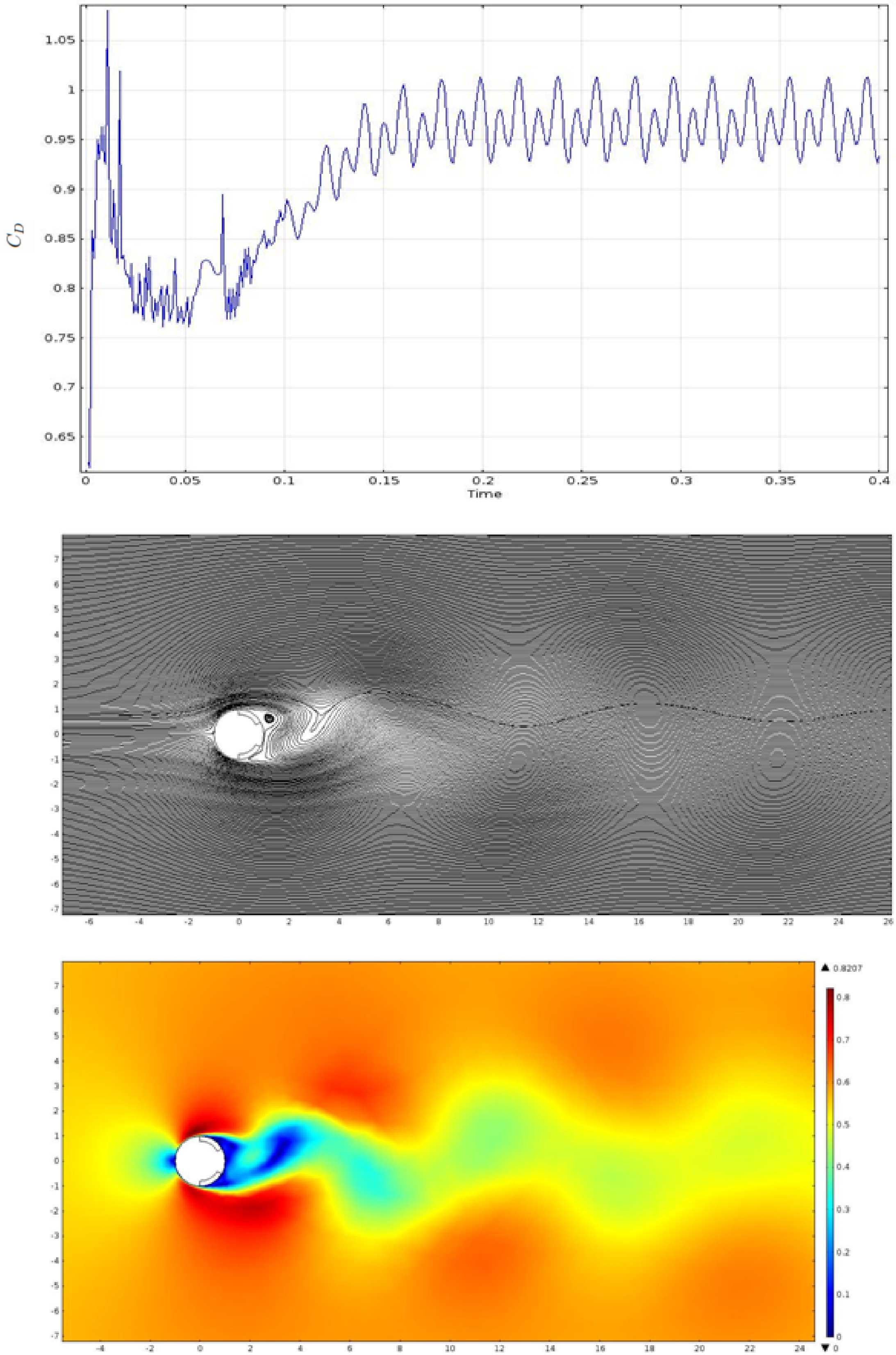

Figure 3.24. Drag Coefficient Graph, Streamline and Velocity Plots for Re=200, N=100 of shear thinning fluid(n=0.2)

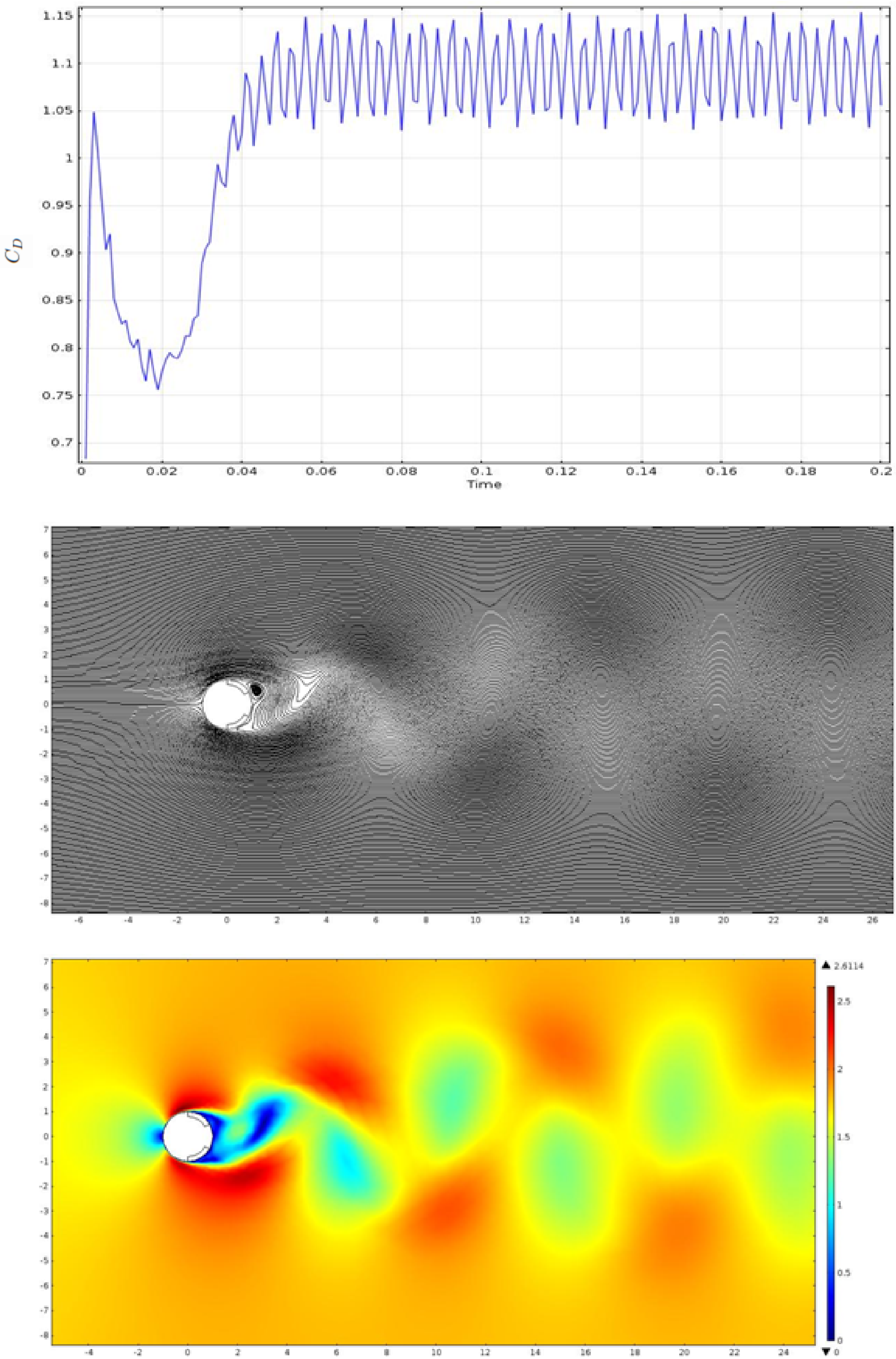

Figure 3.25. Drag Coefficient Graph, Streamline and Velocity Plots for Re=1000, N=0 of shear thinning fluid(n=0.2)

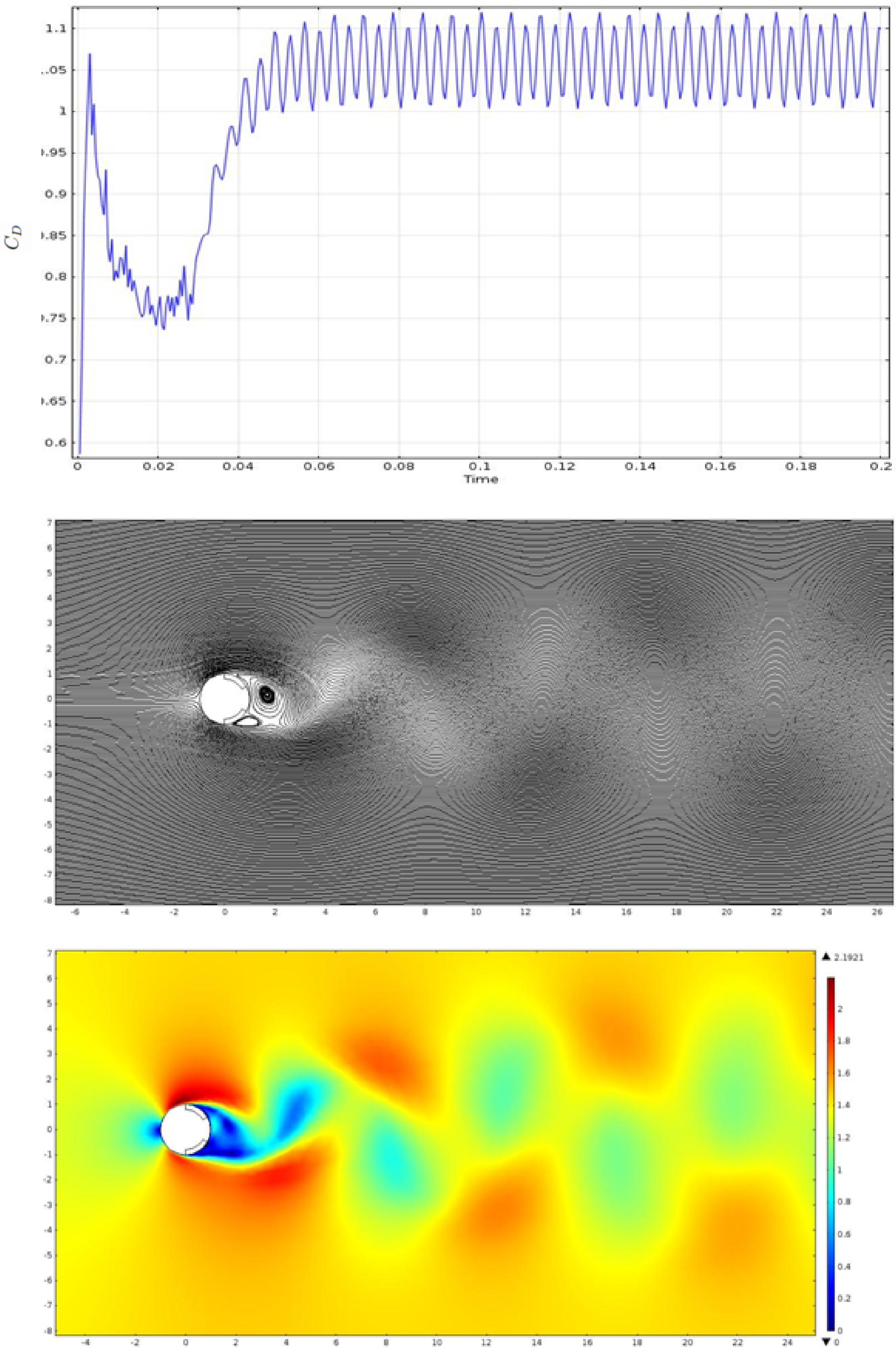

Figure 3.26. Drag Coefficient Graph, Streamline and Velocity Plots for Re=1000, N=10 of shear thinning fluid(n=0.2)

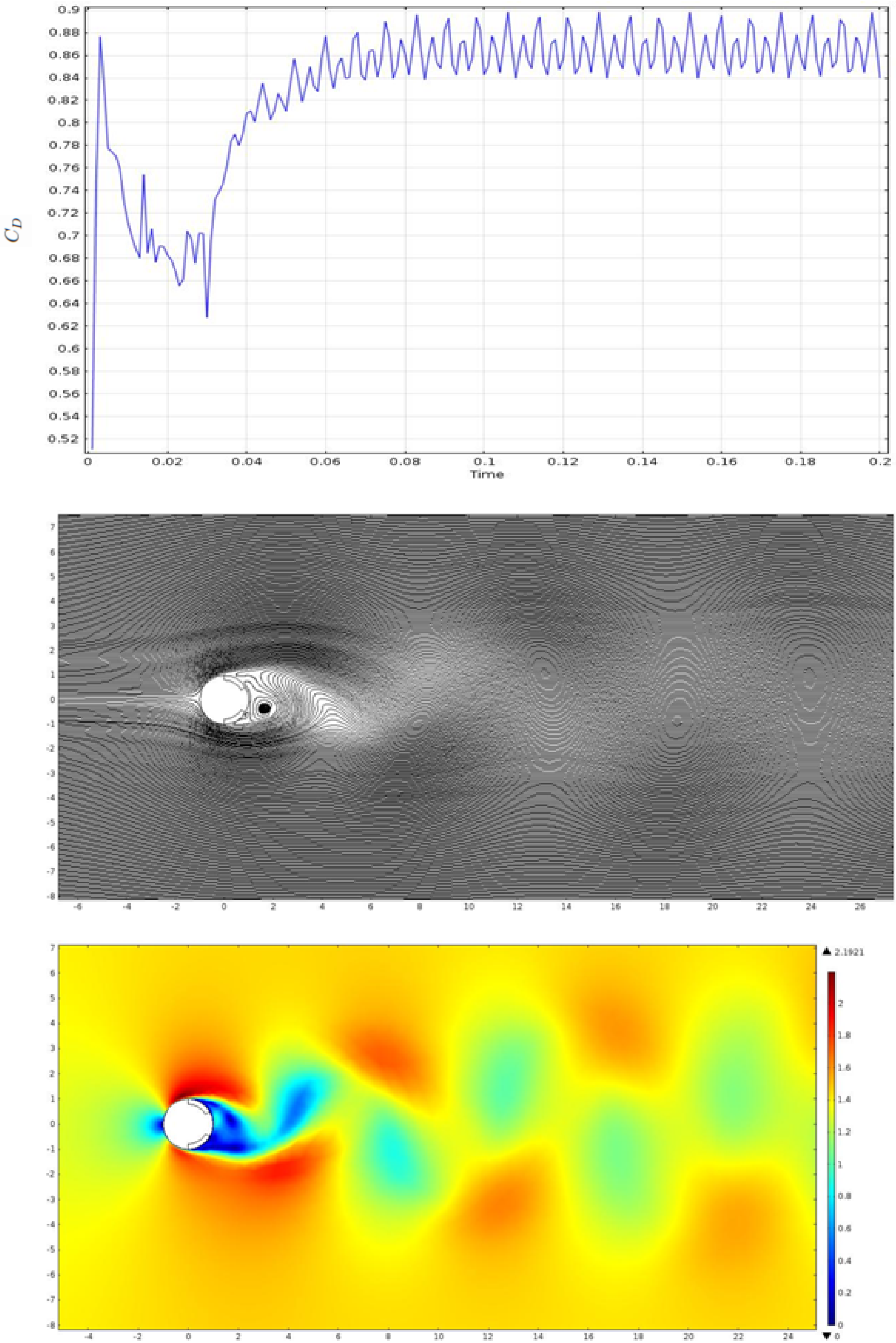

Figure 3.27. Drag Coefficient Graph, Streamline and Velocity Plots for Re=1000, N=100 of shear thinning fluid(n=0.2)

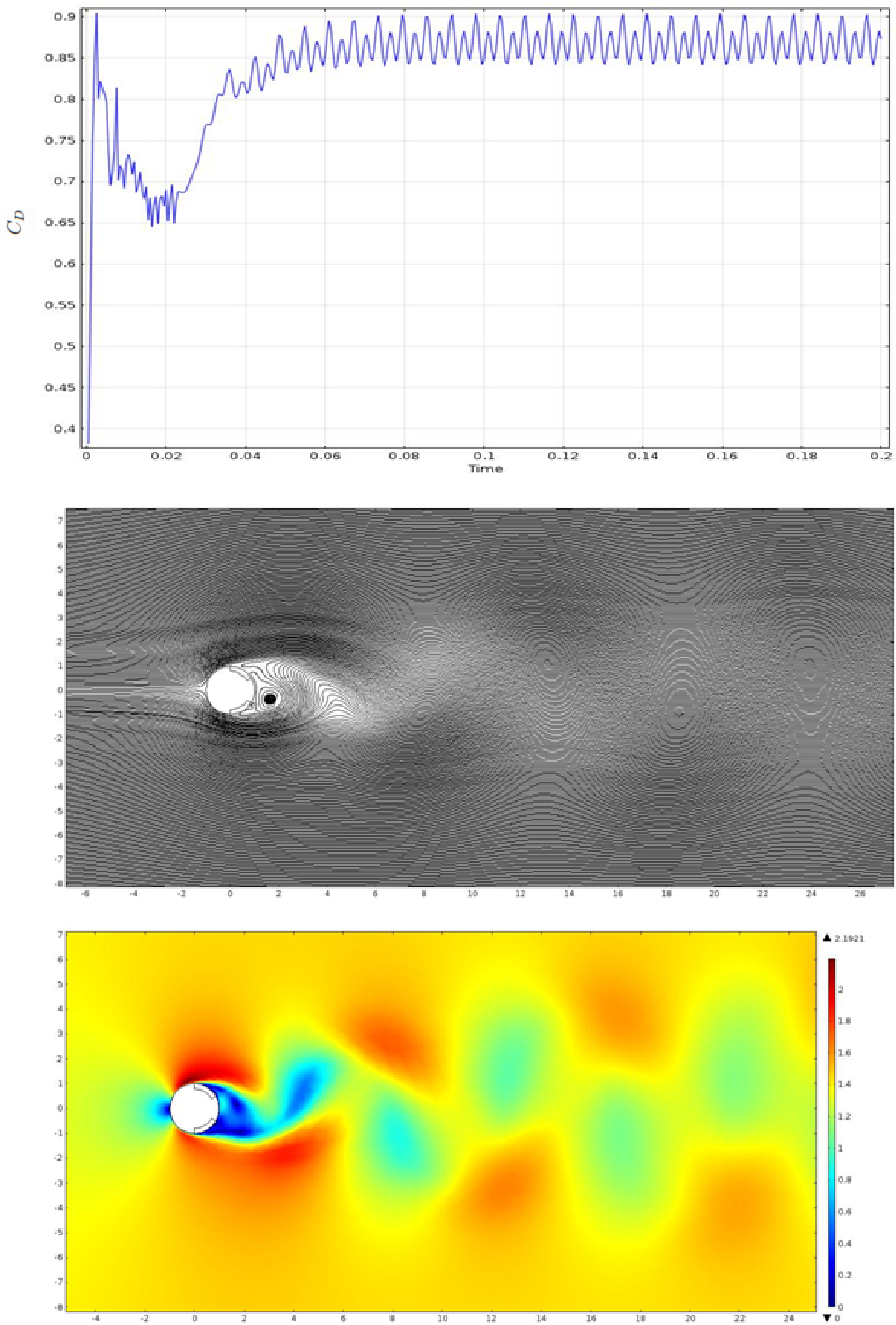

Figure 3.28. Drag Coefficient Graph, Streamline and Velocity Plots for Re=1500, N=0 of shear thinning fluid(n=0.2)

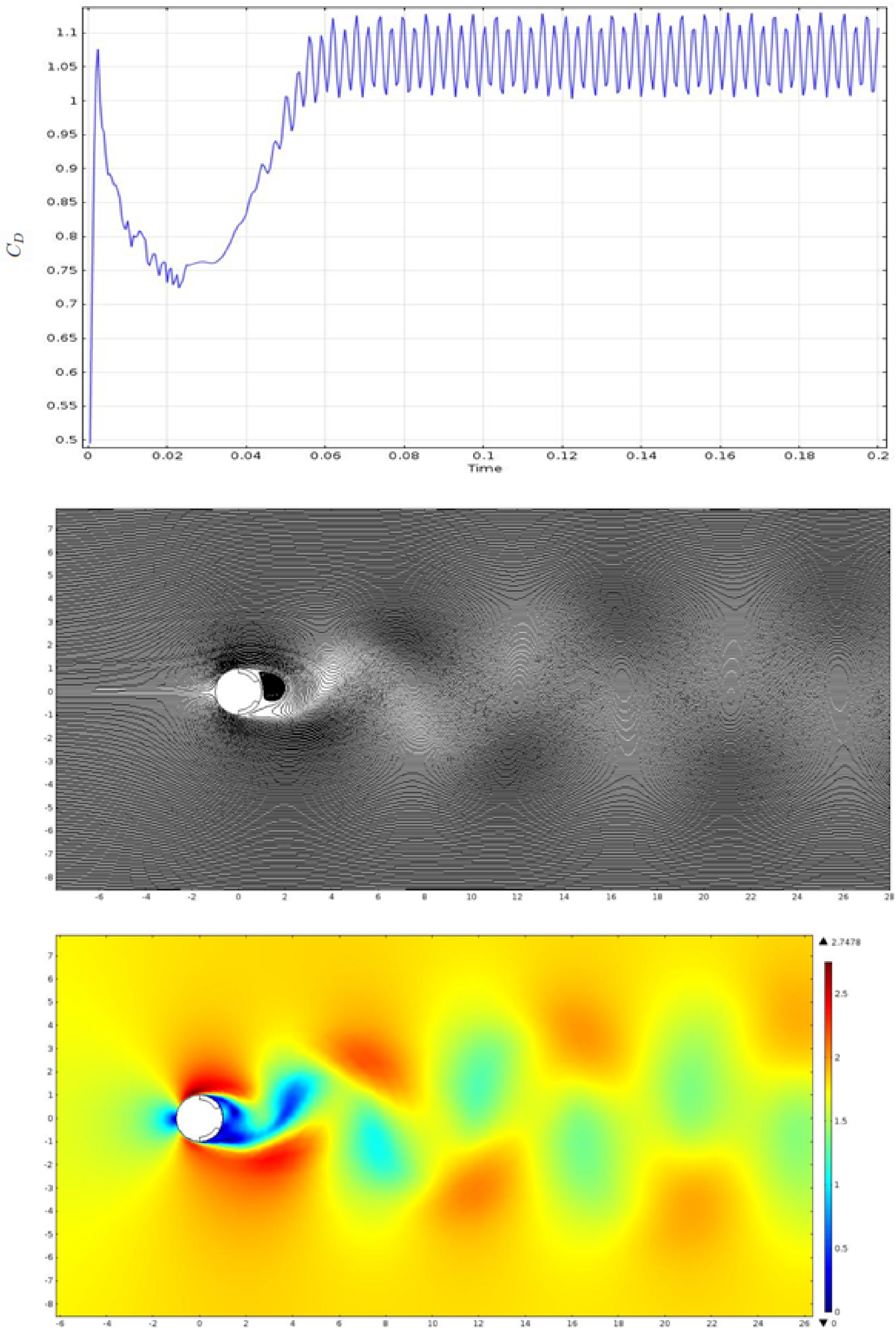

Figure 3.29. Drag Coefficient Graph, Streamline and Velocity Plots for Re=1500, N=10 of shear thinning fluid(n=0.2)

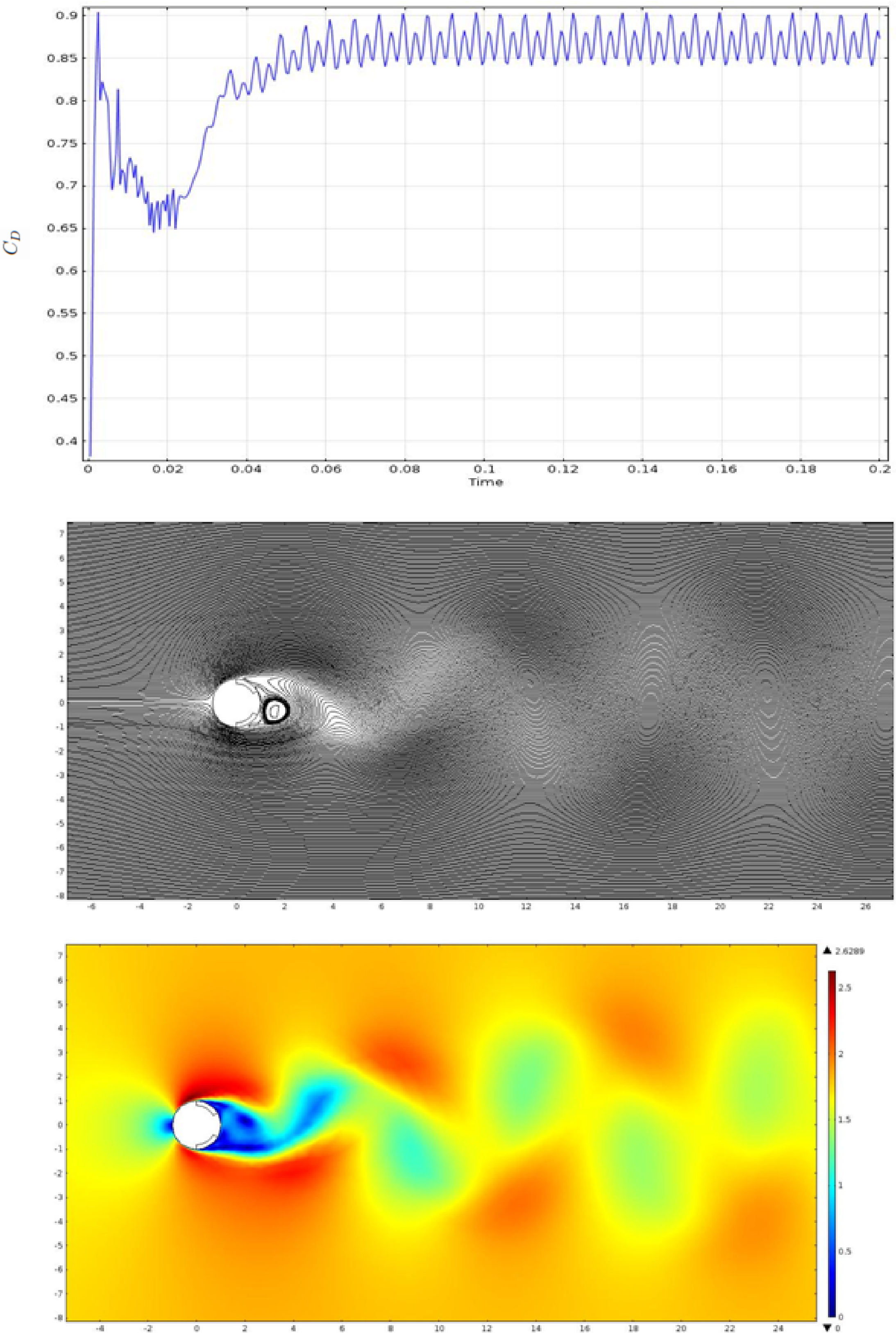

Figure 3.30. Drag Coefficient Graph, Streamline and Velocity Plots for Re=1500, N=100 of shear thinning fluid(n=0.2)

3.3. Shear Thickening Cases

The second non-Newtonian fluid is chosen as shear thickening fluid, since it is also very frequently used fluid type in previous analyses. In order to express the behavior of shear thickening fluid, the power law index has been chosen as n=1.5. In Table 3.5, the computed drag coefficient values of shear thickening fluid flow simulations are tabulated. As seen at Newtonian and shear thinning fluid simulations, the drag coefficient values are decreased with interaction parameter. The stated decrease can be seen at Figure 3.31. The degree of decrease is in range of 5% and 15%, which is close with previously mentioned other fluid types. It is also implied that, the amount of change for lower Reynolds numbers, as Re=50, Re=100 and Re=200, is smaller compared to higher Reynolds numbers as Re=1000 and Re=1500.

Table 3.5. Mean drag coefficients (C_D) with different Reynolds number(Re) values for different interaction parameter(N) of shear thickening fluid(n=1.5)

	N=0	**N=10**	**N=100**
Re=50	1.6275	1.6086	1.5494
Re=100	1.5750	1.5608	1.4988
Re=200	1.4922	1.4030	1.3193
Re=500	1.1615	1.1509	0.9899
Re=1000	1.1153	1.1011	0.959
Re=1500	1.0945	1.0674	0.9324

Calculated Strouhal numbers for shear thickening fluid simulations are given at Table 3.6. The calculation can be made for Re=100, Re=200, Re=500, Re=1000 and Re=1500 at N=0, N=10 and N=100. Accordingly, it is inferred that, the vortex shedding starts earlier then shear thinning model simulations. The Strouhal number values have a decreasing trend similar to Newtonian and shear thickening results. Also, similarly, there is a more clear decreasing trend for higher Reynolds numbers as Re=1000 and Re=1500. At Figure 3.32, the mentioned trends are shown.

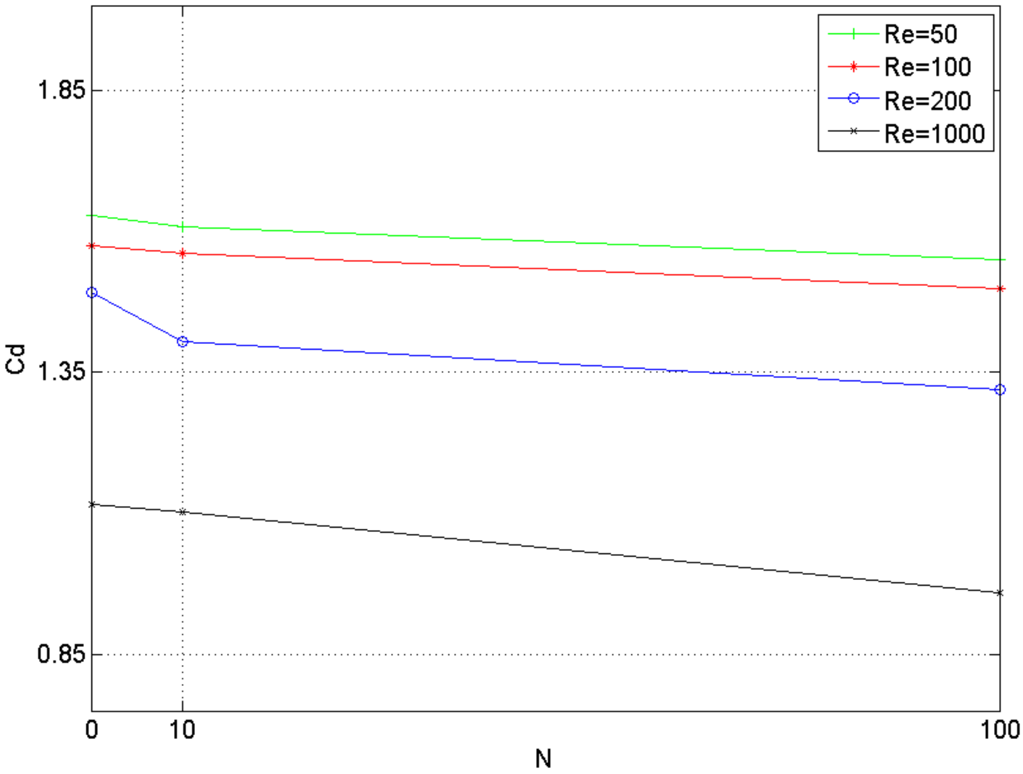

Figure 3.31. Mean drag coefficients (C_D) with different Reynolds number (Re) values for different interaction parameter(N) of shear thickening fluid(n=1.5)

Table 3.6. Strouhal number(St) with different Reynold,s number(Re) values for different interaction parameter(N) of shear thickening fluid (n=1.5)

	N=0	**N=10**	**N=100**
Re=100	0.18121	0.181	0.17754
Re=200	0.18000	0.17851	0.17851
Re=500	0.21667	0.21111	0.19452
Re=1000	0.20282	0.20282	0.19718
Re=1500	0.20825	0.20442	0.19937

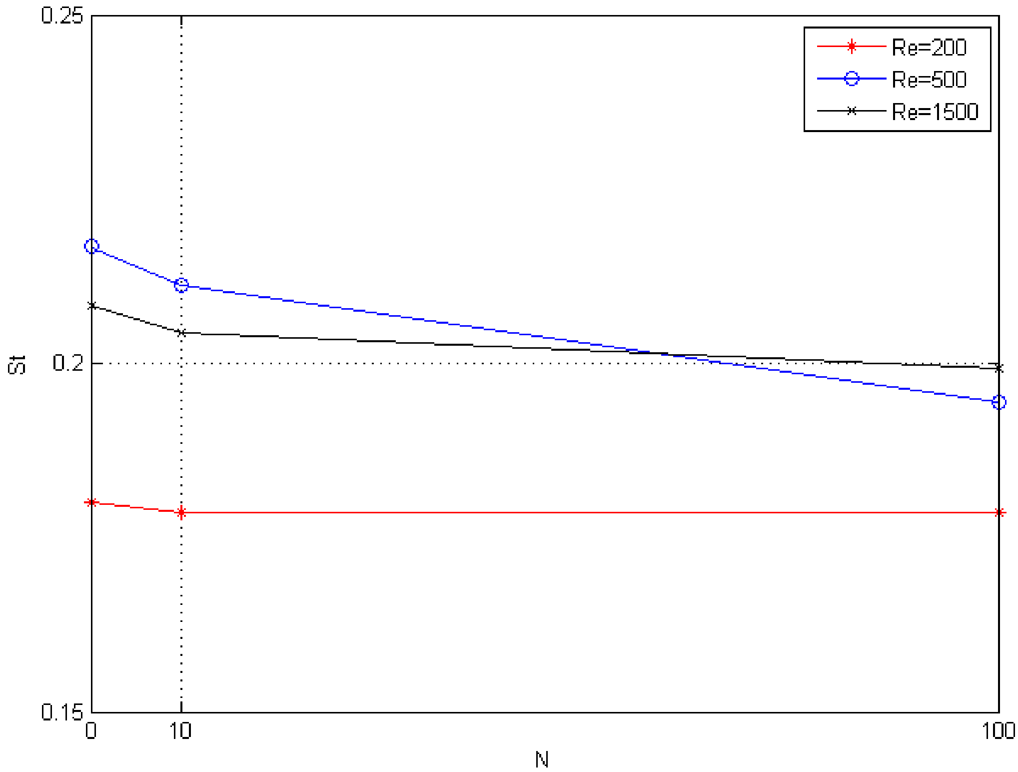

Figure 3.32. Strouhal Number(St) with different Reynolds number(Re) values for different interaction parameter (N) of shear thickening fluid (n=1.5)

From Figure 3.33 to Figure 3.41, time evolution of drag coefficients, streamlines and velocity plots are manifested for Re=200, Re=1000 and Re=1500. The vortex shedding frequency pattern changes with Reynolds number and interaction parameter. Also, streamlines and velocity distribution plots show that vortex formation length becomes higher with magnetostatic force application.

As all of the plots taken into consideration, shear thinning, shear thickening and Newtonian fluid simulations show same trends on vortex formation and vortex shedding frequency with magnetic field application.

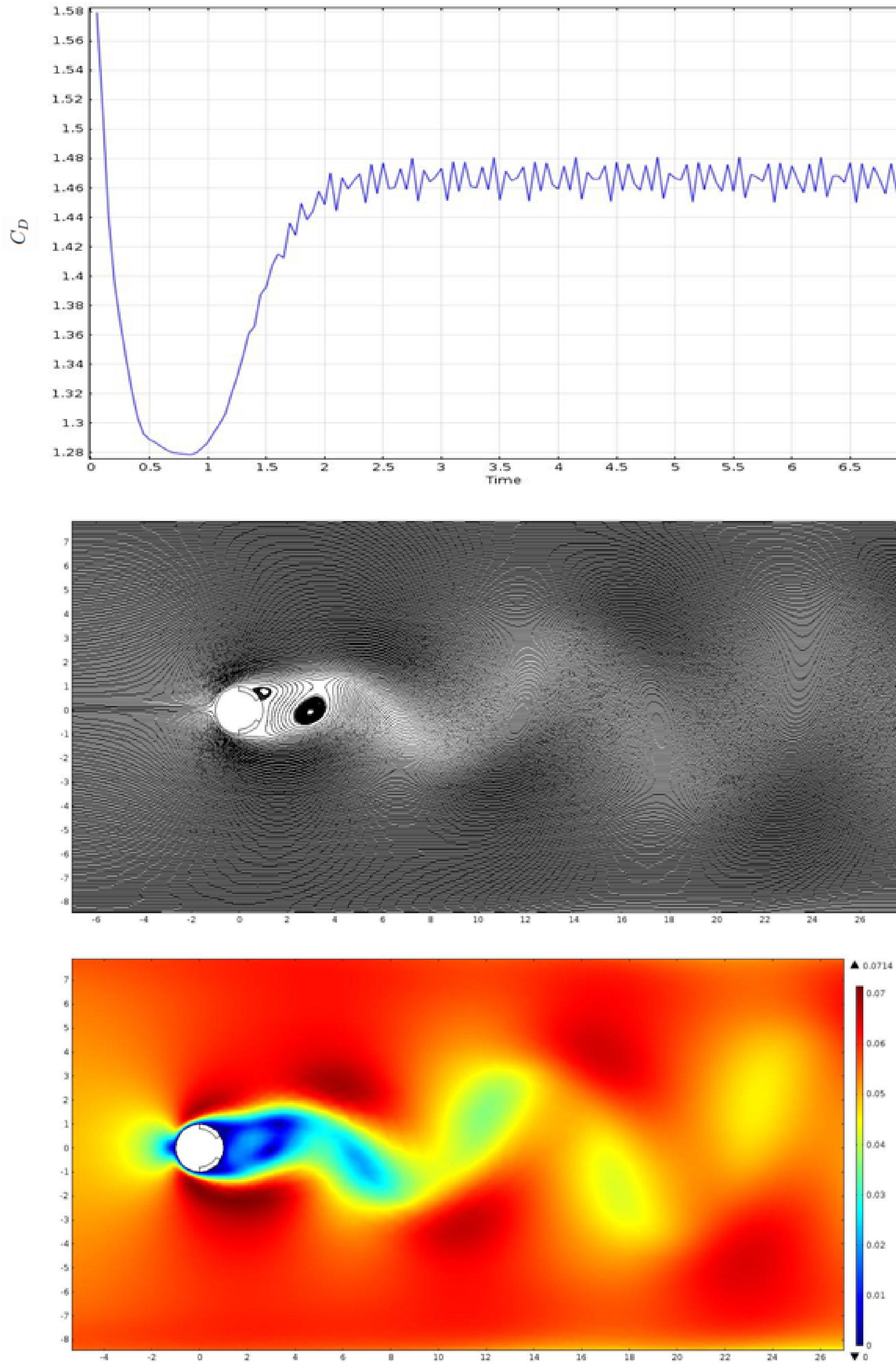

Figure 3.33. Drag Coefficient Graph, Streamline and Velocity Plots for Re=200, N=0 of shear thickening fluid(n=1.5)

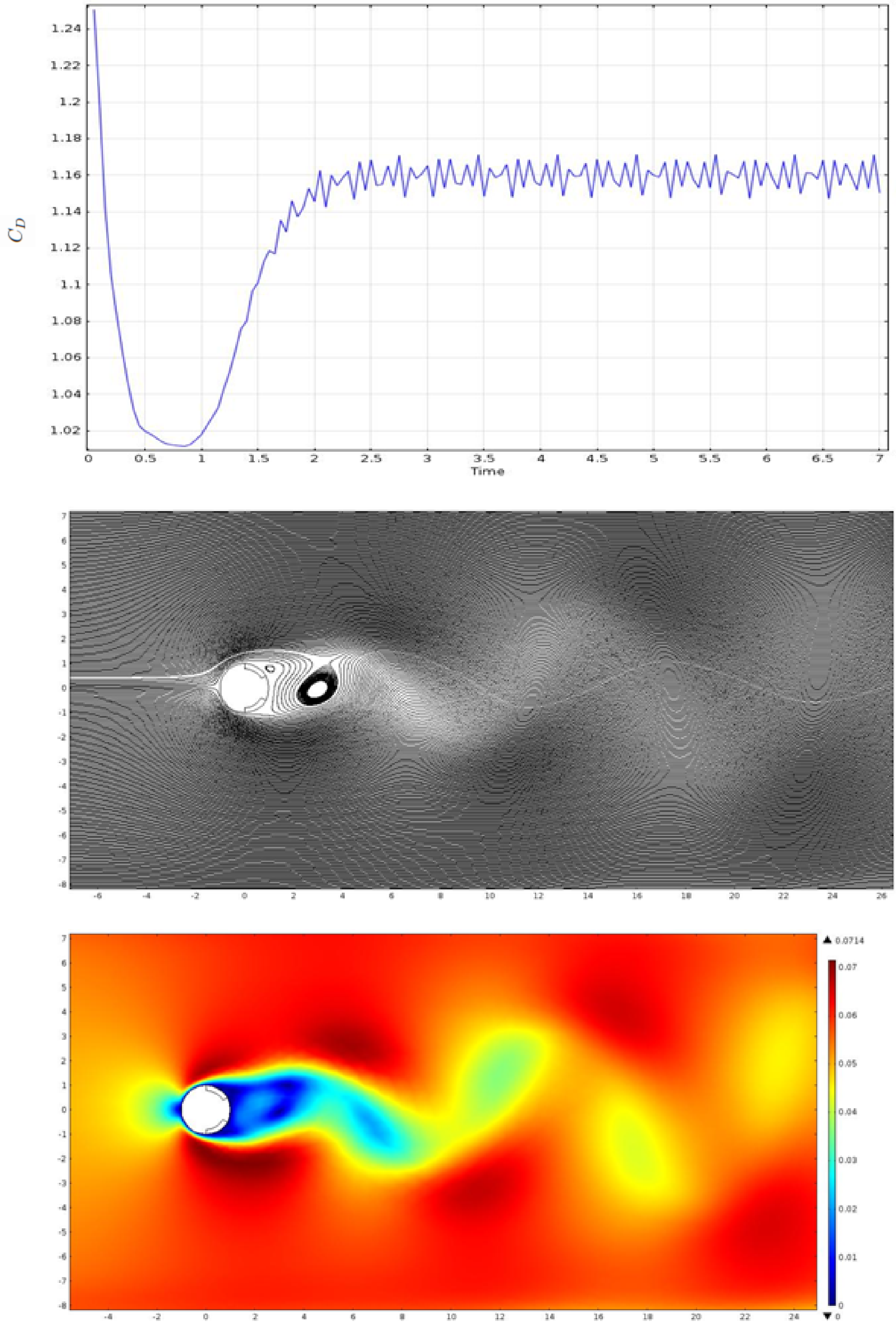

Figure 3.34. Drag Coefficient Graph, Streamline and Velocity Plots for Re=200, N=10 of shear thickening fluid (n=1.5)

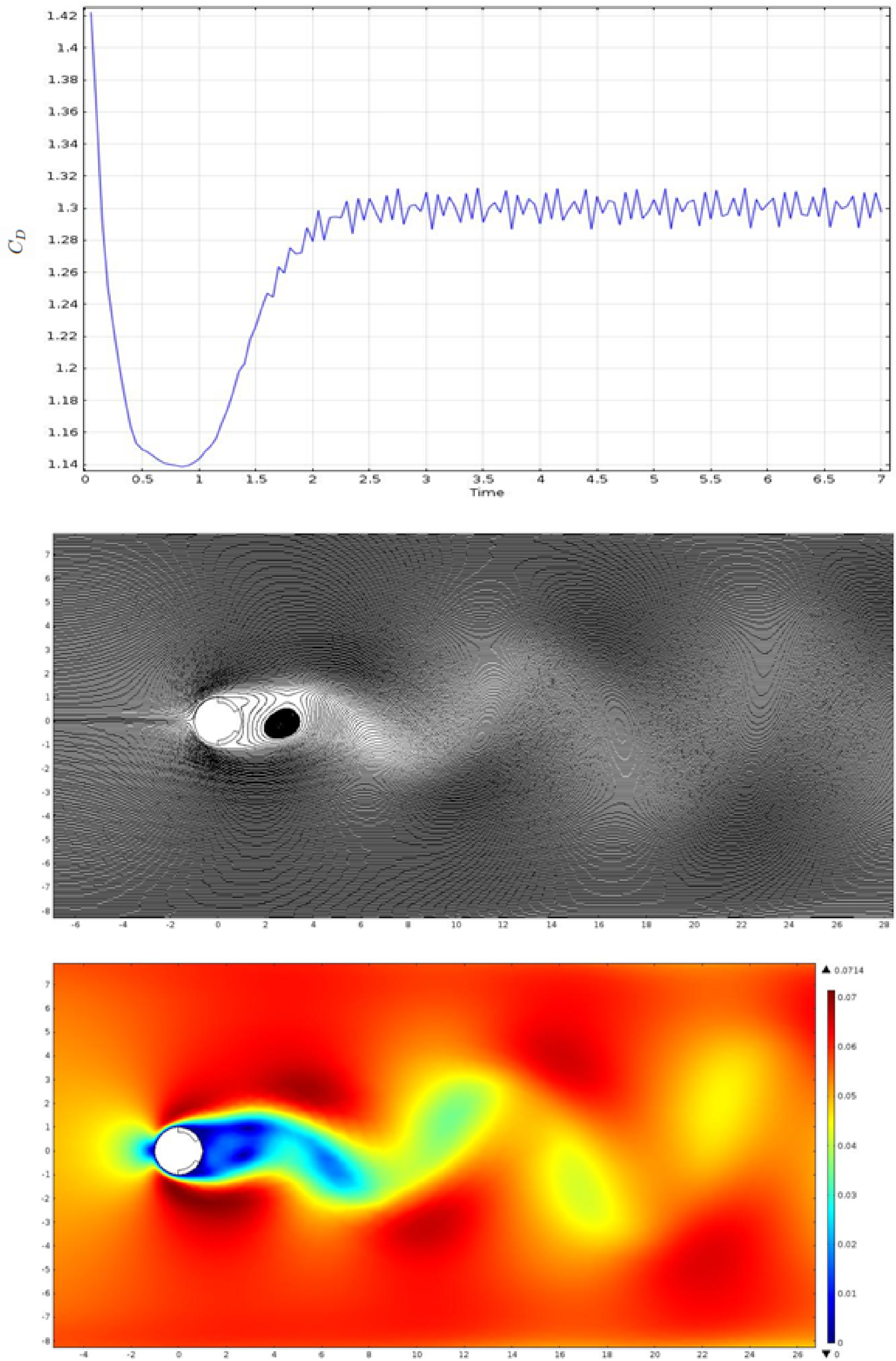

Figure 3.35. Drag Coefficient Graph, Streamline and Velocity Plots for Re=200, N=100 of shear thickening fluid(n=1.5)

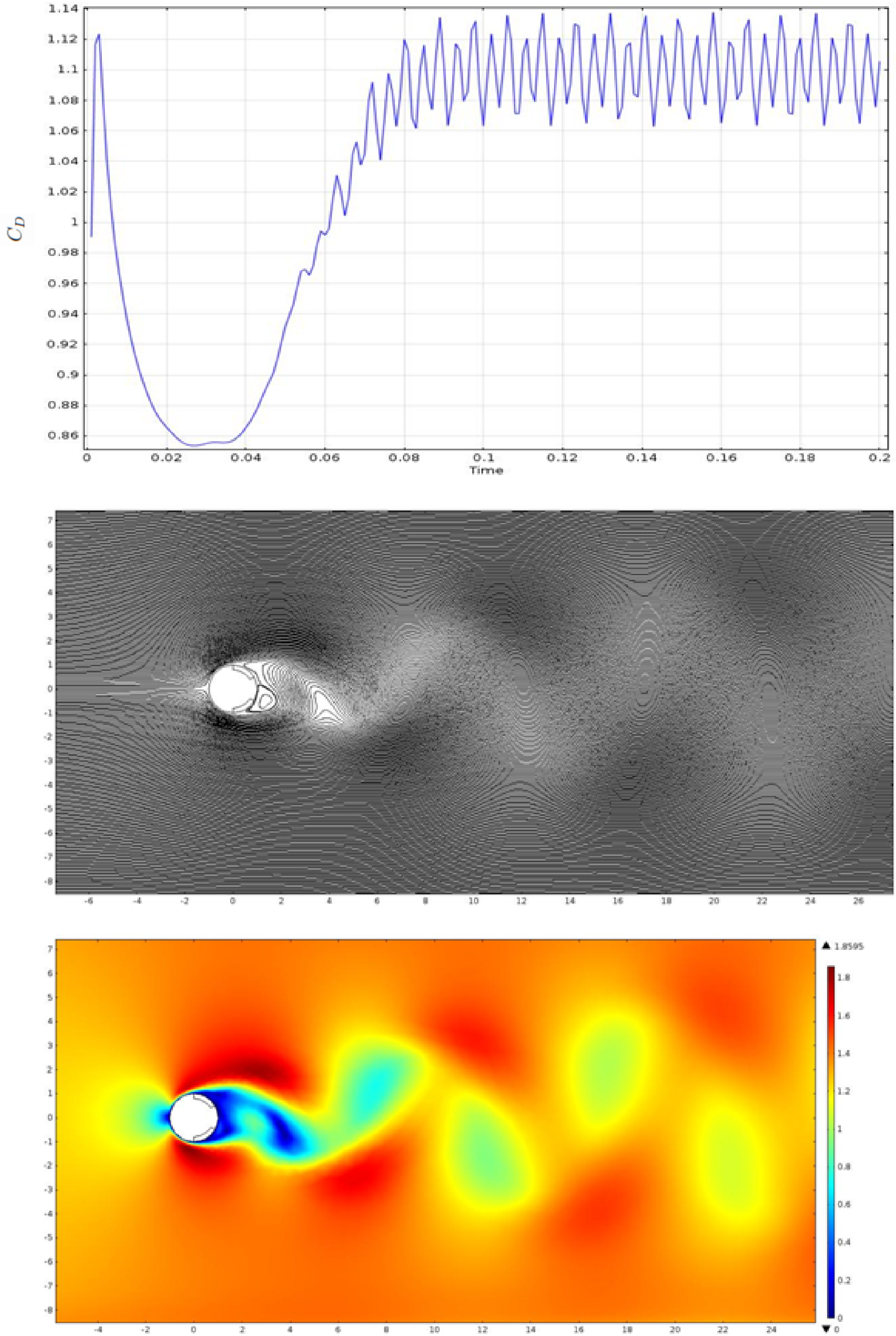

Figure 3.36. Drag Coefficient Graph, Streamline and Velocity Plots for Re=1000, N=0 of shear thickening fluid(n=1.5)

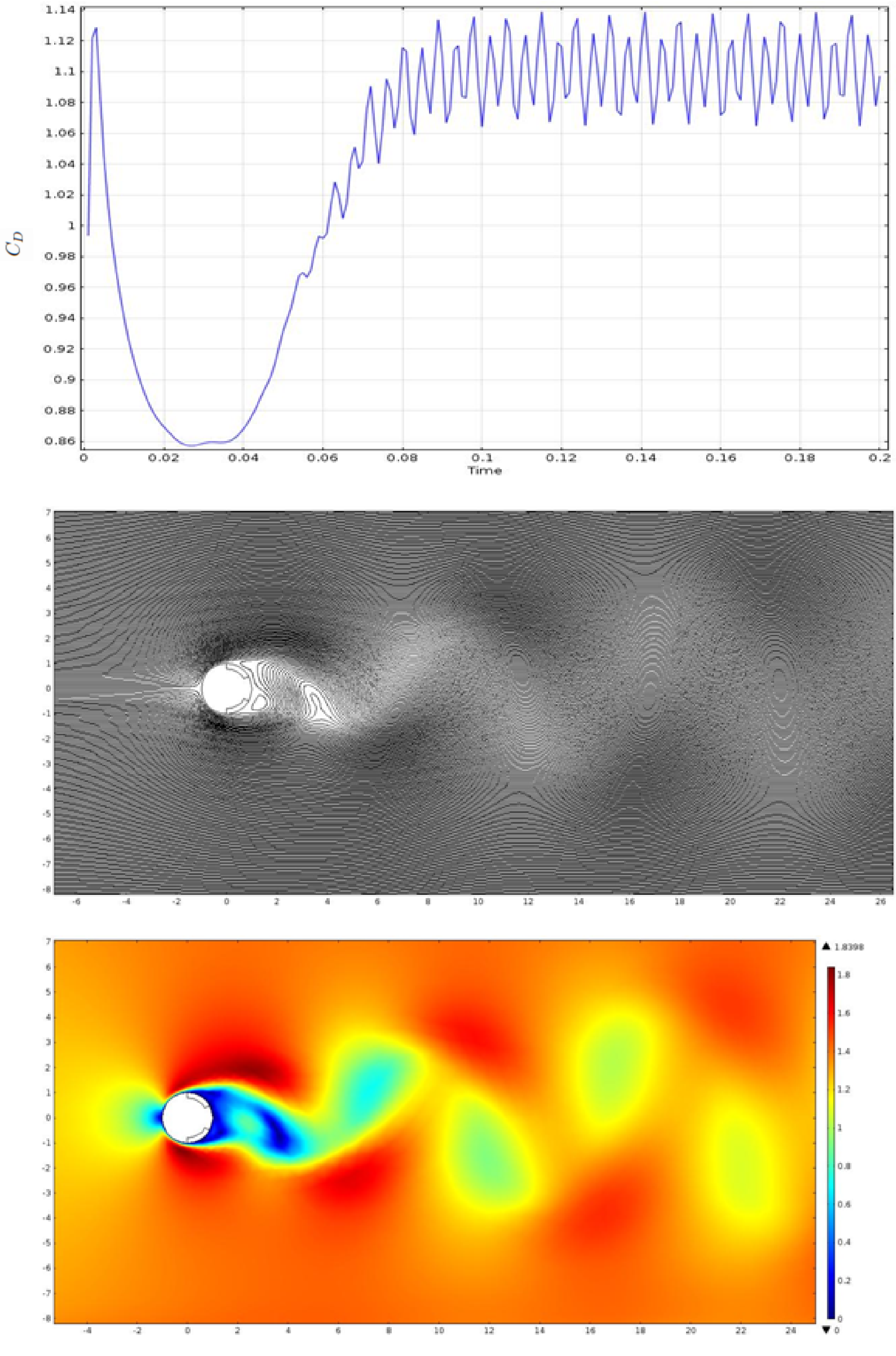

Figure 3.37. Drag Coefficient Graph, Streamline and Velocity Plots for Re=1000, N=10 of shear thickening fluid(n=1.5)

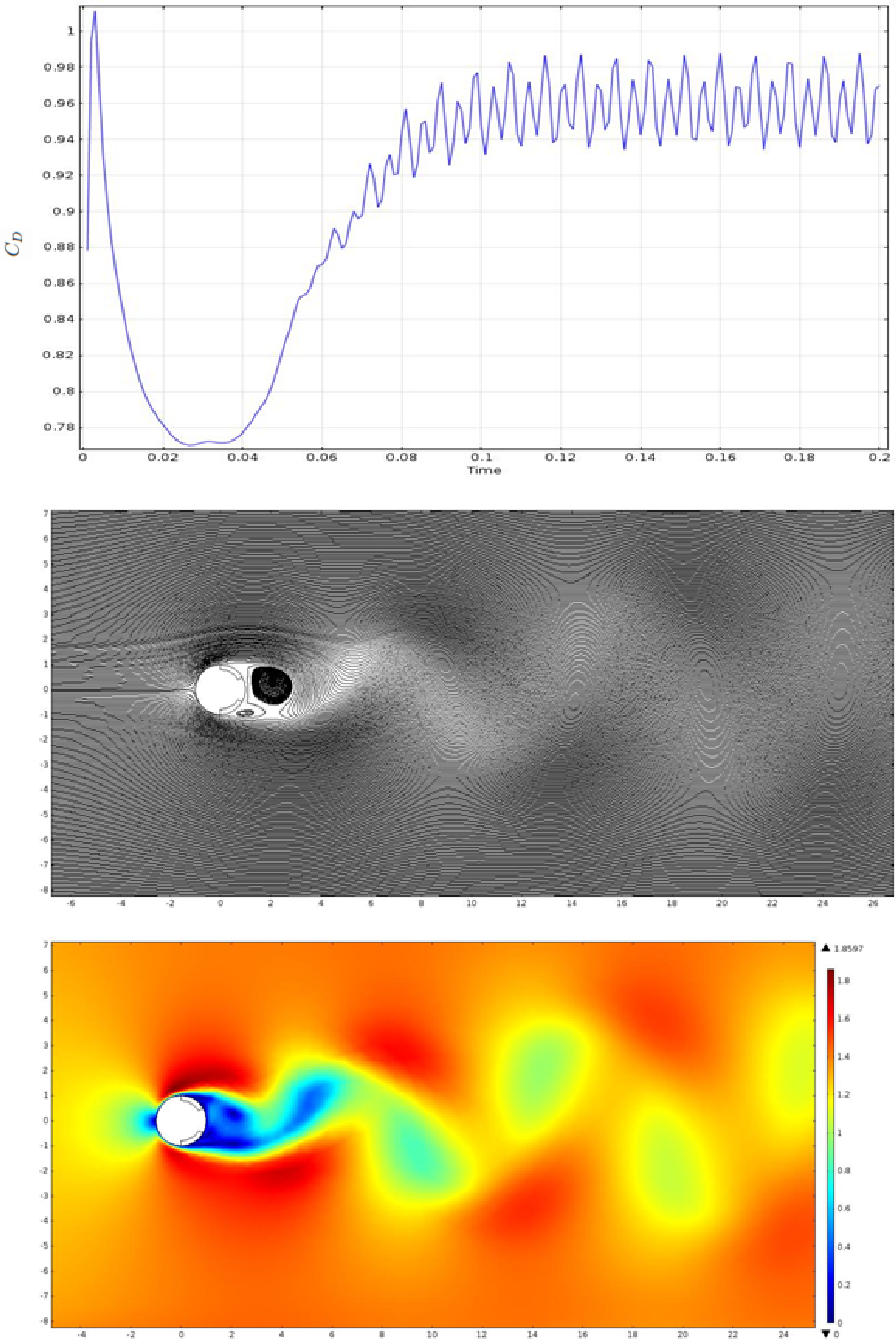

Figure 3.38. Drag Coefficient Graph, Streamline and Velocity Plots for Re=1000, N=100 of shear thickening fluid(n=1.5)

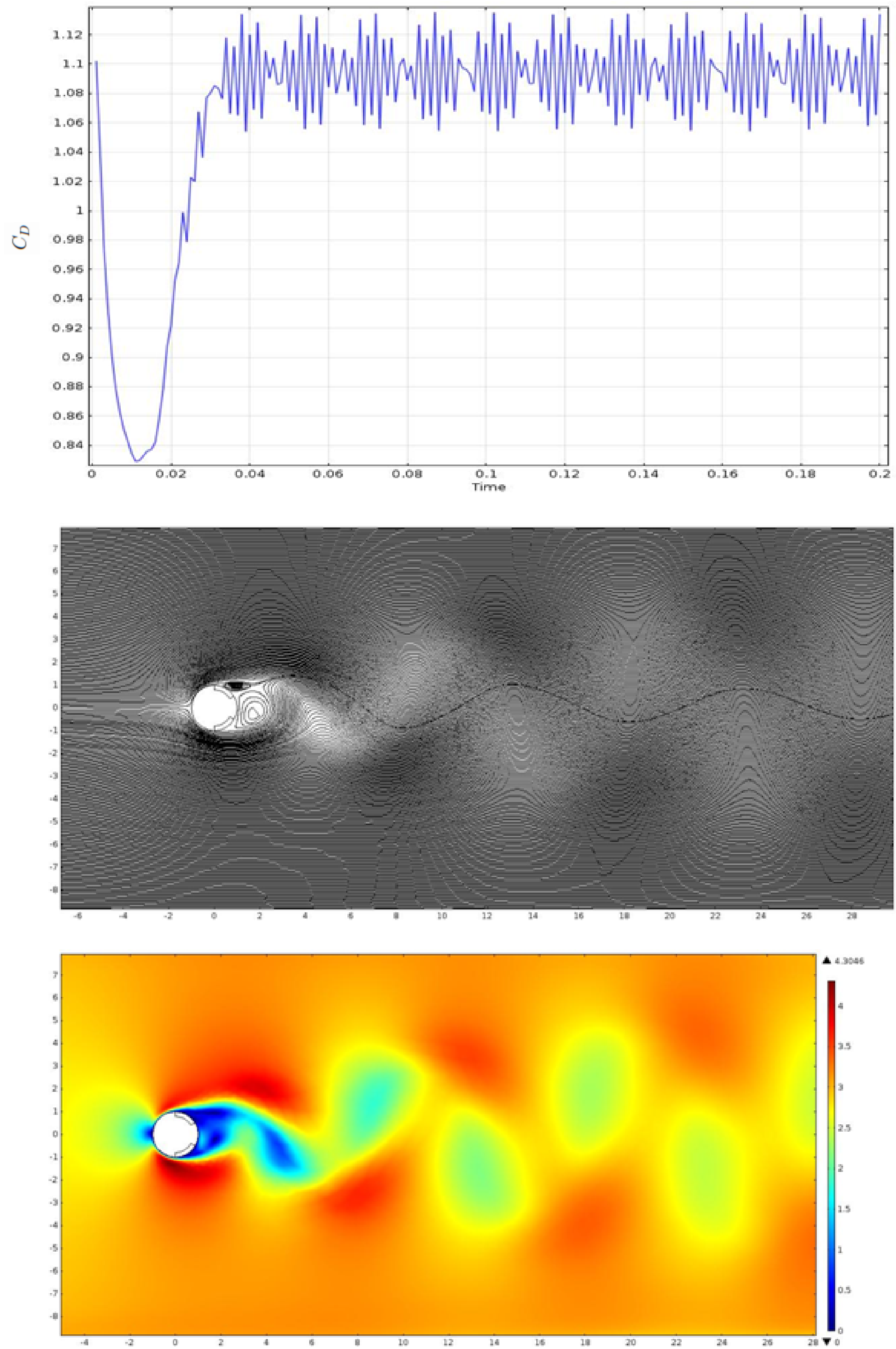

Figure 3.39. Drag Coefficient Graph, Streamline and Velocity Plots for Re=1500, N=0 of shear thickening fluid(n=1.5)

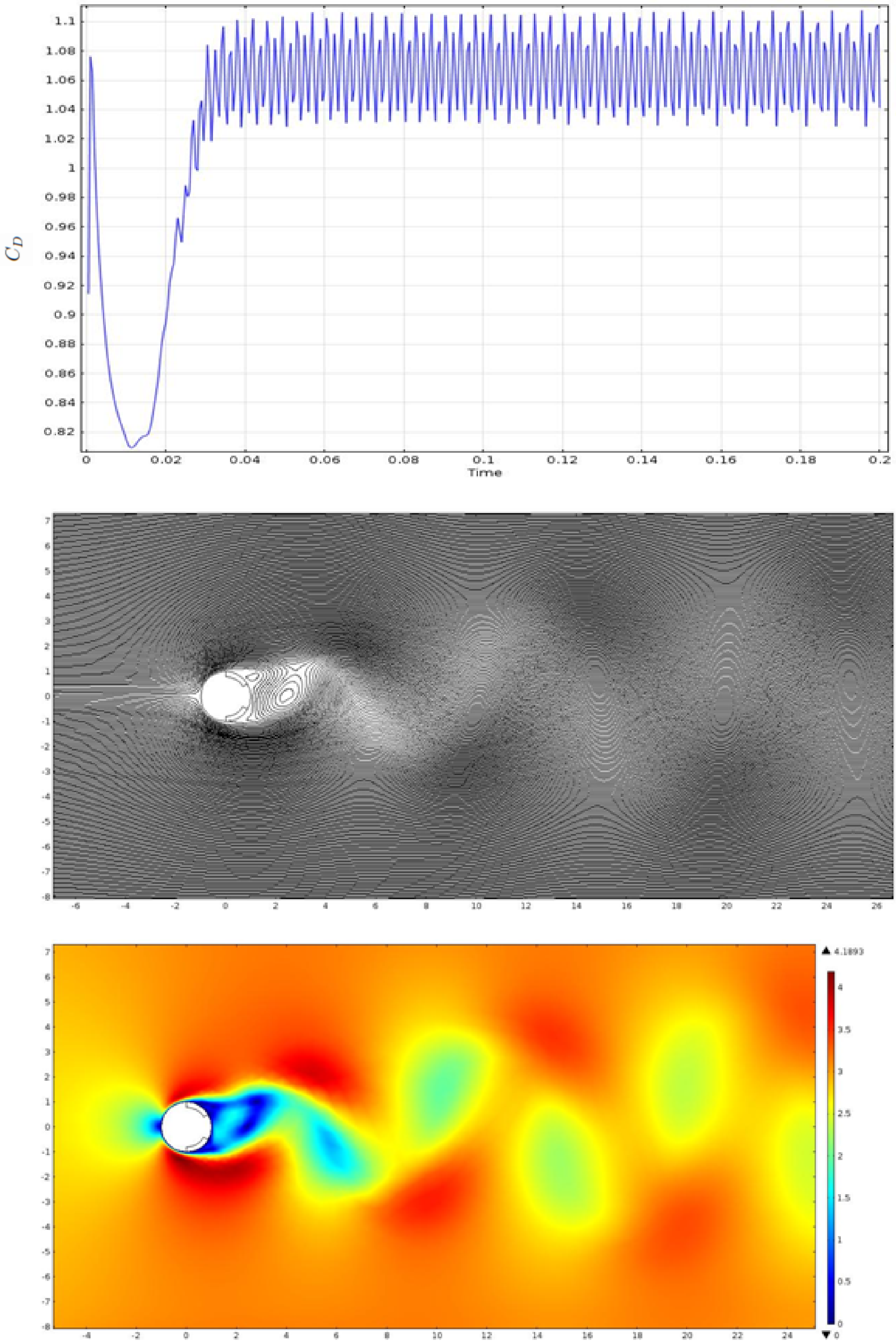

Figure 3.40. Drag Coefficient Graph, Streamline and Velocity Plots for Re=1500, N=10 of shear thickening fluid(n=1.5)

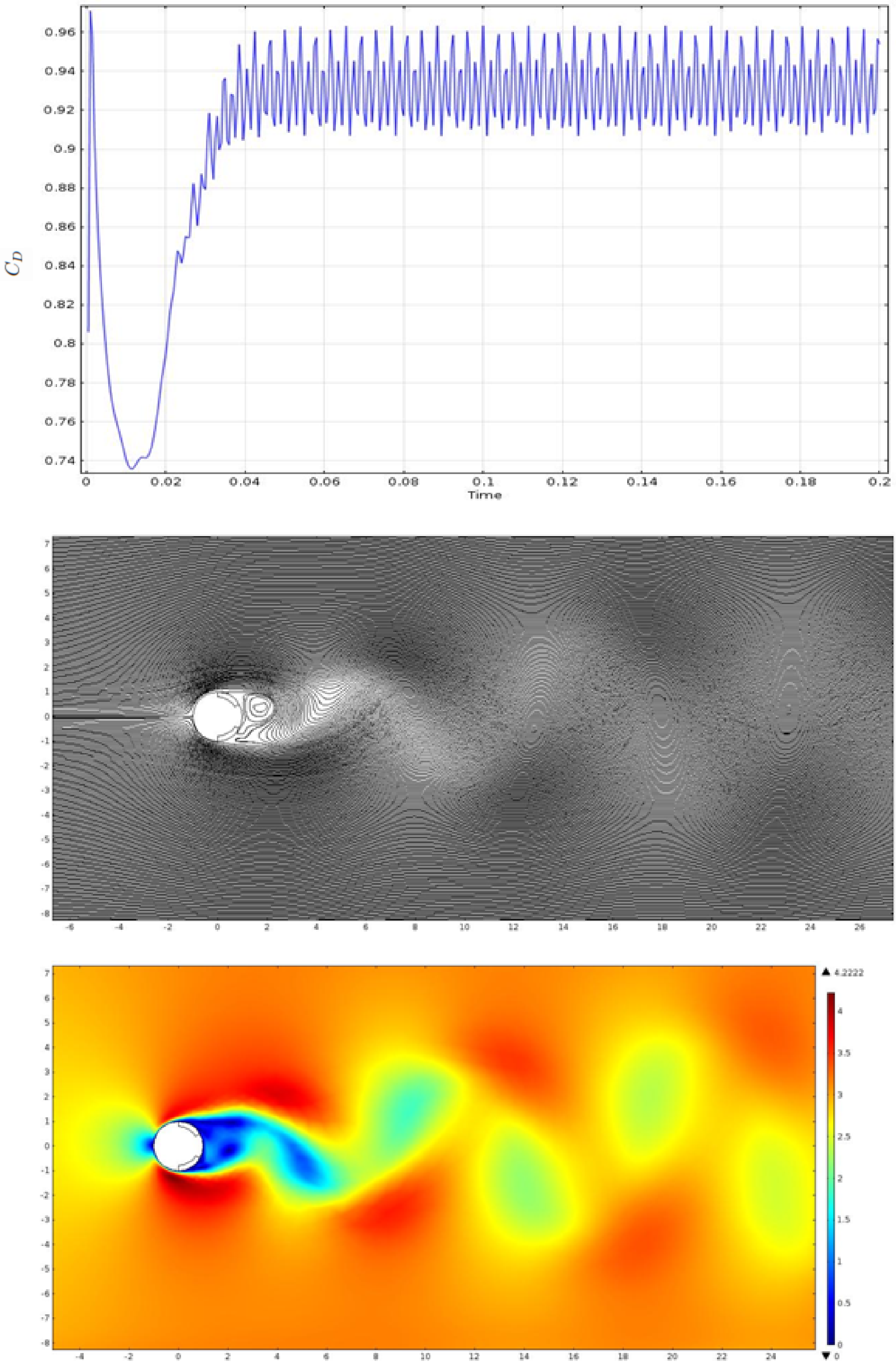

Figure 3.41. Drag Coefficient Graph, Streamline and Velocity Plots for Re=1500, N=100 of shear thickening fluid(n=1.5)

3.4. Comparison of Newtonian and non-Newtonian Fluid Results

In order to monitor the results from other perspectives, Figure 3.42, Figure 3.43, Figure 3.44, Figure 3.45, Figure 3.46 and Figure 3.47 are presented. In those, the drag coefficients and Strouhal numbers are compared with respect to fluid types as Newtonian (n=1), shear thinning (n=0.2) and shear thickening (n=1.5) for different Reynolds numbers as Re=50, Re=100, Re=200, Re=500, Re=1000 and Re=1500.

Firstly, drag coefficient values are compared. In Figure 3.42, drag coefficients of Newtonian, shear thinning and shear thickening fluids for different Reynolds numbers without any magnetic effect are presented. It shows that drag coefficients of shear thickening fluids are higher for any Reynolds number. On the other hand, shear thinning fluids show different characteristics on the basis of drag coefficient. For lower Re values as Re=50, Re=100, drag coefficients of Newtonian fluids are higher compared to shear thinning fluids. After Re=500, the drag coefficients of shear thinning fluids become higher than Newtonian. For flows past an object, when there is no magnetic field, the wake formation is delayed and the wake is shortened for shear thinning fluids compared to Newtonian fluid, and the reverse happens for shear thickening fluids. Therefore the results for the N=0 case are expected for relatively low Reynolds numbers where viscous effects are important, and they are in agreement with trends observed in the literature [27]. When magnetic effects are applied, there is no important change in trends of drag coefficients as seen at Figure 3.43 and Figure 3.44.

Secondly, the Strouhal numbers of Newtonian, shear thinning and shear thickening fluids are compared with respect to Reynolds numbers as Re=200, Re=500, Re=1000 and Re=1500, and presented at Figure 3.45, Figure 3.46 and 3.47. Similarly, trends are very close each other for different magnetic fields. In Figure 3.45, it is shown that Strouhal number of shear thinning fluid is higher for any Reynolds number. In the aspect of this parameter, shear thickening fluid show variable characteristics with Reynolds numbers. For lower Re values as Re=200, Newtonian fluids have higher value than shear thickening fluid, reverse is valid for higher Reynolds numbers. The reason is the acceleration of the particles around the object. For higher Reynolds number values, the viscous effects become more effective and the frequency is higher for shear thickening fluids compared to Newtonian fluids.

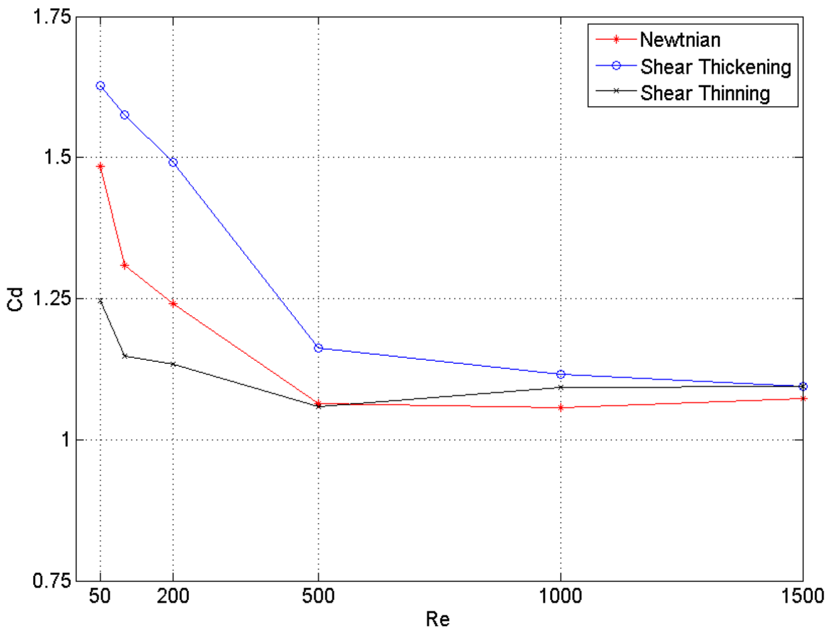

Figure 3.42. Mean drag coefficients (C_D) with different Fluid Types for different Reynolds Number (Re) Values for N=0

Secondly, the Strouhal numbers of Newtonian, shear thinning and shear thickening fluids are compared with respect to Reynolds numbers as Re=200, Re=500, Re=1000 and Re=1500, and presented at Figure 3.45, Figure 3.46 and 3.47. Similarly, trends are very close each other for different magnetic fields. In Figure 3.45, it is shown that Strouhal number of shear thinning fluid is higher for any Reynolds number. In the aspect of this parameter, shear thickening fluid show variable characteristics with Reynolds numbers. For lower Re values as Re=200, Newtonian fluids have higher value than shear thickening fluid, reverse is valid for higher Reynolds numbers. The reason is the acceleration of the particles around the object. For higher Reynolds number values, the viscous effects become more effective and the frequency is higher for shear thickening fluids compared to Newtonian fluids.

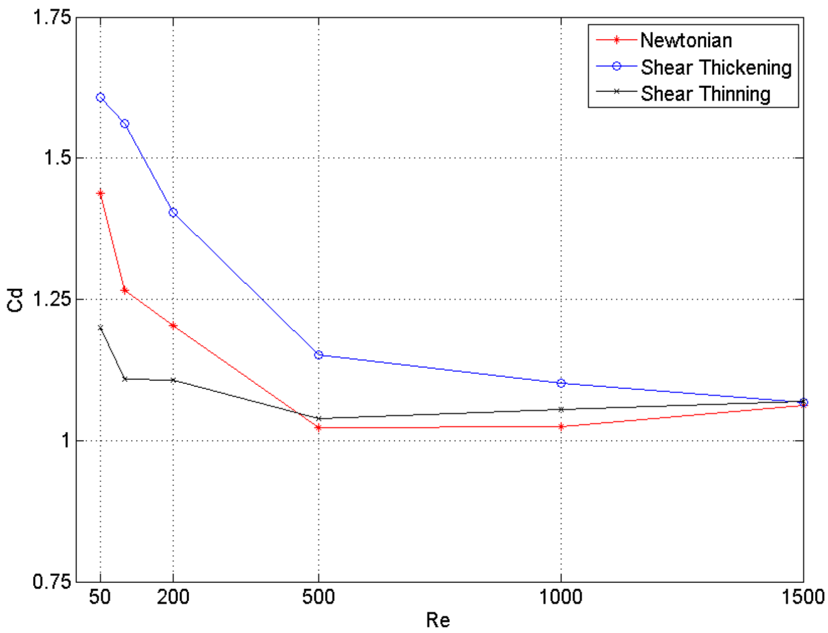

Figure 3.43. Mean drag coefficients (C_D) with different Fluid Types for different Reynolds Number (Re) Values for N=10

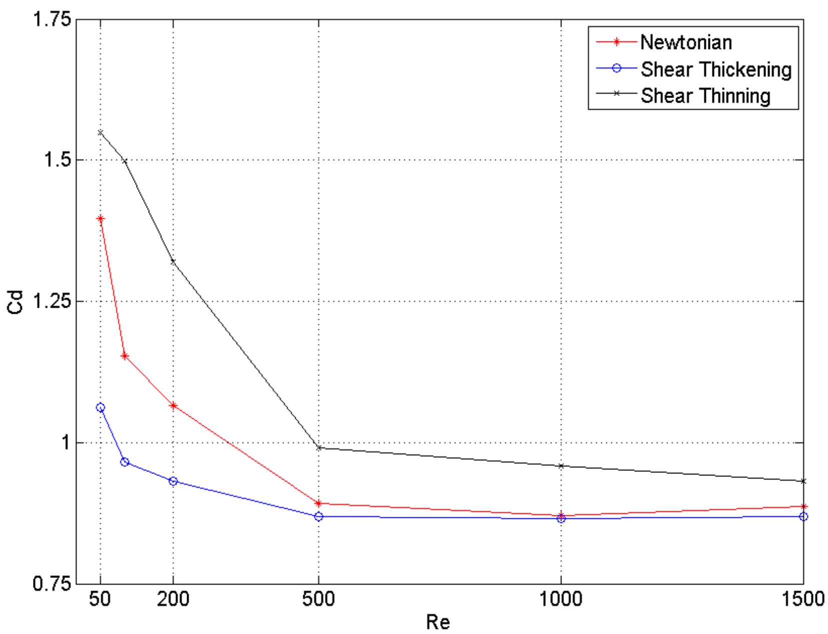

Figure 3.44. Mean drag coefficients (C_D) with different Fluid Types for different Reynolds Number (Re) Values for N=100

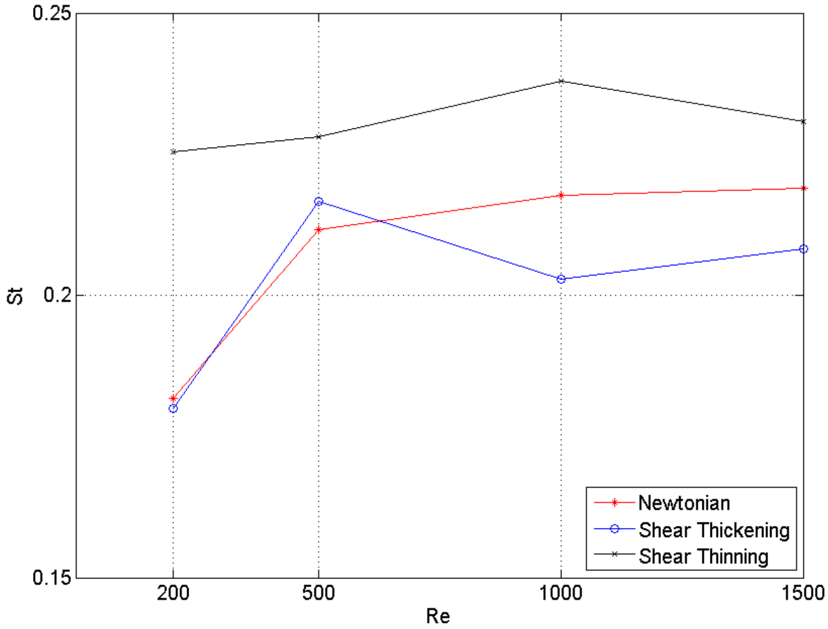

Figure 3.45. Strouhal Number(St) with different Fluid Types for different Reynolds Number (Re) Values for N=0

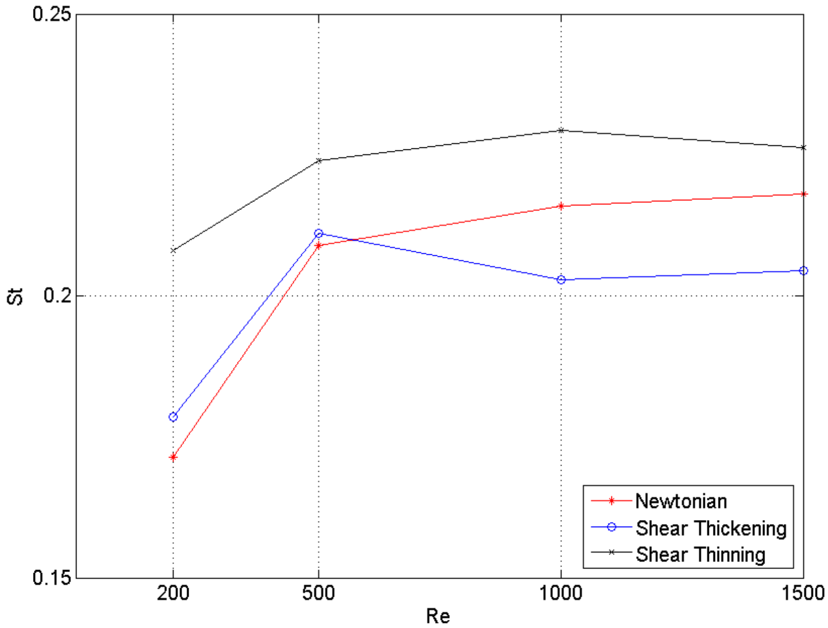

Figure 3.46. Strouhal Number(St) with different Fluid Types for different Reynolds Number (Re) Values for N=10

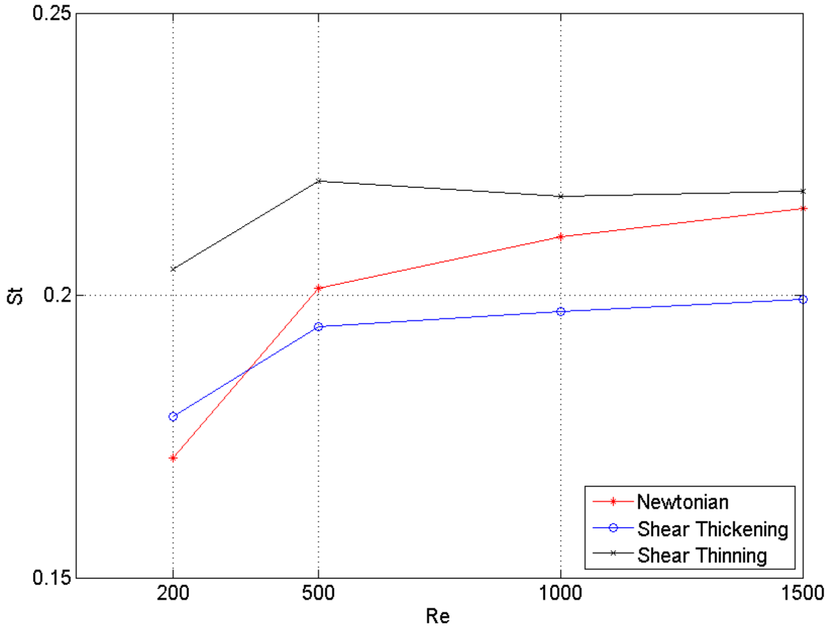

Figure 3.47. Strouhal Number(St) with different Fluid Types for different Reynolds Number (Re) Values for N=100

The final parameter of this study is the vortex formation length. Vortex formation length is the distance from the saddle point behind the cylinder where the vortices cross the central horizontal axis, to the cylinder surface. The literature data can be seen at Figure 3.48[25].

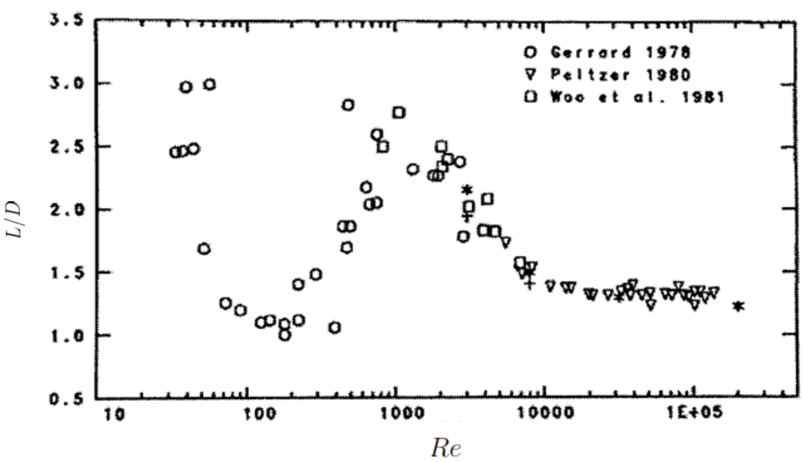

Figure 3.48. Literature data for vortex formation length(L/D) with different Reynolds number values(Re) for Newtonian fluid model(n=1) [25]

First, the validation is made with Newtonian cases like the previous analysis. As seen at Figure 3.49, the results are relevant to the literature data. Also it is seen that, the formation length increases with the interaction parameter value(N) for each Renolds number(Re).

Furthermore, in order to see how vortex formation length data changes for non-Newtonian fluid flows, shear thinning case is investigated. In Figure 3.50, it is possible to see the change of vortex formation length for different Reynolds number (Re) and interaction parameter (N) values. It is implied that, non-Newtonian fluid models show same kind of trend on the basis of vortex formation length point of view. The vortex formation length moves away from the cylinder regardless of type of fluid for flow around the cylinder cases.

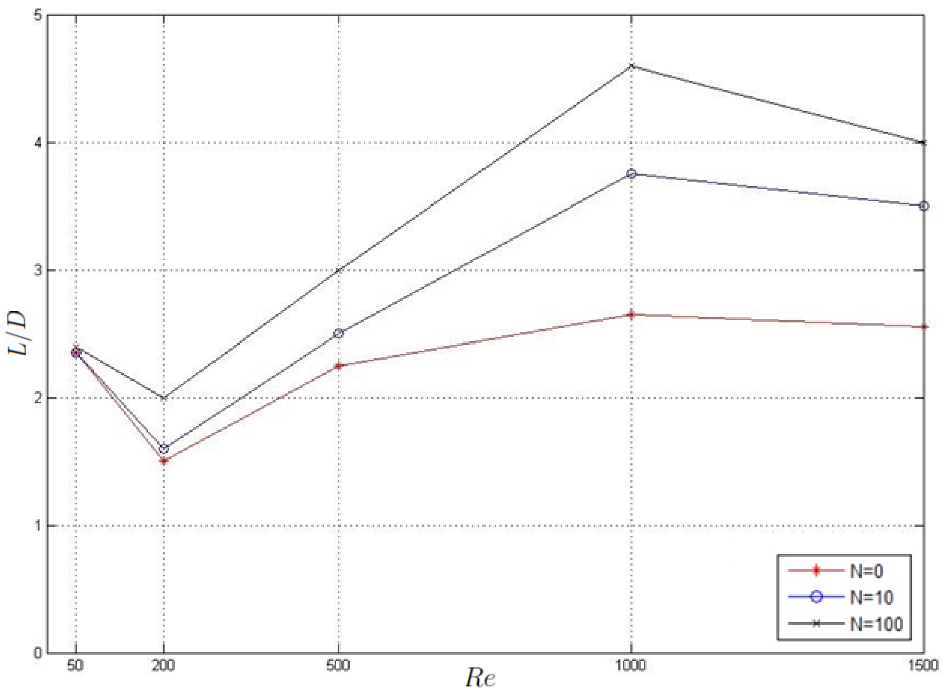

Figure 3.49. Vortex formation length(L/D) with different Reynolds number values (Re) for Newtonian fluid model(n=1)

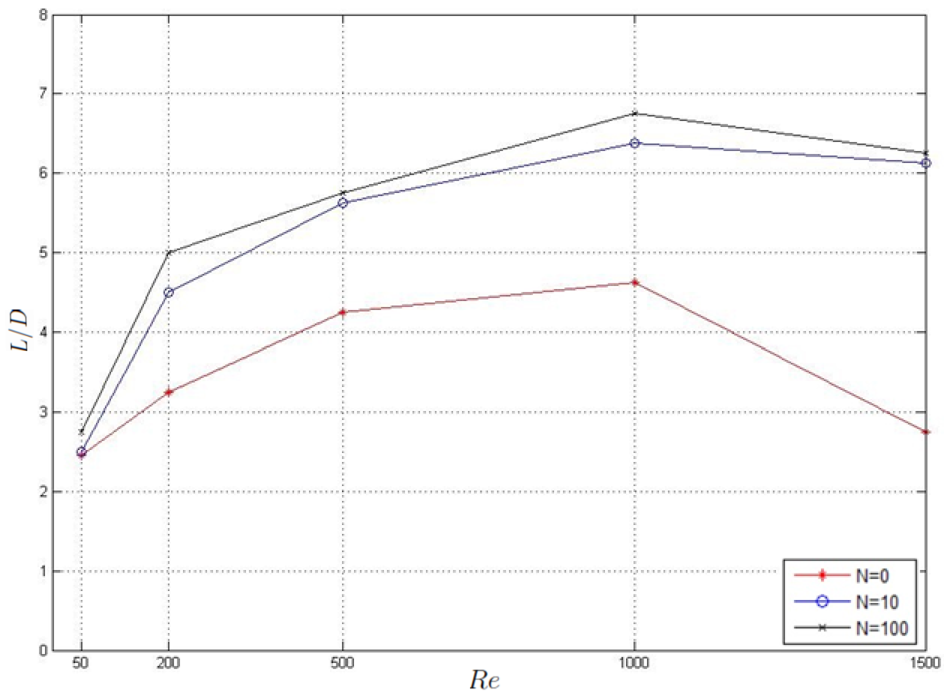

Figure 3.50. Vortex formation length(L/D) with different Reynolds number values (Re) for shear thinning fluid model(n=0.2)

3.5. Magnet Location Effect

Magnet location is another parameter for flow control around the object simulations. There are 3 different configurations, as P0: $90^o - 150^o$ section, P1: $60^o - 120^o$ section and P2: $30^o - 90^o$ section, to investigate the impact of magnet locations, as shown at Figure 3.51.

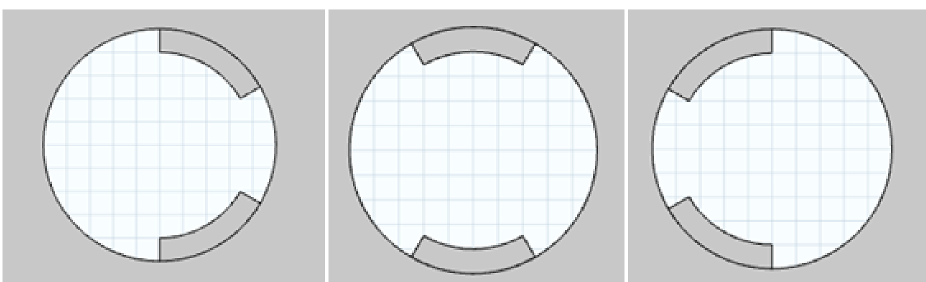

Figure 3.51. Different magnet locations as P0: $90^o - 150^o$ section, P1: $60^o - 120^o$ section, P2: $30^o - 90^o$ section)

In order to show the effects, drag coefficients and Strouhal numbers are calculated at Re=1000 and N=100 for each fluid type. The results are presented at Table 3.7 and Table 3.8. At Table 3.7, it can be seen that drag coefficient values have higher values, when the magnets are located on the back side of cylinder. For Newtonian simulations, from P0 to P1, the drag coefficient value increases 22%. Also, there is 35% difference between configurations P0 and P1. Similarly, shear thinning simulations show same trend. There is 30% difference between P0 and P1, and 55% difference between P0 and P2 as a result of these simulations. Finally, there is 13% increase, when magnets are shifted from P0 to P1 for shear thickening fluid simulations, and this value is 27% for P0 to P2 shift. In contrary, as seen at Table 3.8, Strouhal numbers do not show this kind of drastic changes for configuration shifts. For Newtonian simulations, the increase of Strouhal number between P0 and P1 is 1%, and between P0 to P2, it is 2.6%. Moreover, this increase is slightly higher for shear thinning and slightly lower for shear thickening compared to Newtonian simulations.

Table 3.7. Computed mean drag coefficient values at Reynolds number Re=1000 and at magnetic interaction parameter N=100, for Newtonian (n=1), shear thinning (n=0.2) and shear thickening (n=1.5) fluid models and for different magnets positions (P0: $90^o - 150^o$ section, P1: $60^o - 120^o$ section, P2: $30^o - 90^o$ section)

	P0	**P1**	**P2**
Newtonian	0.8704	1.0657	1.1706
Shear Thinning	0.8648	1.1204	1.3399
Shear Thickening	0.959	1.0814	1.2156

Figure 3.14, Figure 3.52 and Figure 3.53 present the streamline plots, velocity distribution plots and time evolution of drag coefficients graphs for a Newtonian fluid at Re=1000 with N=10 for each configuration. It is shown that wake region becomes wider, when magnets are located on the back side of cylinder with the help of streamline and velocity distribution plots. From the time evolution of drag coefficients graphs,

the change of Strouhal numbers can be seen, although there is no significant change of this parameter.

Table 3.8. Strouhal values at Reynolds number Re=1000 and at magnetic interaction parameter N=100, for Newtonian (n=1), shear thinning (n=0.2) and shear thickening (n=1.5) fluid models and for different magnets positions (P0: $90^o - 150^o$ section, P1: $60^o - 120^o$ section, P2: $30^o - 90^o$ section)

	P0	**P1**	**P2**
Newtonian	0.21039	0.21386	0.21589
Shear Thinning	0.21769	0.22818	0.23643
Shear Thickening	0.19718	0.20426	0.20709

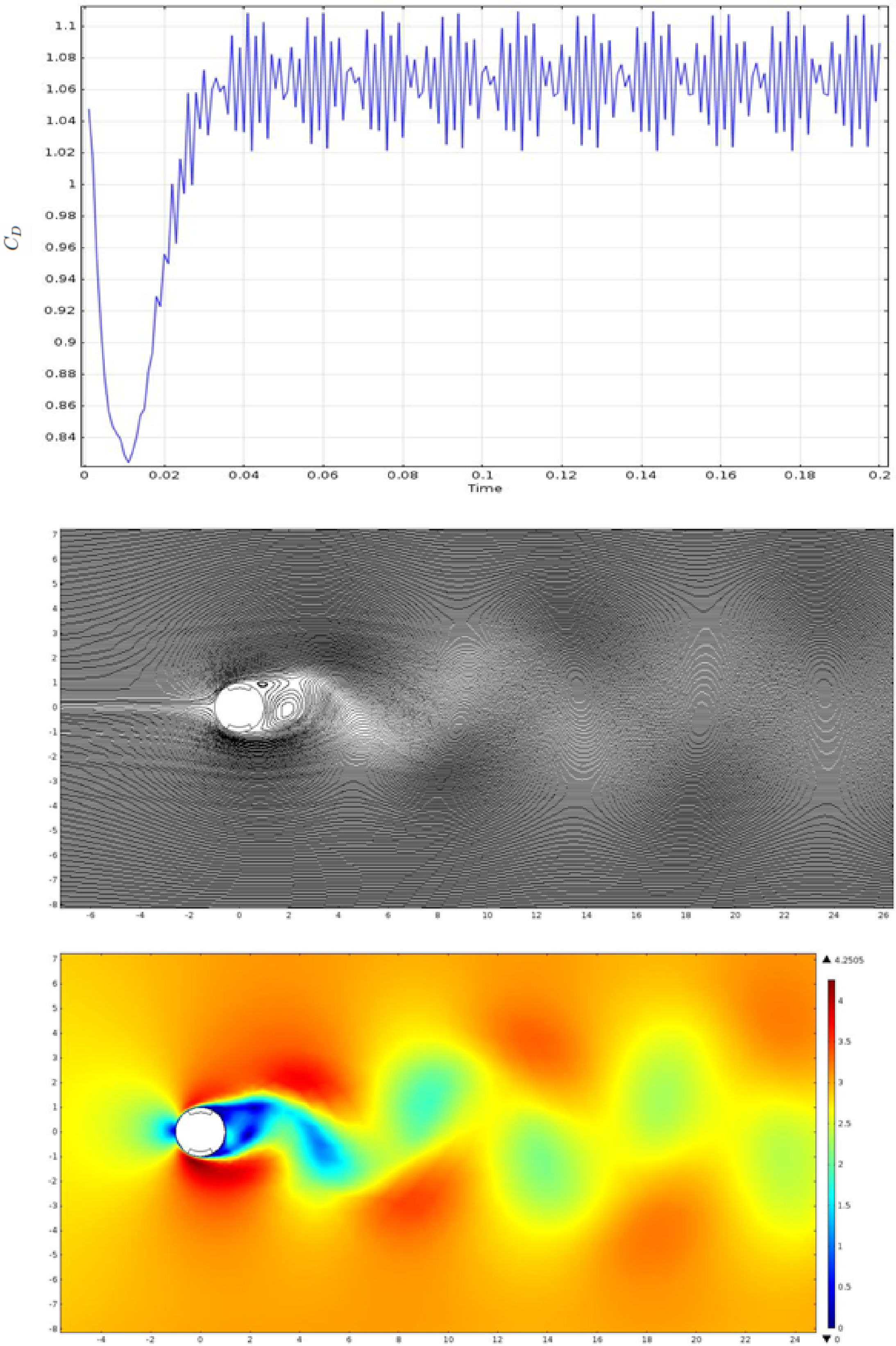

Figure 3.52. Drag Coefficient Graph, Streamline and Velocity Plots for Newtonian flow(n=1) at Re=1000, N=10 at magnet position P1

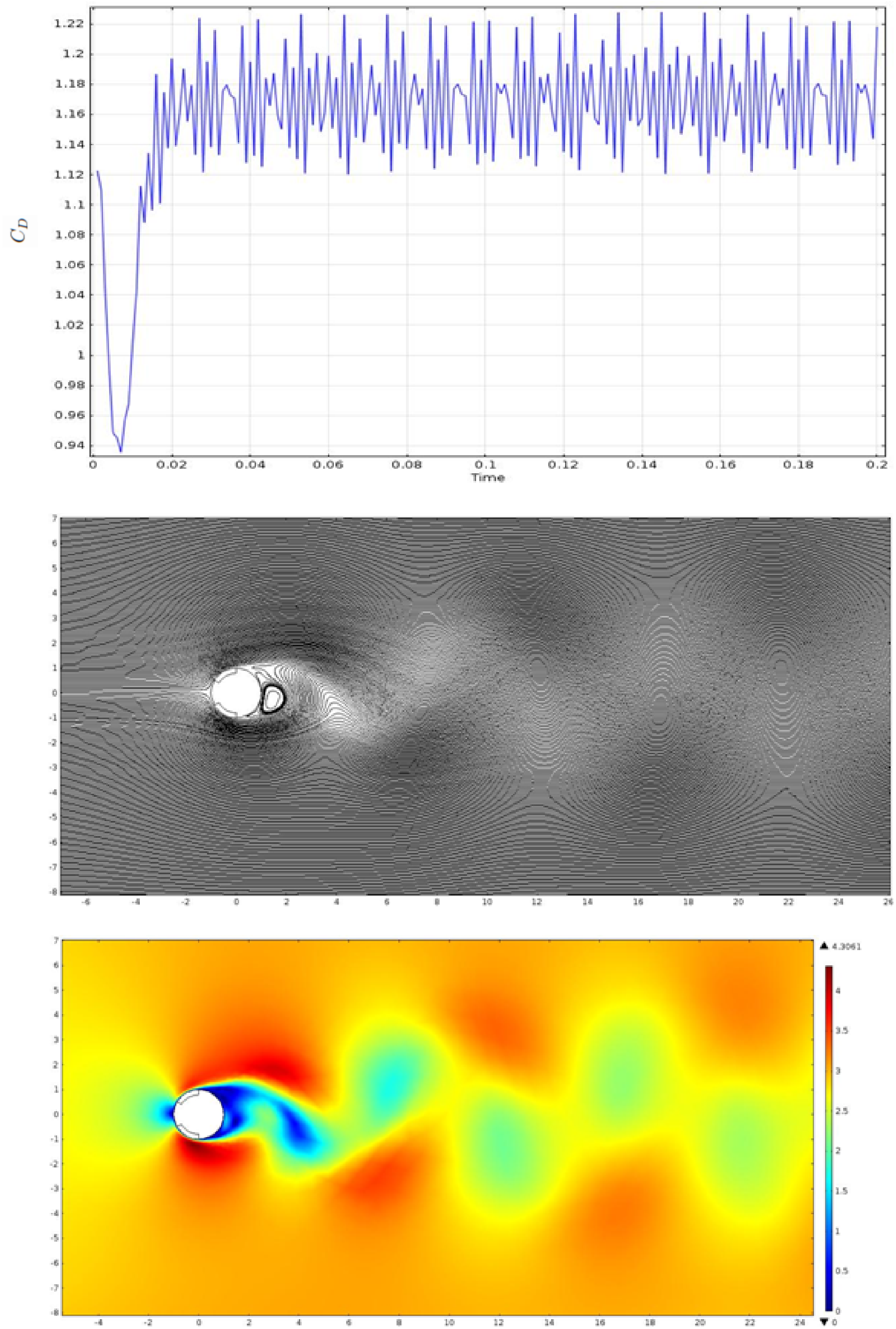

Figure 3.53. Drag Coefficient Graph, Streamline and Velocity Plots for Newtonian flow(n=1) at Re=1000, N=10 at magnet position P2

4. CONCLUSION

This study investigated if magnetostatic field is applicable for flow parameters of flow around a circular cylinder cases on reduction of drag and elimination of the wake region point of views. In order to express the results, 3 parameters are used as Reynolds number for inertial effects, interaction parameter for magnetic effects and power law index for fluid type effect. Two dimensional numerical studies are conducted for Re=50, Re=100, Re=200, Re=500, Re=1000 and Re=1500. The interaction parameter values are selected as N=0, N=10 and N=100, and the power law index values are n=1 for Newtonian, n=0.2 for shear thinning and n=1.5 for shear thickening fluids.

The computed parameters are mean drag coefficient (C_D), Strouhal number (St) and vortex formation length (L/D). General trends have been determined for these parameters on different perspectives. Drag coefficient values are decreased with magnetic field application without any exception. So, it can be inferred that, magnetostatic fields can be used for drag reduction for any kind of fluids. Additionally, the highest reduction rate is observed on shear thinning case, when compared with other applied types. Strouhal number is also decreased with interaction parameter. The decrease for all kinds of fluids is lower than the decrease of drag coefficient. This indicates that magnetic effects have a lower reduction on vortex shedding frequency.Vortex formation length is increased with interaction parameter for all of the fluids. The increase may be happened because of the acceleration of fluid particles under the action of magnetic effects near the separation point and close to the surface of the cylinder. For larger interaction parameter values, the vortex shedding disappears. Nonetheless, when the interaction parameter value becomes much higher, the drag coefficient values get negative values. This shows an unphysical effect, formed because of unrealistic magnetic intensity. Magnet location is also a parameter in this study. After various simulations made for three different configurations, it is implied that the drag coefficient values become higher and the separation points shift to front of the object, when the magnets placed towards the front region.

Some of the results on the subject of this thesis are presented in recently published study of Adiguzel and Atalik[28]. Regarding, there are various different aspects of this subject, it is possible to enhance this study in future. First, in order to have more accurate results for the simulations, especially for higher than Re=50, three dimensional studies can be conducted. For this purpose, smaller amount of data set and higher computational power are needed. By the help of this potential study, not only these trends can be seen again, but also excellent approximation to experimental results can be made and alternative applications can be investigated. Secondly, flow inside the pipe case should be researched, since this subject is also widely applied and popular. Hence, it is important to know how magnetostatic forces affect the friction factor for different pipe flow setups. Also, as magnetic effects are widely applicable for biological studies, oscillatory magnetic and pressure gradients can be used for future studies. This shows higher resemblance to real biological environment. Additionally, there are numerous studies that investigate the thermal behavior under electromagnetic forces for different geometries, so it is possible to investigate the thermal behavior of the Newtonian and non-Newtonian fluids under magnetostatic effects.

REFERENCES

1. Berger T.W., Kim J., Lee C., Lim J., “Turbulent boundary layer control utilizing the Lorentz force”, *Phys. Fluids* 12 (3) 631–649, 2000.

2. O. Posdziech, R. Grundmann, “Electromagnetic control of seawater flow around circular cylinders”, *Eur. J. Mech. B-Fluids*, 20, 255-274, 2001.

3. T. Weier, G. Gerbeth, “Control of separated flows by time periodic Lorentz forces”, *Eur. J. Mech. B-Fluids*, 23, 835–849, 2004.

4. S.J. Kim, and C.M. Lee, “Investigation of the flow around a circular cylinder under the influence of an electromagnetic force”, *Experiments in Fluids*, 28, 252-260, 2000.

5. McBain, James W., “Colloid Science”, Reinhold Publ.Corp., pp. 3-4, 1950.

6. Montgomery, Carol G. “The Magnetization of Colloidal Suspensions”, *Phys. Rev., vol. 38, no. 9*, p. 1782, November 1, 1931.

7. Montgomery, Carol G., “The Magnetic Properties of Nickel Colloids”, *Phys. Rev., vol. 39*, no. 1, pp. 163-164, January 1, 1932.

8. Berkovsky B. and V. Bashtovoy, “Magnetic Fluids and Applications Handbook”, Begell Home, Inc., 1996.

9. Gazeau F.,C. Baravian, J.-C. Bacri, R. Perzynski and M.I. Shliomis, “Energy conversion in ferrofluids: Magnetic nanoparticles as motors and generators”, *Phys. Rev. E* 56(1), 614–618, 1997.

10. P.A. Voltairas, D.I. Fotiadis, L.K. Michalis, “Hydrodynamics of magnetic drug targeting”, *J. Biomechanics*, 35, 813-821, 2002.

11. D.N. Ku, “Blood Flow in Arteries”, *Ann. Review Fluid Mech.*, 29, 399-434, 1997.

12. Tanner RI, Walters K, “Rheology: an historical perspective”, Elsevier, Amsterdam, 1998.

13. Chhabra RP, Richardson JF, “Non-Newtonian flow and applied rheology 2nd edn.”, Butterworth-Heinemann, Oxford, 2008.

14. Ibarz A, Barbosa-Canovas GV, “Unit operations in food engineering”, CRC Press, Boca Raton, FL, 2003.

15. Govier GW, Aziz K, “The flow of complex mixtures in pipes”, Van Nostrand, New York, 1977.

16. Metzner AB, Whitlock M, “Flow behaviour of concentrated (dilatant) suspensions”, *Trans Soc Rheol 2*, 239-254, 1958.

17. P.K.Papadopoulos, P.Vafeas, P.M.Hatzikonstantinou, “Ferrofluid pipe flow under the influence of the magnetic field of a cylindrical coil”, *Phys.Fluids 24*, 122002, 2012.

18. A.P.Rosa, R.G.Gontijo, F.R.Cunha, “Laminar pipe flow with drag reduction induced by a magnetic field gradient”, *Applied Mathematical Modelling* 40, 3907–3918, 2016.

19. R. Kalter, M.J. Tummers, S. Kenjereš, B.W. Righolt, C.R. Kleijn, “Electromagnetic flow control of a bifurcated jet in a rectangular cavity”, *International Journal of Heat and Fluid Flow* 47, 113–122, 2014.

20. Ahmad Sedaghat and Mohammad Ali Badri, “Numerical study on flow separation control over NACA0015 aerofoil using electromagnetic fields”, *Theoretical and Applied Mechanics Letters* 3, 052003, 2013.

21. Zhao Guangyin, Li Yinghong, Liang Hua, Han Menghu, Wu Yun, “Flow separation control on swept wing with nanosecond pulse driven DBD plasma actuators”, *Chinese Journal of Aeronautics*, 28(2), 368–376, 2015.

22. V. Shatrov, G. Gerbeth, “Electromagnetic flow control leading to a strong drag reduction of a sphere”, *Fluid Dynamics Research,* 36, 153 – 173, 2005.

23. T.V.S. Sekhar, R. Sivakumar, T.V.R. Ravi Kumar, “Magnetohydrodynamic flow around a sphere”, *Fluid Dynamics Research*, 37, 357 – 373, 2005.

24. Hui Zhang, Bao-chun Fan, Zhi-hua Chen, “Optimal control of cylinder wake flow by electro-magnetic force based on adjoint flow field”, *European Journal of Mechanics B/Fluids*, 29, 53–60, 2010.

25. D.J. Tritton, “Experiments on the flow past circular cylinder at low Reynolds number”, *J. Fluid Mech.*, 6, 547-567, 1959.

26. M.M. Zdravkovich, “Flow around circular cylinders: a comprehensive guide through flow phenomena, experiments, applications, mathematical models, and computer simulations, vol. 1”, *Oxford University Press*, 1997.

27. R.P. Chhabra, J.F.Richardson, “Non-Newtonian Flow and Applied Rheology”, Elsevier, 2008.

28. Omer Baris Adiguzel, Kunt Atalik, “Magnetic field effects on Newtonian and non-Newtonian ferrofluid flow past a circular cylinder”, *Applied Mathematical Modelling,* 42, 161–174, 2017.